Master of Science Thesis

The Oval Fuselage

A New Structural Design Concept for Blended Wing Body Cabins

M.F.M. Hoogreef B.Sc.

9 August 2012

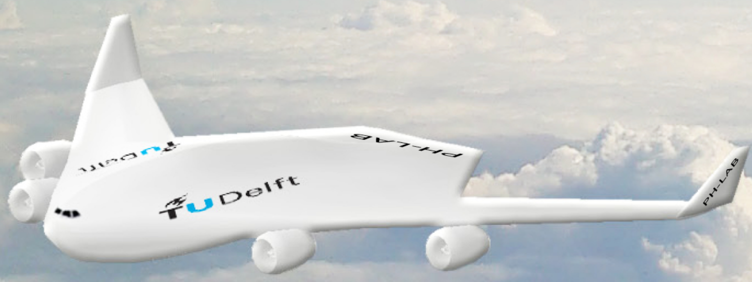

Faculty of Aerospace Engineering · Delft University of Technology

Faculty of Aerospace Engineering

Delft University of Technology

The Oval Fuselage
A New Structural Design Concept for Blended Wing Body Cabins

Master of Science Thesis

For obtaining the degree of Master of Science in Aerospace Engineering at
Delft University of Technology

M.F.M. Hoogreef B.Sc.

9 August 2012

Faculty of Aerospace Engineering · Delft University of Technology

Delft University of Technology

Delft University Of Technology
Department Of
Flight Performance and Propulsion

The undersigned hereby certify that they have read and recommend to the Faculty of Aerospace Engineering for acceptance a thesis entitled **"The Oval Fuselage"** by **M.F.M. Hoogreef B.Sc.** in partial fulfillment of the requirements for the degree of **Master of Science**.

Dated: 9 August 2012

Chairman: ______________________
dr.ir. L.L.M. Veldhuis

Supervisor: ______________________
dr.ir. R. Vos

Reader: ______________________
dr.ir. G. La Rocca

Reader: ______________________
ir. F.J.J.M.M. Geuskens

ABSTRACT

Faced with the decreasing fossil fuel reserves and the need to decrease its environmental footprint, the aviation industry is searching for alternative fuels and more fuel efficient engines and aircraft. With the current designs reaching their limits, the industry has turned its attention to the family of all lifting bodies. Particularly blended wing body aircraft have received much interest, a combination of a lifting fuselage and a flying wing. It is commonly believed that this design has a high aerodynamic efficiency and lower structural weight fraction, which both contribute to a higher fuel efficiency. Though the concept has been around since World War II, no flying full-scale aircraft with a pressurized cabin currently exists. Additionally, the pressure cabins have so far been dictated by the aerodynamic design of the centre body.

This thesis presents an alternative approach in blended wing body design, which has its roots in the design of conventional aircraft. For current aircraft a method called the 'inside-out approach' is used, where the design of the fuselage is dictated by the requirements for the passenger and cargo compartment. Following this approach a blended wing body cabin consisting of four tangentially connected arcs, forming an oval fuselage cross-section with no need for an aerodynamic outer surface is designed. The arcs are supported by vertical and horizontal members, doubling as walls, floors and ceiling for the cabin. The research presented in this thesis describes the geometry determination and weight estimation for this new design, for pressurization, wing bending loads and longitudinal fuselage stresses. The weight estimation method that has been developed determines the thicknesses of the structural members per oval fuselage cross section, described by the four arcs and horizontal and vertical members, for a certain cabin geometry and the aforementioned loads. An imposed airfoil shape over the centre line of the cabin restricts the height of each oval cross-section. By placing these oval cross-sections in sequence, and interpolating between two neighbouring sections, a three-dimensional fuselage can be created that follows the airfoil shape. This airfoil-shaped fuselage is combined with outer wing sections, vertical tail planes, engines and landing gears to generate a complete blended wing body model. This model is analyzed by means of a Matlab optimization tool, which was adapted from a pre-existing blended wing body design tool. In this tool, the developed fuselage weight estimation is combined with a wing-weight estimation and an operative empty weight estimation to calculate the total operative empty weight.

Three different conceptual design studies of blended wing body configurations, for 200, 400 and 800 passengers, have been optimized and assessed to investigate the feasibility of the new structural cabin design. These designs have been compared to another blended wing body cabin design and to conventional aircraft. In comparison to other blended wing bodies a lower fuel consumption, lower operative empty weight and longer range were found for the same maximum take-off weight and the same payload. A 400 passenger 'oval-fuselage' blended wing body showed the most promising results with a 13% lower empty weight, a 6% better fuel consumption and almost 29% longer range. In comparison to the conventional airliners, this particular blended wing body showed a fuel consumption per transported kilogram that was 10% lower than that of the best performing conventional aircraft, the Boeing 777-200LR.

ACKNOWLEDGMENTS

This thesis is part of the graduation of the M.Sc. curriculum at the Faculty of Aerospace Engineering of the Delft University of Technology. It is the result of a 10 months individual research and design project, applying the skills and knowledge obtained during the studies. Though being an individual research and design project, this graduation would not have been possible without the valuable input of others, who I hereby wish to thank.

First and foremost, I wish to thank my supervisor, Dr. Ir. Roelof Vos, for his support and input over the course of this thesis. Without his initial idea on the concept, this thesis would not have been possible. I also want to thank Ir. François Geuskens for his assistance with the structural design and Dr. Ir. Gianfranco La Rocca for his knowledge of aircraft design and optimization. Furthermore, I want to thank Dr. Ir. Leo Veldhuis for his objective point of view in the later stages of the design. In addition I would like thank my fellow students for their support and the brainstorming sessions.

Finally, I want to thank my family and friends for their support and patience in sometimes stressful times during my thesis and my time at the Faculty of Aerospace Engineering.

Delft, The Netherlands M.F.M. Hoogreef B.Sc.
9 August 2012

CONTENTS

LIST OF FIGURES

LIST OF TABLES

NOMENCLATURE

Latin Symbols

A_1	Structural half width of upper member	[m]
A_2	Structural half width of lower member	[m]
B	Structural height of wall	[m]
b_1	Width of cabin front section	[m]
b_2	Width of cabin centre section	[m]
b_3	Width of cabin aft section	[m]
E_{f}	Young's modulus of sandwich facing material	$\left[\mathrm{N/m^2}\right]$
F_1	Force in upper shell	[N]
F_2	Force in side shell	[N]
F_3	Force in lower shell	[N]
F_{crit}	Critical buckling force	[N]
F_{h}	Horizontal component of resultant force	[N]
$F_{\mathrm{h_{bar}}}$	Force in horizontal member	[N]
$F_{\mathrm{n_{max}}}$	Lateral compressive force from maximum load factor	[N]
$F_{\mathrm{n_{min}}}$	Lateral compressive force from minimum load factor	[N]
$F_{\mathrm{n_{ult}}}$	Lateral compressive force, general notation	[N]
F_{res}	Resultant force	[N]
$F_{\mathrm{res_{bottom}}}$	Resultant force in lower node	[N]
$F_{\mathrm{res_{top}}}$	Resultant force in upper node	[N]
F_{v}	Vertical component of resultant force	[N]
$F_{\mathrm{v_{bar}}}$	Force in vertical member	[N]

h	Structural cabin height	[m]
I_{f}	Area moment of inertia of sandwich facing	$[\mathrm{m}^4]$
I_{yy}	Second moment of area of the structure about the y-axis	$[\mathrm{m}^4]$
j	Safety factor	[-]
K_{door}	Factor for door cut-outs	$[-]$
K_{LG}	Factor for landing gear cut-outs	$[-]$
L	Length of structural member for buckling	[m]
L_1	Length of cabin front section	[m]
L_2	Length of cabin centre section	[m]
L_3	Length of aft section	[m]
$(L/D)_{\mathrm{av}}$	Average lift over drag ratio	$[-]$
M	Bending moment	[Nm]
M_{Beng}	Bending moment due to engine allocation	[Nm]
M_{Bf}	Bending moment due to fuel	[Nm]
M_{BL}	Bending moment due to lift	[Nm]
m_{bottom}	Lower member mass	[kg]
$m_{\mathrm{R_1}}$	Mass of top shell	[kg]
$m_{\mathrm{R_2}}$	Mass of side shell	[kg]
$m_{\mathrm{R_3}}$	Mass of lower shell	[kg]
m_{top}	Upper member mass	[kg]
m_{walls}	Wall mass	[kg]
N_{x}	Axial acceleration in g	$[-]$
n_{max}	Maximum load factor in maneuvering	$[-]$
n_{min}	Minimum load factor in maneuvering	$[-]$
$n_{\mathrm{ult_{max}}}$	Ultimate positive load factor	$[-]$
$n_{\mathrm{ult_{min}}}$	Ultimate negative load factor	$[-]$
R	Range	[km]
R_1	Inner radius of top shell	[m]
R_2	Inner radius of side shell	[m]
R_3	Inner radius of lower shell	[m]
S_{TE}	Trailing edge planform area	$[\mathrm{m}^2]$
S_{wet}	Wetted area	$[\mathrm{m}^2]$
t_1	Thickness of the upper shell	[m]
t_2	Thickness of the side shell	[m]
t_3	Thickness of the lower shell	[m]
t_{c}	Sandwich core thickness	[m]
t_{f}	Sandwich facing thickness	[m]
t_{wall}	Wall thickness	[m]

W_{airframe}	Airframe weight	[N]
$W_{\mathrm{fus_{TE}}}$	Fuselage trailing edge weight	[N]
W_{paint}	Paint mass	[kg]
W_{TO}	Take-off weight	[N]
z	Distance from centroid to stress location	[m]

Greek Symbols

α_{max}	Maximum angle of attack during cruise	[°]
Δl	Unit length	[m]
Δp	Pressure differential	$[\mathrm{N/m^2}]$
δ_{max}	Maximum trim deflection	[°]
ρ_{c}	Sandwich core density	$[\mathrm{kg/m^3}]$
ρ_{f}	Sandwich facing density	$[\mathrm{kg/m^3}]$
ρ_{mat}	Material density	$[\mathrm{kg/m^3}]$
ρ_{shell}	Shell density	$[\mathrm{kg/m^3}]$
ρ_{wall}	Wall density	$[\mathrm{kg/m^3}]$
$\sigma_{\mathrm{fatigue_t}}$	Tensile fatigue stress	$[\mathrm{N/m^2}]$
σ_{θ_1}	Hoop stress in upper shell	$[\mathrm{N/m^2}]$
σ_{θ_2}	Hoop stress in side shell	$[\mathrm{N/m^2}]$
σ_{θ_3}	Hoop stress in lower shell	$[\mathrm{N/m^2}]$
$\sigma_{\mathrm{x_A}}$	Longitudinal stress due to axial acceleration	$[\mathrm{N/m^2}]$
$\sigma_{\mathrm{x_B}}$	Longitudinal stress due to bending	$[\mathrm{N/m^2}]$
$\sigma_{\mathrm{x_{p1}}}$	Longitudinal pressurization stress in upper shell	$[\mathrm{N/m^2}]$
$\sigma_{\mathrm{x_{p2}}}$	Longitudinal pressurization stress in side shell	$[\mathrm{N/m^2}]$
$\sigma_{\mathrm{x_{p3}}}$	Longitudinal pressurization stress in lower shell	$[\mathrm{N/m^2}]$

Abbreviations

ALV	All Lifting Vehicle
APU	Auxiliary Power Unit
BWB	Blended Wing Body
CG	Centre of Gravity
CS-25	Certification Specifications and Acceptable Means of Compliance for Large Aeroplanes
EASA	European Aviation Safety Agency
FBD	Free Body Diagram

ISA	International Standard Atmosphere
LE	Leading Edge
MAC	Mean Aerodynamic Chord
MDO	Multi-disciplinary Design Optimization
MLW	Maximum Landing Weight
MMG	Multi-Model Generator
MTOW	Maximum Take-off Weight
NASA	National Aeronautics and Space Administration
OEW	Operating Empty Weight
SFC	Specific Fuel Consumption
TE	Trailing Edge

CHAPTER 1

INTRODUCTION

Over the past few decades various attempts have been made to design, build and fly blended wing body aircraft, with varying degrees of success. Many papers explain the conceptual airframe design of such aircraft for passenger and/or cargo transportation, such as the design of the Boeing Blended Wing Body by Liebeck et al.[1] or the Silent Aircraft Initiative[2] by the Cambridge University - MIT Institute. The main driver behind these studies is the achievable aerodynamic efficiency of this type of aircraft, considering that an improved aerodynamic efficiency will decrease the amount of fuel that is required for a certain range. Hence, lowering fuel cost and decreasing the ever more important environmental footprint of the aircraft.

The blended wing body comprises of a smoothly connected lifting surface, without a distinct fuselage section or tail. Whereas in a conventional aircraft the fuselage section is pressurized to serve as a passenger compartment, a blended wing body does not feature a cylindrically shaped hull, the ideal shape for carrying pressurization loads. Current cabins for these aircraft consist of highly reinforced members to create a pressure vessel inside a non cylindrical shape or a separate pressure vessel (e.g. the multi-bubble[3]) inside an aerodynamic skin, both causing compromises in the structural design and efficiency of the blended wing body. Only very limited information is available on the weight of blended wing body aircraft, and most current weight estimation methods are designed for, or statistically based on, conventional aircraft, perhaps except for the method by Howe[4] or the use of the wing weight estimation method of Torenbeek[5]. However, these methods provide little information on the weight of the ‘fuselage’ section of the blended wing body.

1.1 Research Question and Thesis Goal

A rearranged version of the Bréguet range equation, as presented in Equation (1.1), shows that the fuel weight of an aircraft can be directly related to the operative empty weight and payload weight, as well as the aerodynamic efficiency (L/D), range (R), Mach number (M), speed of sound (a) and specific fuel consumption of a jet engine (c_j).

$$W_\mathrm{F} = (W_\mathrm{OE} + W_\mathrm{P}) \frac{1-\epsilon}{\epsilon} \tag{1.1}$$

where,

$$\epsilon = \exp\left(\frac{-R \cdot c_\mathrm{j}}{M \cdot a} \frac{1}{L/D}\right) \tag{1.2}$$

Hence, a lower operative empty weight will result in less required fuel for the same range and aerodynamic performance. Knowing that most of the operative empty weight is the empty weight, containing the airframe of an aircraft, it appears that an efficient structural design of the airframe may result in less required fuel. Therefore a new fuselage concept based on the inside-out approach, where the cabin requirements dictate the shape of the fuselage pressure vessel around the cabin, dubbed the 'oval-fuselage' concept, was created[6]. This concept consists of tangentially connected arcs forming an oval pressure vessel, supported by horizontal and vertical members. The pressure vessel serves as an aerodynamic outer surface at the same time. From Equation (1.1) it can be concluded that it is desirable to know the operative empty weight of such a concept, in order to compare it to the multi-bubble design. This leads to the research question of this thesis: **"How does the performance of the 'oval-fuselage' blended wing body compare to a multi-bubble concept, for the same configuration and a given set of top-level requirements?"** To assess the performance of the blended wing body, it is important to estimate the operative empty weight, as this greatly determines the fuel weight that is necessary to perform the mission, as can be observed from Equation (1.1). However, no method exists for estimating the operative empty weight. Therefore, a sub-question can be phrased in addition to the research question: **"How can the operative empty weight of the 'oval-fuselage' concept be estimated?"**

The goal of the thesis is the development of a method and tool for the conceptual design and weight estimation of the 'oval-fuselage' blended wing body. By means of this tool, the concept can be compared to the separated pressure vessel concept modeled in an earlier thesis[7], or to conventional long range airliners. The outputs of both tools are Class-II conceptual designs of blended wing body aircraft.

1.2 Thesis Approach

The analysis in this thesis is restricted to the conceptual design phase of aircraft design. This limits the level of detail and introduces several assumptions and simplifications to the model. The phase is very suitable for the application of multi-disciplinary design optimization (MDO). As the subject of this thesis involves a new design concept, there is little information on the road to be taken to achieve the final goal of creating a full blended wing body, estimating its operating empty weight and comparing it to an existing concept. Before creating and evaluating a new fuselage design concept, it is necessary to understand the fuselage design of blended wing body aircraft.

Therefore, the first step in designing a new fuselage concept is to examine the already existing methodologies for the design of aircraft fuselages in general and specifically the blended wing body, for inspiration and background information. The fuselage design of conventional aircraft centres on the 'inside-out' approach, as the outer dimensions are determined by the inner cabin requirements and the tube-like shell is structurally ideal to carry pressurization.

Adopting a similar approach to blended wing body fuselage designs requires the development of a pressure vessel composed of circular segments that are constructed around a certain required cabin. Once a two-dimensional geometrical representation of such a structure is parameterized, a three-dimensional model can be built. This model consists of several two-dimensional fuselage cross-sections being put in sequence to create an aircraft, where variations in the cabin width between cross-sections cause shape variations in the 3D model, e.g. taper of the front section of the fuselage. Controlling the fuselage height of each cross-section allows for the creation of an airfoil-shaped body, whilst maintaining a level cabin floor and ceiling. As this is the first attempt to design a 'oval-fuselage' blended wing body, a symmetric airfoil profile is chosen, to reduce the complexity of what is a completely new design methodology.

Once a geometrical model of the new fuselage is created, it must be combined with the other components of the blended wing body, such as outer wings, vertical tail and engines. The full aircraft can then be assessed through MDO, by means of a tool previously created[7]. Yet, the new fuselage design requires a separate weight estimation methodology for the optimizer to evaluate the aircraft's performance, as there is no existing method to cope with this specific design. Therefore, a method for estimating the operative empty weight of the 'oval-fuselage' concept must be created. This method determines the weight of the fuselage cross-sections under pressurization loads, and the bending moment introduced by the wing lift force. Also longitudinal stresses must be checked against the tensile and compressive fatigue stress limits of the fuselage material. Shear and torsion in the fuselage are not checked at this conceptual design stage, as the final goal is the development of a method and tool for the conceptual design and weight estimation of the 'oval-fuselage' blended wing body, and not the structural design of the cabin.

When the new fuselage geometry and weight estimation are incorporated in the MDO tool, the concept's performance can be evaluated and compared against a multi-bubble blended wing body and conventional aircraft.

1.3 Design Requirements and Fixed Input Variables

The designs to be optimized by the MATLAB tool are to be created within the bounds given by several top-level requirements. An extensive list of input variables (note, not design variables) is also included in the program. These input variables range from engine and aircraft reference data and material properties to assumptions in the fuel consumption during specific phases, such as taxiing. These inputs are provided in Appendix B. Most of the requirements and inputs are taken from the tool developed for the analysis of the multi-bubble blended wing body and altered or extended where it was deemed necessary. In these cases both blended wing body designs, multi-bubble and 'oval-fuselage', were subjected to the same constraints, requirements and input variables. The top-level requirements imposed on the blended wing bodies are listed below.

- Payload, passengers in two classes with luggage and additional cargo. The numbers were changed to evaluate three different concepts.
  - 175 passengers in economy class, 25 in first class with 10,000kg additional cargo
  - 350 passengers in economy class, 50 in first class with 20,000kg additional cargo
  - 700 passengers in economy class, 100 in first class with 40,000kg additional cargo
- Cruise Mach number of 0.82
- Cruise altitude of 11,000m
- Design range of 11,000km at maximum payload. The objective of the aircraft's optimization process was to maximize this range.
- Maximum take-off distance of 2,500m at maximum take-off weight, at sea level conditions.
- Maximum landing distance of 2,500m at maximum landing weight at sea level conditions.
- Stall speed in clean configuration below 80m/s
- Maximum dimensions within the 80m span by 80m length box[8]
- Maximum thickness to chord ratio should not exceed 20 percent
- Compliance with CS-25 regulations

Here, sea level conditions are considered in the international standard atmosphere (ISA) at 15° Celsius. Cruise altitude is at 11,000 meters ISA. CS-25[9] regulations are the Certification Specifications and Acceptable Means of Compliance for Large Aeroplanes, Amendment 11 of the European Aviation Safety Agency (EASA). The box of 80 by 80 meters is considered in order for the designed aircraft to be operational at existing airports[8]. The maximum thickness to chord ratio is set relatively high at 20 percent due to the fact that a significant thickness can be required to provide a sufficiently high cargo hold, able to store currently available cargo containers. An example of a concept with a lower thickness, will be shown in Chapter 5.

For the concept to be examined, a blended wing body with wing mounted engines was chosen, with aft swept wings and winglets as vertical tails, which provide an induced drag advantage. This configuration is commonly found in literature, except for the mounting of the engines. The positioning under the wings was chosen for accessibility and convenience. With body mounted engines, the aft section of the fuselage could for example not, or rather difficultly, be used as a control surface. Moreover the engines are supplied with cleaner airflow and provide bending relief to the wings. The different blended wing body configurations that have previously been evaluated for the multi-bubble fuselage[7] are shown in Figure 1.1.

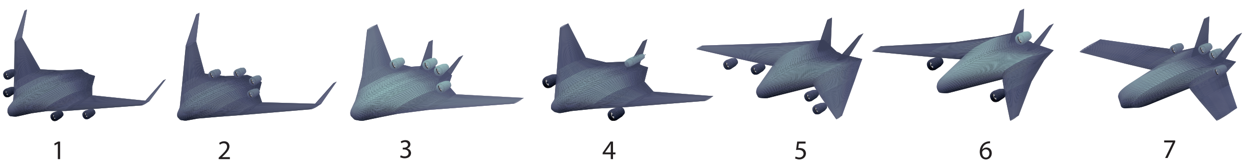

Figure 1.1: Seven different blended wing body configurations[7]

The configuration that has been chosen to examine the oval-fuselage concepts is Nr. 1 in this figure. The forward swept configurations 5, 6 and 7 were discarded because of a lack of information. Also, winglets were chosen over body mounted fins as a vertical stabilizer because of their induced drag advantage. And finally wing mounted engines were considered to be more practical when the aft of the centre body is potentially used as a control surface.

1.4 Report Structure

The report is divided into four main chapters, followed by a fifth and final chapter containing the conclusions and recommendations. Chapter 2 contains the necessary background information on blended wing body cabins. This chapter presents an overview of the findings of a literature research preceding the actual thesis. A brief introduction to the concept of all lifting vehicles is given, followed by a discussion of non-structural requirements on aircraft cabins and a discussion of the different fuselage concepts for blended wing bodies. Here, the 'oval-fuselage' concept is introduced.

Chapter 3 introduces the structure of the MATLAB optimization program that was used to evaluate and optimize the concepts. The original program for the multi-bubble is briefly explained and then the most important changes that were made to accommodate the new fuselage concept are highlighted and discussed. The chapter also introduces the multi-model generator of the program that generates the geometric model of every concept that is evaluated. Here, the geometric definition of the cabin is explained, as well as how the pressure shell is constructed around the cabin and finally how a three dimensional model of the aircraft is generated. The different steps are mentioned, the theory behind the sizing, however, is not yet presented here.

In Chapter 4 the theory behind the weight estimation of the blended wing body fuselage is explained. This structural design is the driver of the geometric design. First, an overview of the Class-II weight estimation from Torenbeek[10] for the operative empty weight is presented, followed by an explanation of the weight estimation of the outer wings, as can be found in Appendix A and the thesis by Van Dommelen[7], respectively. Then the fuselage sizing for pressurization is discussed, followed by a section on the longitudinal stresses in the fuselage. The chapter is concluded by a section on the changes made to the centre of gravity calculation of the aircraft.

The analysis of the concepts is presented in Chapter 5. Three different sizes of blended wing bodies for the 'oval fuselage' are compared to the multi-bubble in terms of performance. In the final section of this chapter a critical reflection on the blended wing body is added, after the 'oval fuselage' concept is compared to conventional airliners.

Chapter 6 presents the conclusions and recommendations that follow from this thesis on the performance and weight estimation of the 'oval fuselage' blended wing body aircraft.

CHAPTER 2

BACKGROUND INFORMATION

This chapter provides the findings of a literature study on the requirements for Blended Wing Body (BWB) cabins and the different fuselage concepts for BWB aircraft. It provides the necessary background information for the design of a new BWB cabin and the subsequent performance evaluation. The first section contains a very brief overview of the family of all lifting vehicles, which the BWB belongs to. A second section presents the findings of the study on requirements for cabin design. The chapter is concluded by a section on the different structural concepts for the design of blended wing body cabins. It is here that the 'Oval Fuselage', or 'conventional approach' to the structural design of a BWB cabin is introduced.

2.1 The All Lifting Vehicle

This section gives a brief introduction into the concept of all lifting vehicles of which the blended wing body is one amongst several other types. Only the different concepts are briefly highlighted and illustrated here. For more detailed information on the history of blended wing bodies, a website, such as "The history of the flying wing"[11] presents a good overview.

The Blended Wing Body is an aircraft design, where the entire aircraft generates the lift required to fly. It is part of the family of All Lifting Vehicles (ALV's). Wood et al.[12] offer the following definition for the ALV: "A vehicle that has all horizontal orientated elements (i.e., wing, fuselage, tail, etc.) continuous and aerodynamically shaped to contribute proportionally equivalent amounts of lift throughout the flight envelope." This includes flying wing, tailless and all wing aircraft, as well as lifting body vehicles. However, aircraft with non-lifting fuselages are not considered ALV's.

ALV's can be split into three categories. First of all there is the flying wing, either tailless or an all wing aircraft according to Northrop's Definition[13]. A good example of this is the B-2 Spirit, as seen in Figure 2.1. The second category is the flying fuselage, which can be divided in the lifting

Figure 2.1: The Northrop Grumman B-2 Spirit[14]

fuselage and lifting body. The lifting fuselage has separate wings and an airfoil-shaped fuselage, that contributes to the total lift generation. The lifting body is a type of aircraft that generates all, or the majority of it's lift through its body. Leaving the impression that the aircraft does not have any wings. Several experimental lifting bodies were build in the United States in the 1960's as can be seen in Figure 2.2.

Figure 2.2: Various United States experimental lifting bodies[15]

The third category is formed by a hybrid solution, the Blended Wing Body. The aircraft has clearly distinctable wings and fuselage and may or may not have a vertical tail plane, and/or winglets. The body itself generates a large part of the lift and blends smoothly with the wings, hence the name 'Blended Wing Body'. An example of this type of aircraft is shown in Figure 2.3.

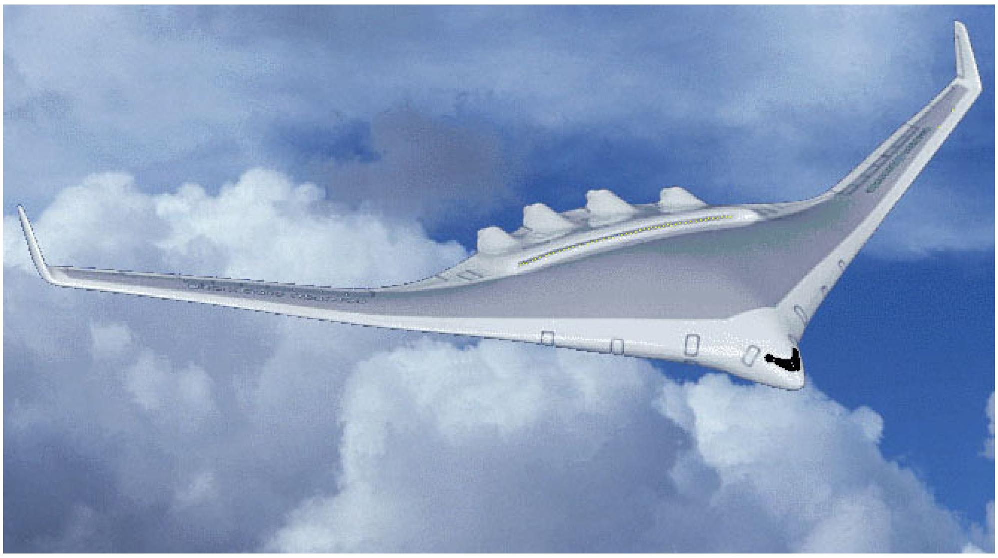

Figure 2.3: A Blended Wing Body concept[16]

2.2 Requirements on Cabin and Fuselage Design

Next to the structural and aerodynamic requirements on the fuselage cabin of a BWB aircraft, there is a considerable amount of requirements from airworthiness regulations, airline operations and passenger well-being. Not all of these are clearly defined and they can be unpredictable, coming from psychological, social, economic, technological or even political environments. In this section, some of these requirements will be discussed, focusing on the operation of BWB aircraft.

2.2.1 Safety

One of the key elements of safety regulations is the amount and location of emergency exits on an airplane, to ensure that all passengers and crew members can rapidly exit and reach the ground. To quote CS-25.803(c)[9]:

> *For airplanes having a seating capacity of more than 44 passengers, it must be shown that the maximum seating capacity, including the number of crew members required by the operating rules for which certification is requested, can be evacuated from the airplane to the ground under simulated emergency conditions within 90 seconds. Compliance with this requirement must be shown by actual demonstration using the test*

> *criteria outlined in Appendix* J *of this* CS-25 *unless the Agency find that a combination of analysis and testing will provide data equivalent to that which would be obtained by actual demonstration.*

Galea et al.[17] have performed computer simulations on the evacuation of several BWB configurations, based on a standard configuration with 1020 passengers in a single class configuration, with 25 crew and 20 floor level type-A exits. Over 10 simulations, with the exits on one side of the aircraft being unavailable, the out of aircraft time varied between 80.6 seconds and 92.8 seconds and an average of 85.6 seconds. Although the average is below the time required by regulations, some 3 seconds have to be added to find the 'on-ground' time. This would mean that even more of the simulations would not meet safety requirements[9]. Striking detail of the study was that the exits located in the aft most corner of the cabin were used much less compared to the others, leaving room for improvements. To validate the results of the simulations, real life experiments using a section of the aircraft were conducted, actually confirming the behaviour in the computers simulation. Fire simulations from the same study showed that the BWB would provide equivalent or even better levels of safety than conventional airliners. Galea et al.[17] found that flashover, the almost simultaneous ignition of all combustible material, is possibly not the primary factor in passenger survivability for BWB, in contrast to wide- or narrow-body aircraft. Whilst Eelman et al.[18] advocate the use of wide aisles and a 'type-0' exit, with a capacity of 200 passengers per minute and twice the size of a 'type-A' exit, Galea et al. suggest improving the familiarisation of the passengers with the cabin layout and the use of improved visual aids to achieve the required on-ground time. Eelman et al.[18] also suggest a rather unconventional and perhaps far fetched approach for quick opening of the emergency exits. Namely, to blast away wing emergency exits and open big tail doors if possible[18], in contradiction with current certification rules. Although this radical approach may be very efficient in getting the passengers quickly out of the aircraft, it is most likely a structurally very challenging design, considering the explosive and the large tail doors. Moreover, aviation authorities will most likely have issues with the presence of explosives, to blast away the emergency exits.

2.2.2 Passenger Well-Being

When considering passenger well-being, several aspects have to be addressed. There is the passenger acceptance of the configuration and cabin lay-out and there are psychological aspects and on top of those, there is passenger health. Passengers can have high demands for the level of comfort and service in the aircraft, depending on their cultural background and wealth. Yet also religion and culture can be key aspects[18], requiring specific on board features. Next to this there are the more obvious cabin requirements, such as requirements for class ratios, seat pitch and dimensions, toilets, galleys and crew members per passenger and luggage compartments. These vary with passenger background and wealth, as well as with time and the type of airline. As Eelman et al.[18] point out; the growth of the dimensions of human beings, means that seating dimensions have to be modified over the service life of an aircraft. E.g. when the body height increases with 1.5 centimeters over 30 years, it justifies a seat pitch increase of about 2.5 centimeters over an operational life of 30 years. For a BWB, this could result in a single row, taken over the entire aircraft. Thus directly influencing capacity and operational profit for an airline. Then there are the technological demands, as society is ever more interleaved by information technology. These could be: broadband Internet connections, wireless support of mobile equipment and information systems (e.g. flight information, news, cameras with night-vision outside of the aircraft, etc.).

Wittmann[19] used a questionnaire to gain insight into the psychological and physiological aspects with the acceptance of blended wing bodies by passengers. Roughly two-third of the respondents favoured the establishment of service and entertainment areas, due to the increase in cabin area. For example bars, lounges or fitness areas, which could according to Eelman et al.[18] be located on the lower deck. Next to that on-board entertainment, Internet and virtual-reality systems were high on the list of desired features. For the aforementioned lack of windows on board of the BWB, video systems were considered an acceptable alternative by most respondents, integrated in the entertainment system in the headrest of the seat in front. Night-vision capabilities of this system would be highly appreciated, according to the study. The Wittmann study[19] also pointed out that flexibility of the cabin lay-out, allowing changes before every flight is very popular with the participants of the questionnaire.

A paper by Hinninghofen and Enck[20] of the University Hospitals Tübingen, Germany, presents the interactions between cabin environment conditions and passenger health. One of the responses to the lowered cabin pressure, which results in a lower oxygen saturation is hyperventilation to compensate, the other is the expansion of gases according to Boyle's law. This has an influence on the air-filled cavities of the body, such as the ear and gut, as well as the skull and tooth fillings. Expansion of the air in these cavities can lead to several forms of discomfort, including nausea, vomiting and dyspeptic symptoms (when the gut is concerned). Also the motion and vibrations inside the aircraft can lead to discomfort and motion sickness, especially when considering that in blended wing bodies "...passengers at the most outward position of the aircraft – large distance from the airplane's longitudinal axis – are exposed to significantly increased vertical accelerations during roll manoeuvres"[19]. And according to Hinninghofen and Eck[20], this can be especially discomforting in combination with the low humidity, especially on long-haul flights. Wittmann argues that "...a reduction of roll rates during flight manoeuvres to less than $0.5\,°/s$ can already promise great success particularly in cruise"[19] and Liebeck[21] states that the angle of attack during cruise should be smaller or equal $3\,°$ Also the video systems can help in comforting passengers and reducing motion sickness, according to Wittmann. With respect to the seat dimensions mentioned earlier, there is also the problem of deep-vein thrombosis when persons are cramped in the same position over a longer time, making seat comfort and enough room for short walks or exercises very important. Hinninghofen and Eck also consider the quality of the upholstery, leg room and possible angle of recline of the seat as important parameters for seat comfort. Cabin air quality (fresh air supply), humidity, CO_2 concentrations and noise are also of great importance to the comfort level experienced by passengers. Other interesting results from Wittmann's study [19] indicate that 34% of the respondents suffer from fear of flying, which matches statistics, and that agoraphobia is more prevalent than claustrophobia (8.7% to 4.5%). As a solution to the different phobias, Wittmann suggests to divide the large cabin of the BWB, which would be favourable from a structural point of view when considering the multi-bubble or integrated skin and shell designs. However, these designs limit the amount of daylight reaching the centre of the cabin, which may be experienced as unpleasant by the passengers. The large cabin also allows for a large degree of freedom in placing toilets and operational items such as galleys.

2.2.3 Airline Requirements

Next to requirements by aviation authorities and passenger acceptance issues, there are also influences on the acceptance of blended wing body cabin designs by the airlines having to operate and buy them. Airlines strive for the highest possible profit, directly implying low operating cost, hence fuel efficient aircraft. Also high flexibility of the cabin lay-out is required, with the possibility to quickly change the configuration. This, combined with the ever increasing environmental awareness, has a considerable impact on the cabin design in terms of demand for lightweight and environmentally friendly materials.

Cargo volume and access are aspects that could actually present themselves as 'show-stoppers' for BWB aircraft. Whilst the plane may be aerodynamically efficient and even a structurally sound design can be made, a badly accessible cargo hold or reduced cargo volume in comparison to conventional designs may prevent airlines from buying the aircraft. A reduced volume could decrease the profit per flight and a difficult to access cargo hold will increase the non-operational time, thereby reducing the flight hours. Also the unit load devices have to be considered, since they are designed for conventional aircraft and might not fit easily or efficiently into blended wing bodies, shown in Figure 2.4. As can be seen from this figure, the volume of the aircraft may not be used that efficiently after all. This might require a redesign of these devices, with additional cost to airlines.

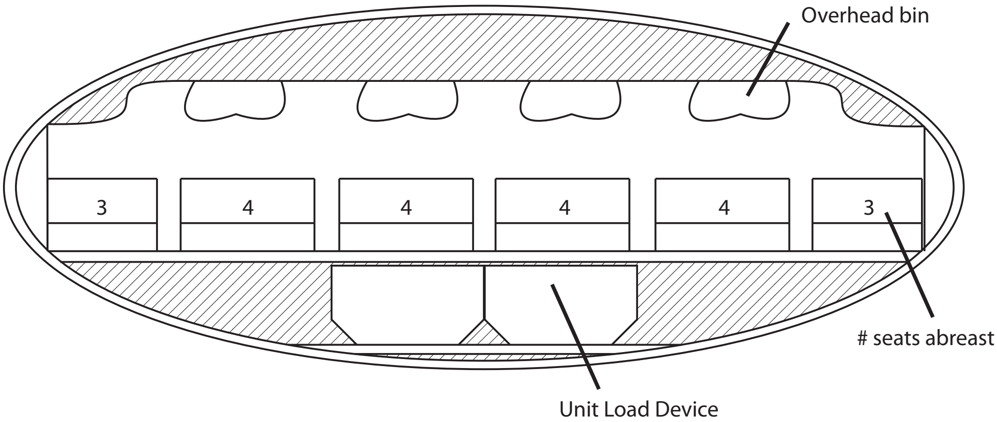

Figure 2.4: Example cabin cross section showing unit load devices in the cargo hold

2.3 Fuselage Concepts

This section discusses the three different types of structural concepts that can be used to construct a BWB fuselage. Sub-section 2.3.1 and Sub-section 2.3.2 elaborate on two common methods, often discussed in literature. Sub-section 2.3.3 discusses a new approach for BWB aircraft, it applies the conventional 'inside-out approach' used to design traditional wide-body aircraft.

2.3.1 The Integrated Skin and Shell Concept

This concept integrates the structural, aerodynamic and pressurization functions in one single structural solution. The concept consists of a thick sandwich upper and lower structure, carrying both the wing bending loads and the pressurization loads and providing an aerodynamic shape at the same time. An example of this concept, taken from Liebeck[21], can be seen in Figure 2.5.

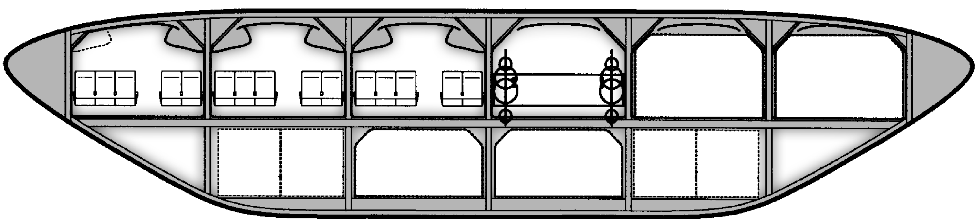

Figure 2.5: The integrated skin and shell concept[21]

From Figure 2.5 it can be observed that the cabin of this configuration is typically split into several longitudinal compartments, either by beams, walls or pillars. Although this may have structural advantages, and may even be required for the load carrying capabilities of the structure, it can provide difficulties in the passenger acceptance of the BWB, limiting the amount of daylight entering the cabin. Also cabin flexibility may be limited because of these walls and there is a loss of usable cabin volume. Please, refer to Section 2.2 for a more elaborate discussion on the cabin design and passenger acceptance.

As Mukhopadhyay[22] points out, the nearly flat shells in this particular concept are not very well suited for coping with a pressure difference. Internal pressure can much better be handled by cylindrical shapes. Another issue, as noted by Mukhopadhyay[22] is the number of highly stressed T-junctions in the cross-section. This would result into over-dimensioning in order to cope with fatigue loading[23]. The advantages of this concept are the relative simplicity of the construction, the reduced volume of the honeycomb filler material in the sandwich panel compared to the segregated shell concept[22] (Sub-section 2.3.2) and the lack of an additional outer aerodynamic shell[21], combined with an efficient aerodynamic design. Emergency egress from the passenger compartment can be achieved in a similar fashion as for conventional airliners, where only the outer structure needs to have cut-outs. However, the segregation into compartments by the vertical walls could hamper passengers in their attempt to find and reach an unobstructed exit in an emergency situation.

2.3.2 The Segregated Pressure Shell Concept

The segregated pressure shell concept, or multi-bubble concept, uses a separate pressure shell and aerodynamic shell. The outer wing skin is connected through a thick sandwich structure, with a high volume of honeycomb core material, to the inner pressure cell. The impression in Figure 2.6 illustrates this concept.

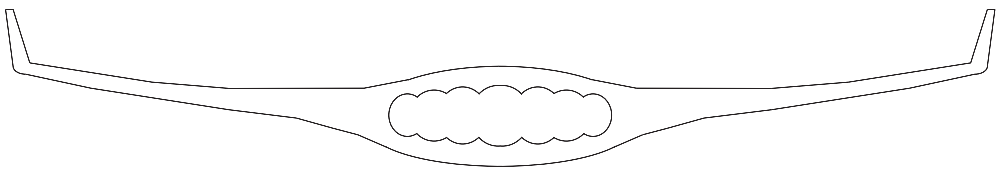

Figure 2.6: Impression of the Segregated Pressure Shell Concept

This sandwich is used to "…transmit the external aerodynamic load from the outer skin, and to prevent local buckling."[22] Fabrication of this type of fuselage is also difficult. Another way would be to connect the outer aerodynamic skin through several beams to the inner multi-bubble pressure cell, as illustrated in Figure 2.7. However, this may result in volume that is lost for payload transportation. The aerodynamic skin has no distortions and is therefore expected to be very efficient in normal flight conditions. This way the skin is connected via the load-carrying longitudinal beams to the columns in the multi-bubble, removing the need for walls or thick beams in the cabin. A problem for both multi-bubble designs, according to Liebeck[21] is the need for the outer skin to be designed to withstand the internal pressure in case the inner pressure shell has a rupture, imposing an additional weight-penalty. Geuskens et al.[25] show that: "…the shape of the cross-section (amount of bubbles, diameter of bubbles) does not influence the structural efficiency"

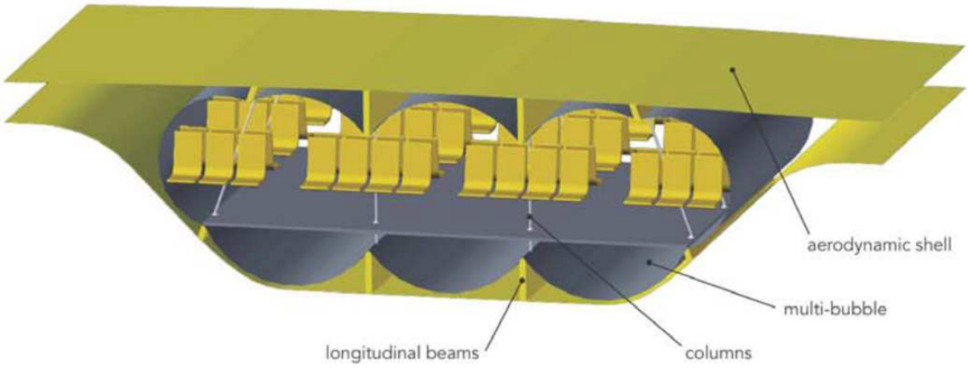

Figure 2.7: The Segregated Pressure Shell Concept[24]

and that "...the 'effective area' of the multi-bubble improves by the number of bubbles", meaning that the multi-bubble could be very well suited as a pressure vessel. Keeping in mind that in real-life reinforcements at intersections are needed and stresses will not be constant, increasing weight and decreasing structural efficiency. In another paper by Geuskens et al.[3] it is shown that "the multibubble is an articulated pressurizable structure that enables pressurization of a volume with substantial spatial freedom." In other words, a multi-bubble fuselage with a large number of bubbles can be constructed without harming the structural efficiency of the cross-section, that can also be used as a pressurized cabin whilst still allowing a degree of spatial freedom (e.g. a dihedral in the cabin section or multi-story multi-bubbles). Constructing this type of fuselage would also yield an improved 'effective-area', where the 'effective area' is in this case defined as the ratio of the largest inscribed rectangle and the frontal area, as illustrated by Figure 2.8. Like

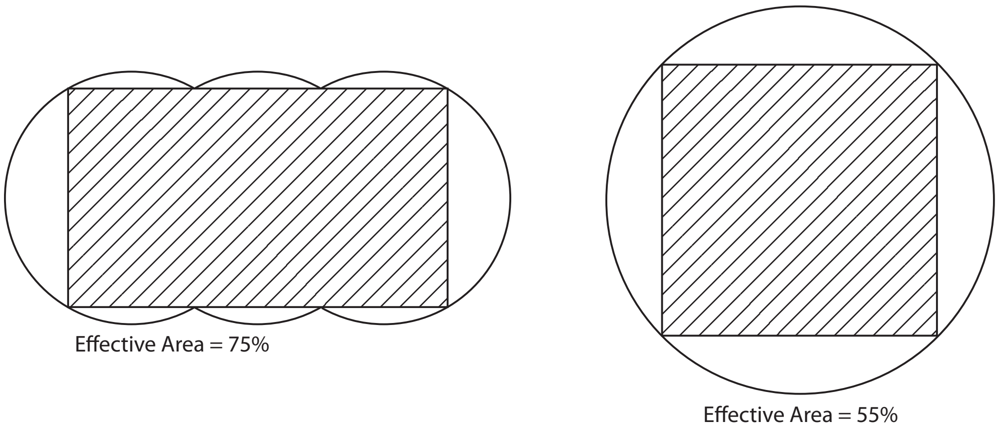

Figure 2.8: The effective area of a multi-bubble and a cylinder with the same frontal area[25]

the integrated skin and shell concept, the multi-bubble has either wall, beams or pillars separating the large cabin in smaller compartments or sections. These can be obstructing the daylight and can therefore be disadvantageous for passenger acceptance, though they can be helpful in reducing phobias (see Sub-section 2.2.2). These walls also limit the cabin flexibility freedom, hence making the concept less acceptable for airlines. Emergency egress has the same issues as the integrated skin and shell concept. The difficulty of adding emergency exits however, is increased by the need to have cut-outs in both the aerodynamic shell and the multi-bubble.

2.3.3 The 'Oval-Fuselage' Concept

The 'oval-fuselage' uses the 'inside-out' methodology that is commonly used in the design of the fuselage of conventional airplanes. The approach is new to the design of BWB aircraft and may yield interesting results, although the research is still in an early phase.

'Inside-out' in this case means that the outer aerodynamic surface is dictated by the required cabin area. The cabin is sized by requirements for the number of passengers, number of seats per row, seat dimensions, payload and cargo capacity and passenger well-being. This approach is commonly used for conventional airliners, to obtain a structurally efficient cabin that is also capable of coping with the pressurization load, yet has aerodynamic compromises. In typical BWB design however, the dimensions of the cabin are dictated by an aerodynamically optimized shape in which compromises are made concerning the efficiency of the structure. It is assumed that the aerodynamic outer shape provides the best solution to fulfill a particular mission with maximum aerodynamic efficiency. However, for jet aircraft, the Bréguet range equation can be used to show that the required fuel weight for the cruise is also dependent on the operating empty weight (OEW), see Equation (1.1). Therefore it could be argued that actually the structural weight, and thus the structural design, should drive the fuselage design of a BWB[23]. The 'inside-out' design, or 'oval fuselage' concept instead tries to create a structurally optimized BWB shape, determined by cabin requirements.

The 'Oval Fuselage' does not have a complex double shell construction. Instead, it carries pressurization via in-plane loading. Four tangentially intersecting arcs, two identical ones at either side of the cabin and a top and bottom arc, make up the outer aerodynamic surface, as illustrated in Figure 2.9.

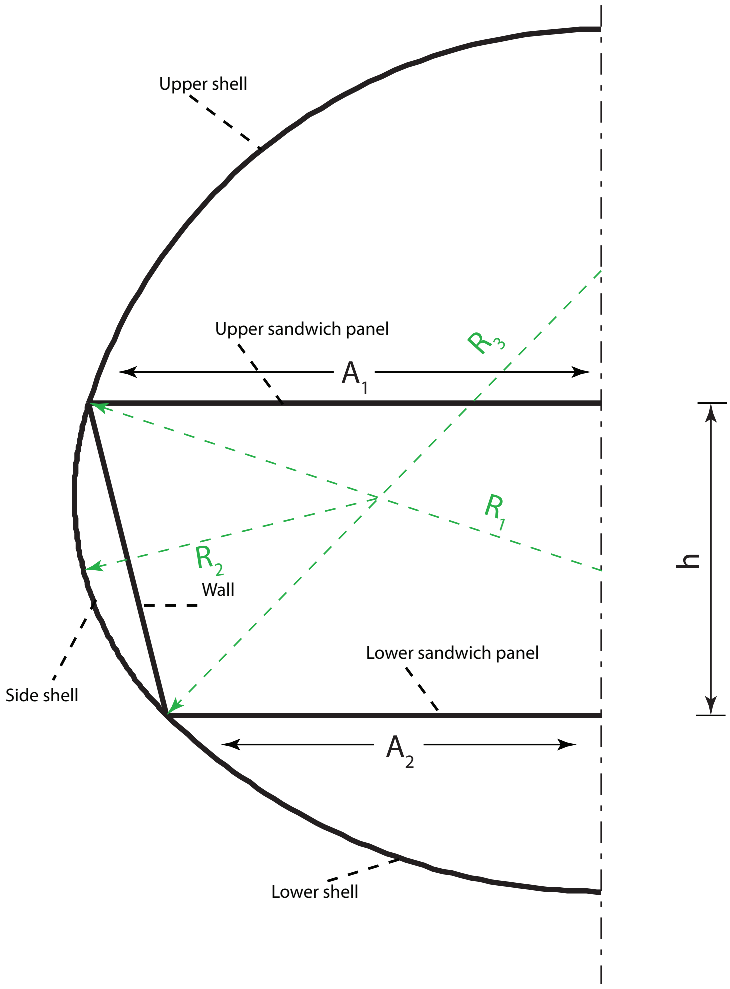

Figure 2.9: Sketch of the 'Oval fuselage' semi cross-section

The semi cross-section shown in Figure 2.9 shows a great resemblance to a conventional wide-body airliner. However, by changing the radius of curvature of the top and bottom arc, a much flatter cross-section can be created. Because the cross-section is non-cylindrical, pressurization will result in in-plane stresses that differ with radius of curvature. Therefore the horizontal and slanted vertical members are added to maintain structural integrity. (In the case where the upper and lower arc have the same radius of curvature, the walls are perfectly vertical.)

The horizontal members are loaded in compression, whereas the vertical members are loaded in tension, provided that the side arc has the smallest radius of curvature. The horizontal members also act as the carry-through structure for the wing-box. An elaboration on the pressure shell construction and force balance, structural concept and weight estimation of the 'oval fuselage' is provided in Sub-section 3.2.2 and Sub-section 4.3.1, respectively. Now, from Figure 2.9 it can be observed that, once the cabin floor width is increased, e.g. due to more seats per row, R_1 and R_3 and subsequently R_2 must be increased to accommodate the wider cabin floor while maintaining cabin height and passenger level of comfort. This influences the aerodynamic cross section of the aircraft, yet the overall shape remains similar. These horizontal members are modeled as sandwich structures and have to resist the resultant horizontal force from the shells due to pressurization and the compressive lateral force introduced by the wing bending moment, as visualized in Section 4.3. Underneath the lower horizontal member, a cargo hold is located, which is sized to accommodate typical LD-3 unit load devices. The volume above the passenger cabin is also used as a second cargo hold, for bulk cargo.

This design could also have major benefits in passenger acceptance as it provides an unobstructed cabin, hence no pillars, beams or walls dividing the cabin. It also provides a very spacious cabin, allowing natural light to reach the centre of the body, from the scarce windows allowed by the BWB configuration. The unobstructed cabin provides the possibility to find a compromise between the issues of agoraphobia and claustrophobia mentioned in Sub-section 2.2.2. Also chairs, galleys, toilets and other operational equipment can be positioned more freely, providing airlines with the necessary flexibility. The possibility to transport standard LD-3 unit load devices could also favour this concept with respect to airline acceptance. Emergency egress is similar to that of conventional aircraft, however, the design may have a larger amount of wasted pressurized space than the other concepts as the volume is used less efficiently. Since the design is a compromise between structural and aerodynamic efficiency, some weight penalties may be imposed because of instabilities in the compressed horizontal members or when the radius of curvature becomes too large[23]. From an aerodynamic point of view, several fairings could be required to insure a smooth transition between the outer wing and the centre-body to form a true “blended” wing body. A too large radius of curvature, i.e. wide cabin, is also not favourable from the perspective of passenger well being, as passengers seated at the outer most positions from the centre-line are heavily influenced by rolling motions, however, this is true for all blended wing bodies, as mentioned in Sub-section 2.2.2.

CHAPTER 3

PROGRAM STRUCTURE AND GEOMETRY DEFINITION

To evaluate the performance of the 'oval-fuselage' BWB, an adapted version of the 'Blended Wing Body Initiator' created as part of the thesis of J.L. Van Dommelen[7] is used. This program was originally designed for a 'multi-bubble' BWB, with a carbon fibre pressure shell. A second version of the original program was created containing the equations for the Class-II OEW estimation by Torenbeek[10], whereas the original program contained the method of Raymer[26]. The second version includes all operational items, of which several were not incorporated into the original version and a corrected landing gear weight estimation. Both programs still use the Torenbeek Class II.5[5] method for the estimation of the wing weight, which is why the Raymer method was substituted, for uniformity. A small mistake concerning the calculation of the cantilever ratio was corrected.

The optimization program for the 'oval fuselage' also contains the Torenbeek Class II OEW estimation and the Class II.5 wing weight estimation for the outer wing. However, it needs to incorporate a new airframe mass prediction method and the geometry definition for the 'oval-fuselage'. Therefore, some changes had to be made to the second version of the optimization tool. Section 3.1 presents an overview of the program structure and the most important changes with respect to the structure of the 'Blended Wing Body Initiator' and is followed by Section 3.2 on the geometry generation of the 'oval fuselage' BWB. The weight and balance methodology of the new BWB concept is discussed in detail in Chapter 4.

3.1 Program Structure

In order to analyze the 'oval-fuselage' concept, several changes had to be made to the MATLAB optimization program for the 'multi-bubble' BWB. Although most of the files that constitute the program had to be altered, only the input to Multi-Model Generator (MMG) and the weight estimation module were fundamentally changed. Their structures were adapted to accommodate the 'oval-fuselage' and its analysis modules. The alterations to the other files are restricted to re-assigned variables and some minor corrections, whereas the methodology remained the same.

The structures of the 'multi-bubble' and 'oval-fuselage' BWB's are visualized in Figure 3.1 and Figure 3.2, for easy comparison.

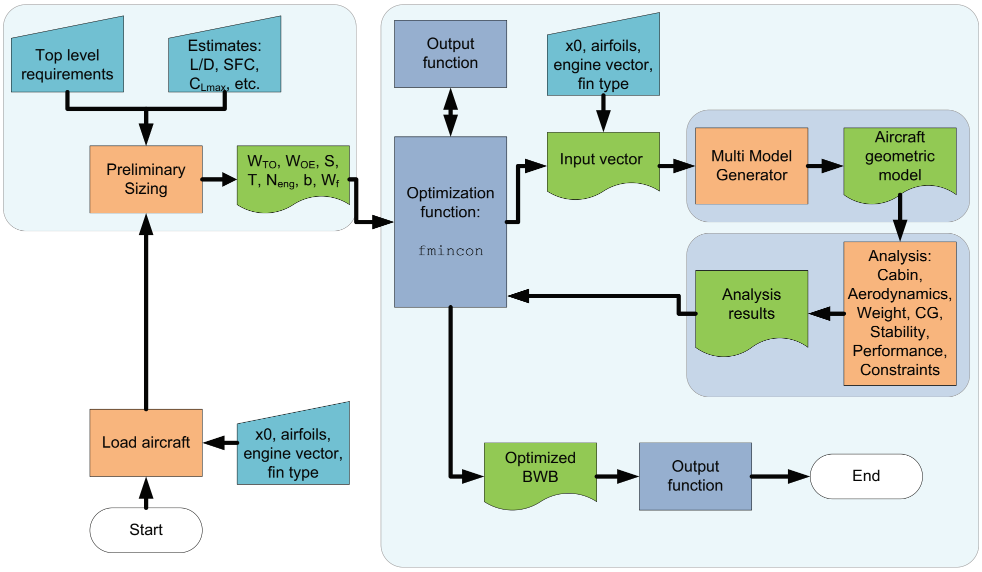

Figure 3.1: Main program structure of the original BWB initiator[7]

Figure 3.1 shows the optimization structure of the BWB initiator by Van Dommelen[7]. Here an input vector is created containing: chord, span, twist, sweep, dihedral, thickness to chord ratio of six sections along the aircraft semispan, the height and type of vertical tail, the number and position of the engines and the airfoils used. This input vector is then loaded and, together with the top-level requirements and estimates on aerodynamic performance, handed to the initial sizing routine. This routine constructs some preliminary geometry, performance and weight estimates based on statistical data. Reference data consists of conventional airliners and BWB aircraft from different design studies. The MMG then generates the full aircraft geometry, including wingbox, fuel tanks, engines, empennage and 'multi-bubble' cabin. The analyzer performs calculations on the cabin, aerodynamics (using Tornado[27]), weight and balance, stability and performance and checks the constraint violations. The output is returned to the optimization function, which either alters the input vector for another iteration or ends the optimization procedure. As can be seen in Figure 3.1, the optimization routine consists of only one loop, with a fixed direction and no feed-back loops. Any results from the analysis are not used to re-evaluate the model or previous analyses of the current iterate.

It must also be noted that the optimization algorithm that is being used, the `fmincon` 'Active Set Algorithm', can find the minimum of constrained, multi-variable and non-linear problems using the Karush-Kuhn-Tucker equations, however, it is highly dependent on the start position, or initial guess for the input vector, as it is a gradient-based approach. Therefore it cannot guarantee a global minimum, as it locally searches in the direction of the steepest descent. Thus a start point that already meets most of the constraints is best used for the optimization, to prevent the routine from running into infeasible local minima or requiring excessive computation time.

Whilst the optimization algorithm is maintained for the 'oval-fuselage' optimization, there are several notable changes in the program structure, as shown in Figure 3.2. Here, the original program is masked and the most important changes to the program are highlighted. The steps mentioned in the description below this figure will be explained in Section 3.2.

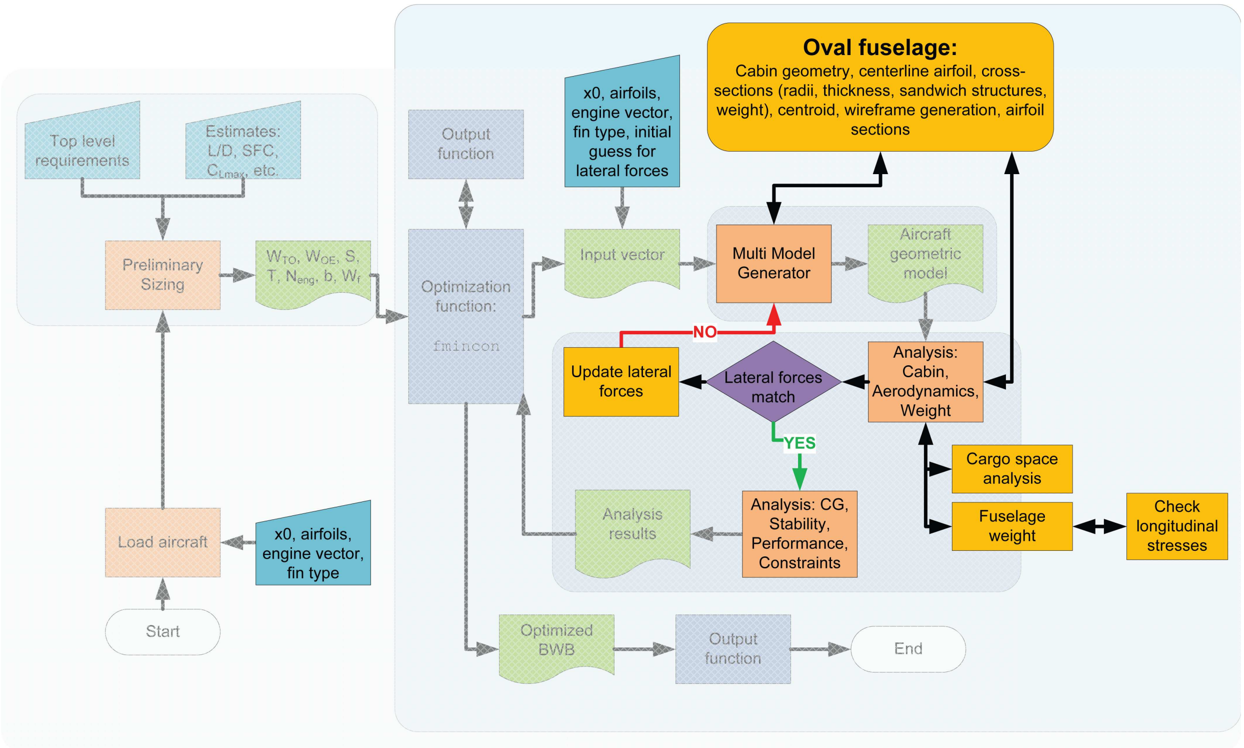

Figure 3.2: Main program structure of the 'oval fuselage' BWB initiator

Already at the very beginning of the program, an important difference to the original version must be noted. The input vector is adapted to suit the 'oval-fuselage' concept. Instead of 30 design variables, the problem is reduced to 19 design variables. Where previously the design variables described six spanwise airfoil sections, the new variables only describe two outer wing sections and the 'oval-fuselage' cabin. (The construction of the cabin from the design variables is explained in Sub-section 3.2.1.)

The design of the cabin is split up into several cross-sections along the fuselage length, which are later combined to form a cabin. Since the cabin is also sized to withstand lateral forces, resulting from the wing bending moment, an initial estimate on these forces is provided as an input to the MMG. Similar to the original program an input file is called before the actual aircraft geometry is constructed. This input file to the MMG now creates the 'oval fuselage'. It defines the cabin geometry and constructs all cross-sections along the longitudinal axis of the cabin. Each cross-section, as shown in Figure 2.9, consists of the selection of appropriate shell radii to suit an imposed airfoil profile over the centre line of the aircraft. This is followed by the calculation of the thicknesses of the structural members.

A 3D wireframe model of the cabin is constructed by placing the cross-sections in sequence after each other and the airfoils at four spanwise sections are obtained from the cabin shape, by longitudinal interpolation of the cross-sections at a given spanwise station. These are the four airfoil sections that were previously used for the design variables. The inputs for the MMG are determined from the calculated fuselage geometry and complemented by the inputs for the outer wings, vertical tails, engines and landing gear, as was the case in the original program. The MMG itself no longer contains the cabin construction for obvious reasons.

Important to note is that the methodology explained in Section 3.2 and Chapter 4 can be applied when cambered, hence asymmetric, airfoils are used. However, the construction of the centre line airfoil and wireframe model and the subsequent determination of the four airfoil sections are not yet capable of handling asymmetric airfoils. It was decided to limit the analysis of the 'oval-fuselage' concept to symmetric airfoils at this stage, since asymmetric airfoils would make the cabin-construction steps overly complicated. The asymmetric shape can be created, however, at this point not with the required level cabin floor.

The aircraft model is passed to the analysis modules, similar to the original program. However, these modules now contain feed-back loops. The analysis modules are split up into two groups, one within the feed-back loops, the other outside of these loops. Within the loops, the cabin analysis is altered and now calls functions that determine the upper and lower deck cargo space. Here a specific clear height is used for both cargo decks and the lower deck is checked for the number of LD-3 containers that would fit the available space. On the upper deck only the volume meeting this clear height is calculated. The aerodynamics module remains unchanged.

The weight estimation module is changed quite dramatically. Not only is the Torenbeek Class II

OEW estimation implemented, in addition to this, the weight of the cabin needs to be calculated. This is done by calculating the weight of all longitudinal cross-sections, as explained in Chapter 4, and interpolating the result. The lateral forces from the wing bending moment, which has now been calculated, are used to resize all cross-sections. Hence a loop to the cross-section calculations is present, to update the fuselage for the lateral forces. Furthermore all longitudinal stresses are checked against the compressive and tensile fatigue stress limits and if necessary the shell thicknesses are resized, and the weight estimation of the fuselage section is evaluated again.

The loop containing the MMG, cabin analysis, aerodynamics and weight estimation is evaluated as long as the difference between the lateral forces (input is set to calculated values after each loop) is smaller than 1kN. (This is normally the case within 2 or 3 iterations.) As soon as this loop is exited, the other analysis modules are called and the centre of gravity position, balance, stability and performance is evaluated, followed suit by the evaluation of the nonlinear constraints.

Because of the increased complexity of the weight estimation module, the structure is visualized in Figure 3.3. This figure shows the steps taken in this module in detail.

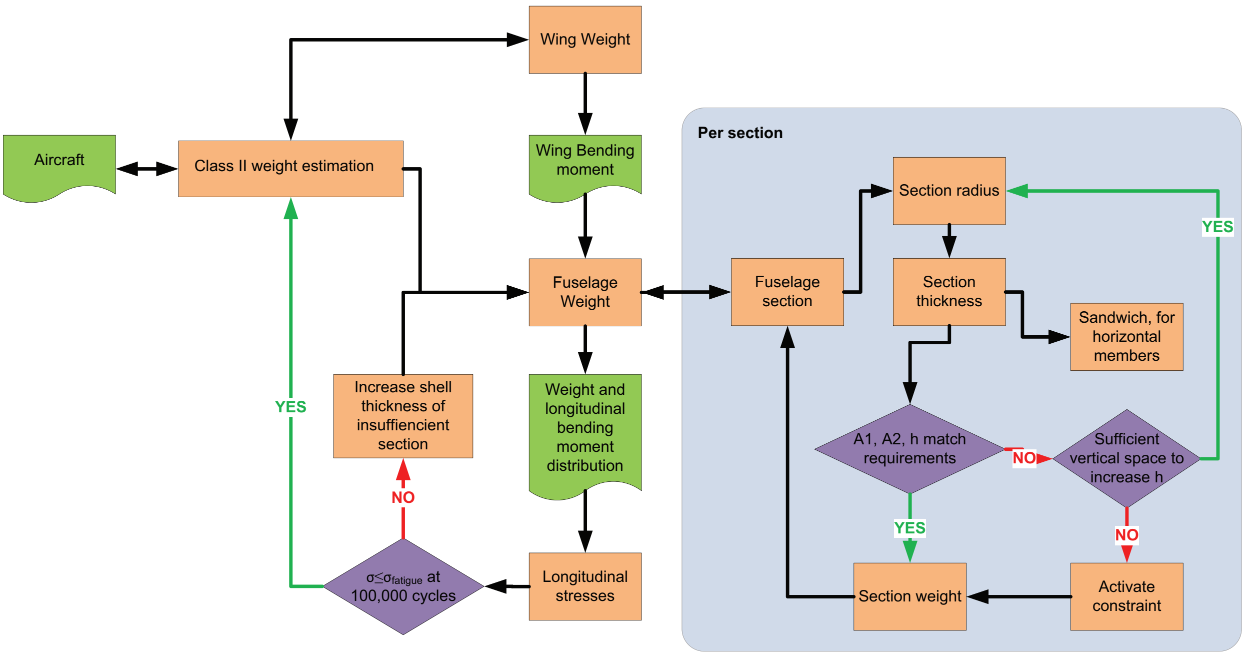

Figure 3.3: Structure of the new weight estimation module

The input to the weight estimation is the geometry created in the MMG and the results of the cabin analysis and the aerodynamic module. First to be calculated are the components of the Torenbeek[10] weight estimation which contain several inputs to the Torenbeek Class II.5[5] wing weight estimation. Here the bending moment in the wing is calculated from the aerodynamic results, taking into account bending relief due to fuel and engines. All data is then forwarded to the fuselage weight estimation function. From the calculated wing bending moment, the lateral forces are updated and the fuselage cross-sections are iterated until the desired cabin geometry is achieved. (Should this geometry be unachievable a constraint is activated and the whole aircraft iterate is declared infeasible). Once the weight of all cross-sections is known, the longitudinal stresses due to fuselage bending and pressurization are evaluated and checked against the fatigue limit compressive and tensile stresses. If the stresses are higher than the allowable stresses, the shell thickness is increased and the entire fuselage weight estimation is evaluated once more. The actual weight estimation methodology can be found in Chapter 4, where the calculations regarding the weight and balance and the longitudinal stresses are explained.

3.2 The Multi-Model Generator

This section provides an overview of the structure of the Multi-Model Generator that had to be altered, in order to accommodate the 'oval-fuselage' geometry for the optimization. The discussion of the new structure is followed by Sub-section 3.2.1, where the cabin definition of the 'oval-fuselage' and its design variables are discussed, Sub-section 3.2.2, on the generation of the geometry of the pressure shell cross-sections and Sub-section 3.2.3, with a description of the generation of the 3D cabin and aircraft model for the 'oval-fuselage'.

Figure 3.4 shows a schematic of the structure of the new Multi-Model Generator and its inputs.

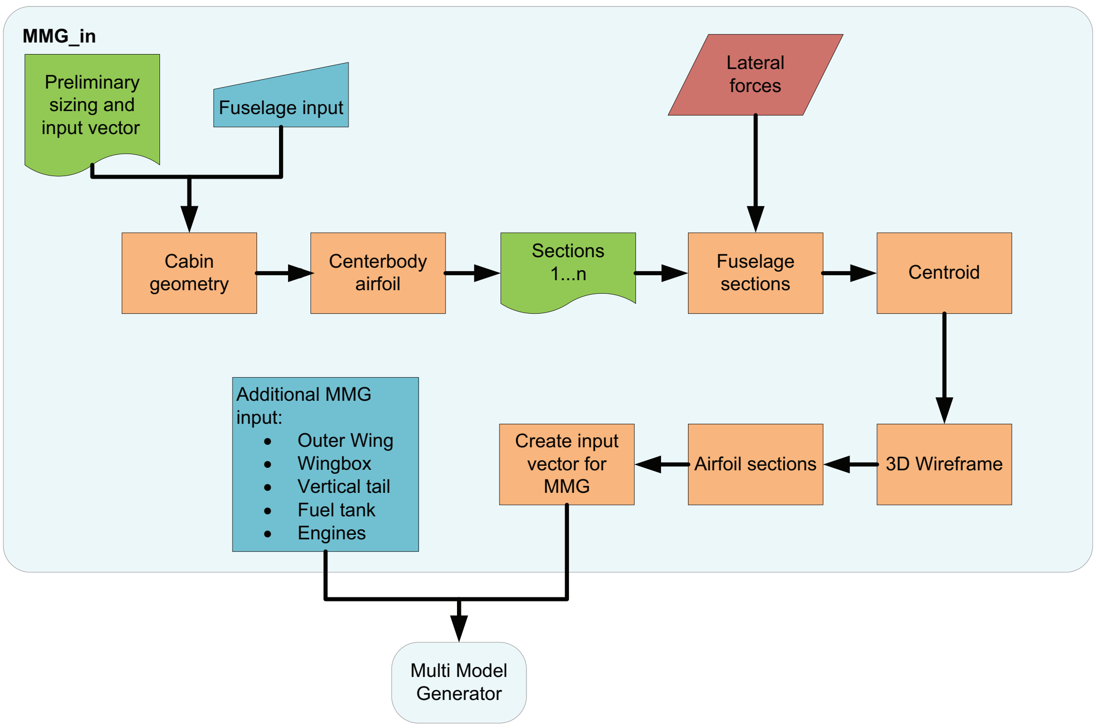

Figure 3.4: Detailed overview of the construction of the 'oval-fuselage' for the MMG

The original MMG contained a module to create the multi-bubble pressure shell, However, the new MMG inherits the cabin from the MMG-input file. In the new version, the cabin generation is not limited to the geometry. Already an analysis of the material thickness needed to resist the external and pressurization loads is performed. The original MMG-input file would simply convert the input vector, initial sizing and requirements into the correct inputs for the MMG.

The results from the preliminary sizing module, together with the input vector are passed to the MMG-in file. The material input for the cabin generation is loaded and all inputs are passed to the cabin geometry module. Here, the geometry of the cabin is determined and divided into sixteen sections along the length of the cabin. Sub-section 3.2.1 explains this process. Based on the cabin length an airfoil over the centre line of the aircraft is determined. The thickness to chord ratio of this airfoil is one of the design variables and this airfoil determines the maximum height of a cross-section, locally (at each of the sixteen stations). The length of the airfoil is based on the length of the cabin. It is assumed that:

- The cabin makes up 70% of the chord of the centreline airfoil
- 2% chord is located in front of the cabin to form the nose of the BWB
- The remaining 28% of chord acts as the trailing edge

The creation of the fuselage sections is shown in a more detailed overview in Figure 3.5.

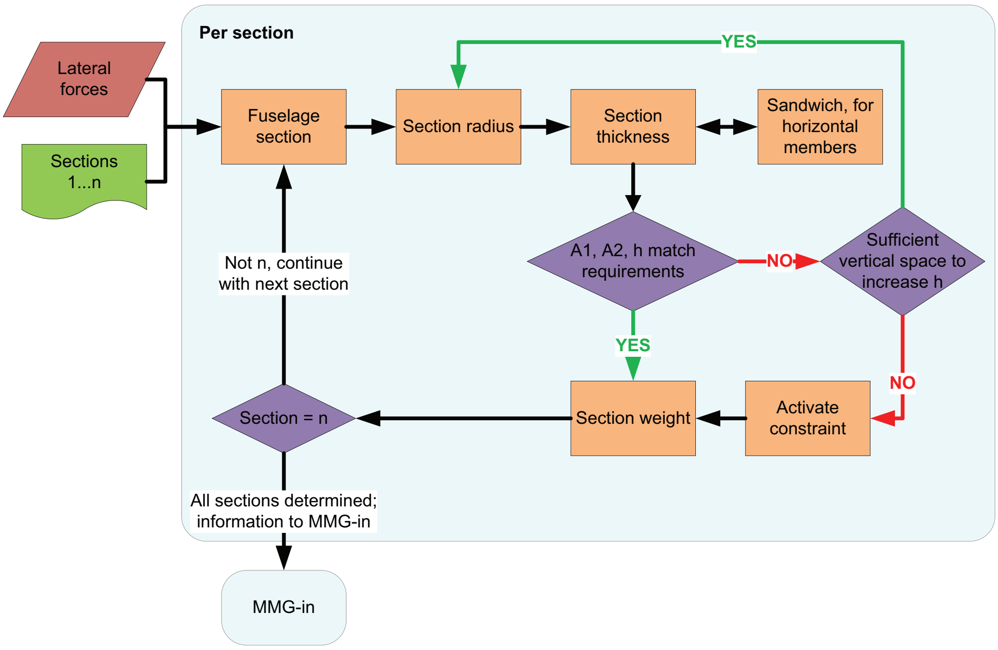

Figure 3.5: Detailed overview of the construction of the 'oval-fuselage' sections in the MMG-in file

The fuselage cross-sections, with the information on the maximum cross-sectional height, are combined with the estimated (or pre-determined, in case of an iteration) lateral forces and a fuselage cross-section with shells, walls and horizontal members is determined per section. First the radii of the shells are selected, then the thicknesses of the shells, walls and horizontal members are determined, as explained in Sub-section 3.2.2. This is iterated until the desired cabin height and width at ceiling and floor, (h, A_1 and A_2, respectively) are obtained. Then the section weight is determined. Should a section not be possible within the maximum height of the fuselage cross-section, i.e. when h, A_1 and A_2 cannot be obtained due to the height restraint from the airfoil, a constraint is activated.

Returning to Figure 3.4, it can be seen that the next step is to determine the centroid and second moment of area of each of the cross-sections. Then, the wireframe module creates the geometric representation of each of the sections and passes this to the airfoil sections module which determines the airfoil sections at pre-determined fuselage stations. (More on this in Sub-section 3.2.3.) Once the 'oval-fuselage' is generated, the input vector for the MMG is constructed for the outer wings, the wingbox, the vertical tail(s), fuel tanks and engines. The MMG then constructs these items and it also sets the initial landing gear positions.

3.2.1 Cabin Definition

The actual 'oval-fuselage' is constructed around the passenger cabin with a certain, constant, cabin height. This cabin height is a fixed input. The planform of the cabin is determined from seven variables, where two are set equal to each other, such that six design variables remain, as can be seen in Figure 3.6. Here, the cabin is highlighted in green and the design variables are indicated. Important to note is that b_1 is fixed in the program. It serves as the cockpit width and is kept constant because cockpit design is not possible at this stage. Therefore it was decided to use the same cockpit width and cockpit floor area for all designs (also for the multi-bubble) for better comparison. This leaves five design variable for the optimizer to work with, divided over a front, mid and aft section: b_2, the maximum width of the cabin, b_3, the width of the aft of the cabin and L_1, L_2 and L_3, the lengths of the three sections. The front, mid and aft sections of the cabin are divided into five equal length sections each, yielding 16 design stations. These design stations serve as the locations where the fuselage-cross sections are divided and it is assumed that the design varies linearly between two fuselage stations. An additional design variable is the thickness to chord ratio of the centreline airfoil as mentioned in Section 3.2. The aft most location of the cabin, i.e. at the end of L_3, where the rear pressure bulkhead is located, is integrated with the position of the aft-spar of the wingbox, as can be observed from Figure 3.6.

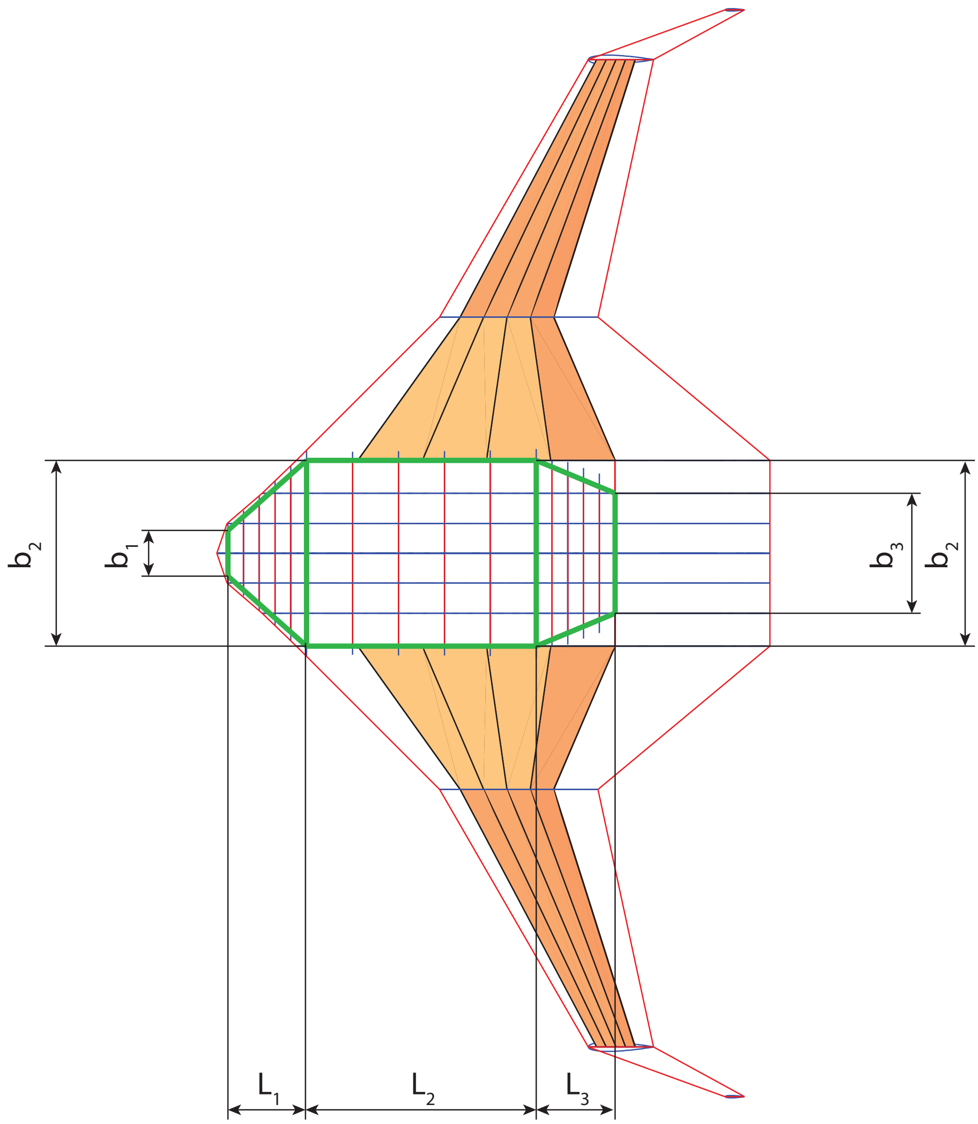

Figure 3.6: Schematic top view of an 'oval-fuselage' BWB, including cabin and wingbox

3.2.2 Pressure Shell Construction

Before it is possible to make any statements on the weight and balance of the BWB fuselage, or the weight and balance of the whole BWB itself for that matter, the fuselage must be defined and modeled. For this purpose, the pressure shell of the aircraft, containing the passenger cabin, is cut into sections that are evaluated per unit length. A cross-section, at a certain station along the longitudinal axis of the pressure cabin, is described by the dimensions of the passenger cabin in lateral and vertical direction. Along the lateral axis, the cabin is described by the ceiling and floor half-width, A_1 and A_2 respectively. In vertical direction, the height of the cabin, h, is the required input parameter. With these input parameters provided, the radii of the shells circumscribing the passenger cabin must found. The boundary condition for these radii is that in the upper and lower nodes, where two shells meet, the tangency is maintained. In other words, the tangent line through R_2 and R_1 in the upper node is the same. Similarly, for the lower node, the tangent line through R_2 and R_3 is the same. This is illustrated in Figure 3.7, where an example of such a pressure shell, satisfying the tangency condition is drawn. This tangency ensures that the resultant force is exactly tangent to the shell in the node. The resultant force, together with the lateral force originating from the wing bending moment is to be carried by the “vertical” wall and the ceiling, or floor, depending on the node that is considered. This is explained in Section 4.3.

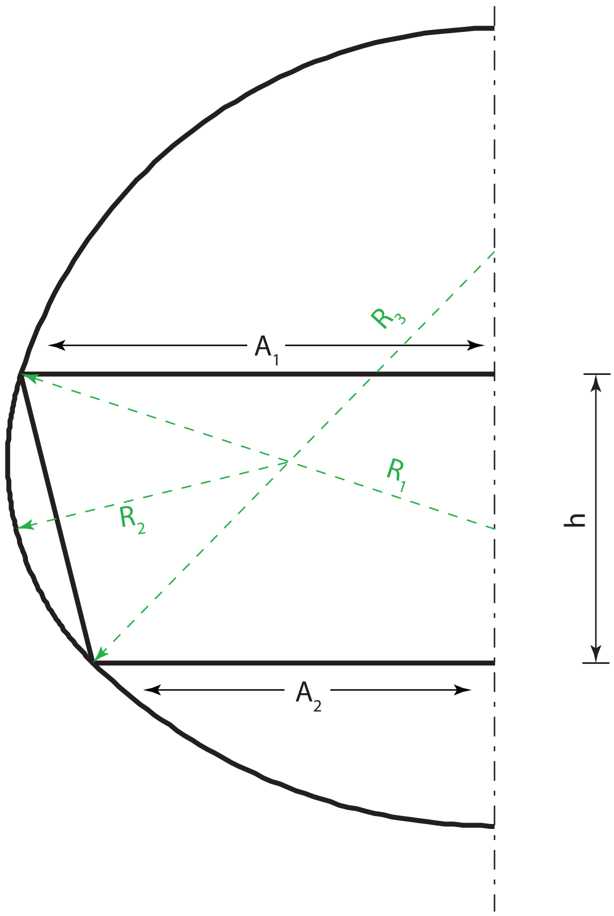

Figure 3.7: Semi cross-section of an ‘oval-fuselage’

As noted in Section 3.1 and Section 3.2 the actual pressure shell construction is an iterative process. Whilst this section describes the geometric relations used to determine these cross-sections, it is important to keep in mind that these relations are valid for infinitely thin lines only. Therefore, in the actual program these lines, except for the arcs, are considered as the centrelines of the structural members. The lines describing the arcs are used as the inner radius of the pressure shell, according to the definitions of the equations for hoop stresses[28]. These lines, together with the structural thicknesses are shown in Figure 3.9. In the iterative process of determining the geometry, the thickness of the horizontal members and that of the arcs is considered in determining the combination of radii suiting the aerodynamic cross-section, such that the desired cabin height is achieved. The thickness of the walls and that of the horizontal members is also considered in determining the width of the section, such that the desired cabin interior dimensions are achieved. Thanks to this iterative process, the cabin interior will match the desired specifications, the wire-frame model, however, can vary from section to section as it shows the centerlines (or inner radius) of the structural members.

From Figure 3.7 it can be observed, that next to the radii also the respective centres of these circles must be determined. From the tangency condition it is already known that the centre of R_2 must be at the intersection of a line through the upper node and the centre of R_1 and a line through the lower node and the centre of R_3. Also, because of the plane of symmetry in vertical direction, the centres of R_1 and R_3 must be on this symmetry axis. In order to determine combinations of radii satisfying the tangency condition and circumscribing the passenger cabin, Figure 3.8 is constructed. Here all the angles and lengths necessary for the analysis are indicated.

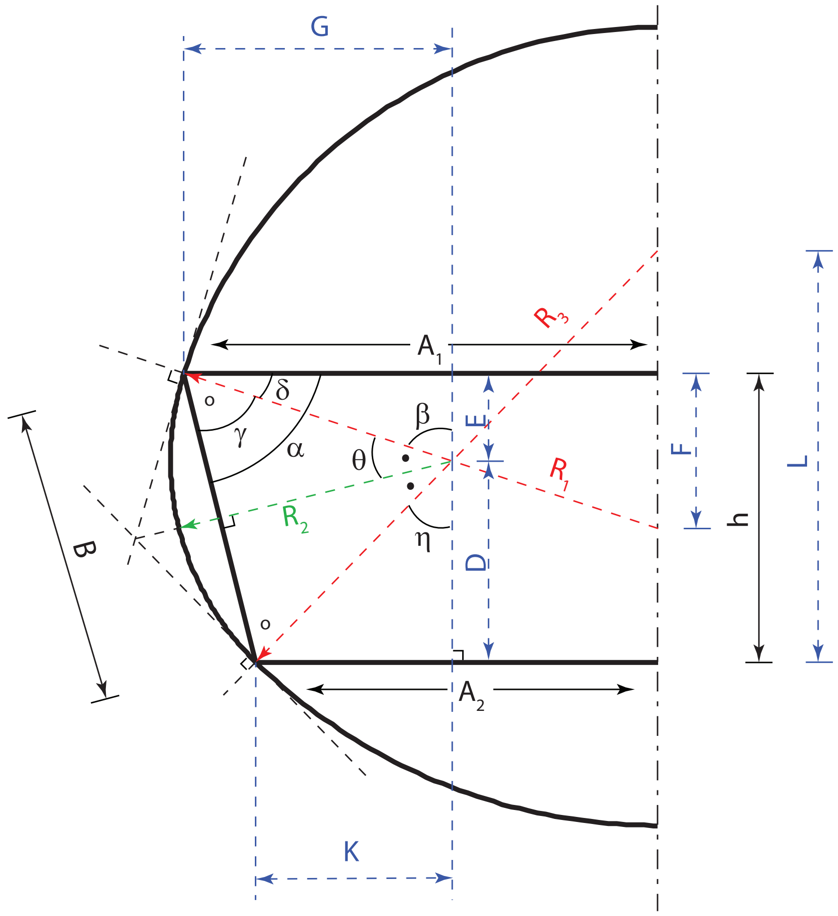

Figure 3.8: Semi cross-section of an ‘oval-fuselage’ for geometry determination

From the input geometry of the lateral and vertical dimensions of the passenger cabin, two parameters in Figure 3.8 can already be determined at first glance. These are α and B, as given by Equations (3.1) and (3.2).

$$\alpha = \arctan\left(\frac{h}{A_1 - A_2}\right) \tag{3.1}$$

$$B = \sqrt{h^2 + (A_1 - A_2)^2} \tag{3.2}$$

To find combinations of radii satisfying the tangency condition, a MATLAB program was constructed performing the calculations described in this chapter. The code uses a vector containing multiple values of R_2 as input, to find the corresponding values of R_1 and R_3. Now that R_2 is considered an input, all other angles in Figure 3.8 can be determined according to Equations (3.3) through (3.7).

$$\theta = \arcsin\left(\frac{B}{2R_2}\right) \tag{3.3}$$

$$\gamma = \arccos\left(\frac{B}{2R_2}\right) \tag{3.4}$$

$$\delta = \alpha - \gamma \tag{3.5}$$

$$\beta = \frac{\pi}{2} - \delta \tag{3.6}$$

$$\eta = \pi - 2\theta - \beta \tag{3.7}$$

With all angles in Figure 3.8 determined, the radii of the top and bottom shell, R_1 and R_3 follow suit, as shown in Equations (3.8) and (3.9).

$$R_1 = \frac{A_1}{\cos(\delta)} \tag{3.8}$$

$$R_3 = \frac{A_2}{\sin(\eta)} \tag{3.9}$$

The construction of the pressure shell is not concluded yet, as the positions of the centres of these shells must still be determined. Since there lateral position is already known from symmetry, two additional trigonometric relations provide the positions of the centres of the top and bottom shell along the vertical axis, according to Equations (3.10) and (3.11).

$$F = R_1 \cdot \sin(\delta) \tag{3.10}$$

$$L = R_3 \cdot \cos(\eta) \tag{3.11}$$

The position of the centre of the side shell, with radius R_2 can be found through Equations (3.12) and (3.13).

$$G = R_2 \cdot \cos(\delta) \tag{3.12}$$

$$E = R_2 \cdot \sin(\delta) \tag{3.13}$$

The combination of radii that is selected for the fuselage section is the one that best fits the allowable height. This maximum fuselage height is obtained from the desired shape of the airfoil over the centre section of the fuselage. The process is looped per section until the desired cabin interior dimensions are obtained, taking into account the structural thicknesses of the cross-section, as schematically shown in Figure 3.9. The geometric relations have been derived for the black lines in this figure, where, according to the definition of the hoop stress, the inner radius is used. The inner radii are connected to the centre lines of the horizontal and vertical members in the node for proper force decompositions.

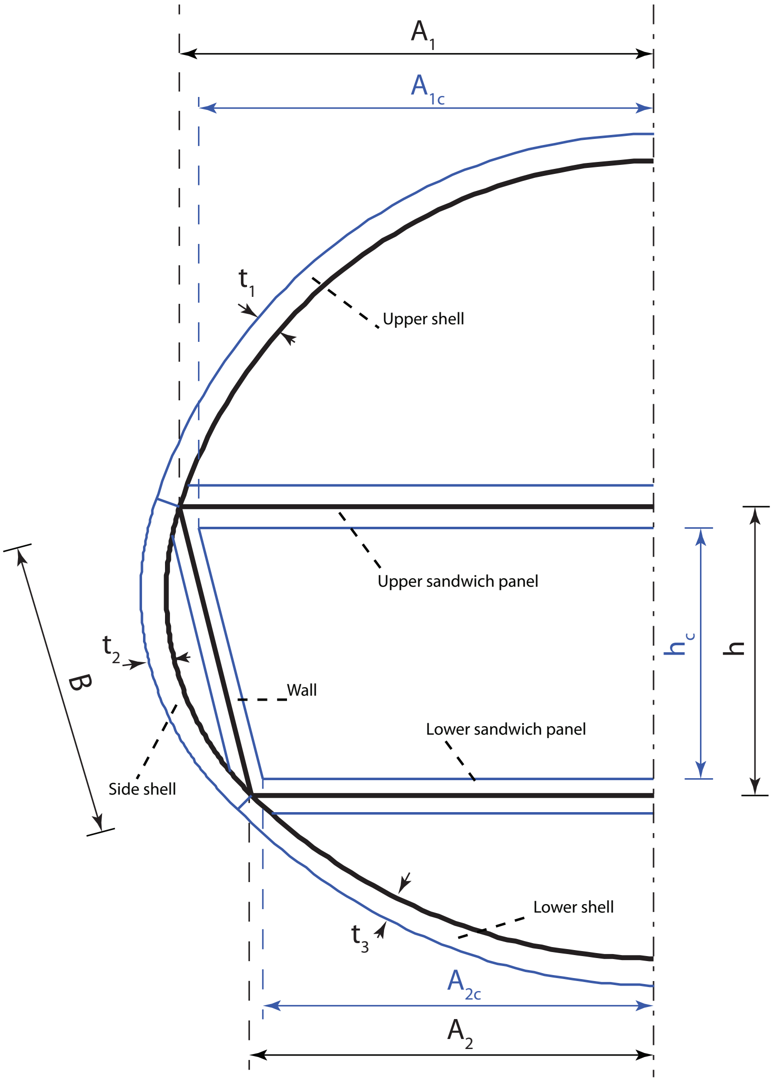

Figure 3.9: Semi cross-section with structural thicknesses

3.2.3 BWB Model Generation

Once the cross-sections at all fuselage stations are determined and iterated, such that the cabin interior dimensions match the desired specifications, a 3D wireframe model of the cabin section can be created simply by positioning all sections according to there location along the cabin length.

An example of this is shown in Figure 3.10, where also the location of the cargo floor is shown in green. The cargo floor is positioned at a clear height of 1.68m, similar to the cargo hold clear height in a Boeing 747-400[29]. This clear height is sufficient to allow for LD-3 unit load devices to be stored in the lower deck cargo hold. The actual check on the amount of cargo volume available is performed in the cabin analysis module, where it is checked whether this clear height is available and how many cargo containers fit a floor located at this distance below the lowest cabin floor member. The same check is performed at the kink-height of the LD-3 container, that has a slanted edge.

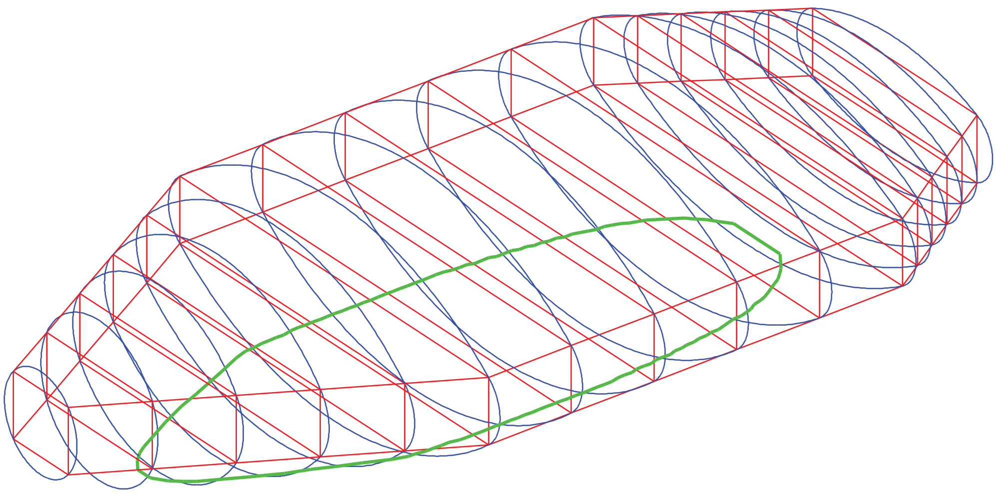

Figure 3.10: 3D view of a wireframe model generated for the 'oval fuselage' cabin, with the cargo floor indicated in green

A similar check on the same clear height is performed for the upper deck cargohold (not drawn in this figure), yet here the volume that satisfies this height is calculated for the storage of bulk cargo. The outer dimensions[30] and structural volume (and weight) of the LD-3 containers are considered in the analysis and a cargo density of 190kg/m^3 from Torenbeek[10] is used. A top view of the fuselage, with fuselage, cabin and cargo floor perimeter indicated, is shown in Figure 3.11.

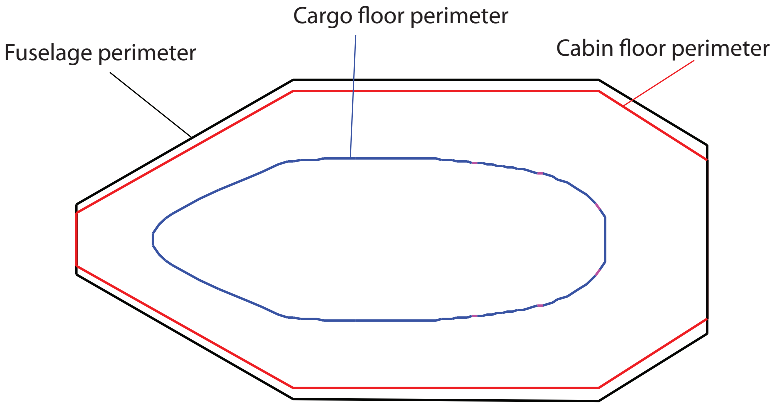

Figure 3.11: Top view of a model generated for the 'oval fuselage' cabin

Now that the cabin of the 'oval-fuselage' concept is constructed according to the new input vector, the correct input for the MMG has to be generated. The MMG still uses the information from the original input vector where for six airfoil sections, chord, span, twist, sweep, dihedral and thickness were used as design variables. However, with the new design variables, these parameters are only input for the outer two sections, illustrated in Figure 3.12. Therefore the information that was contained in the original input vector is obtained from the the 'oval-fuselage' at the four inner stations. Here, the twist of the cabin sections is set to zero, similar to the original program.

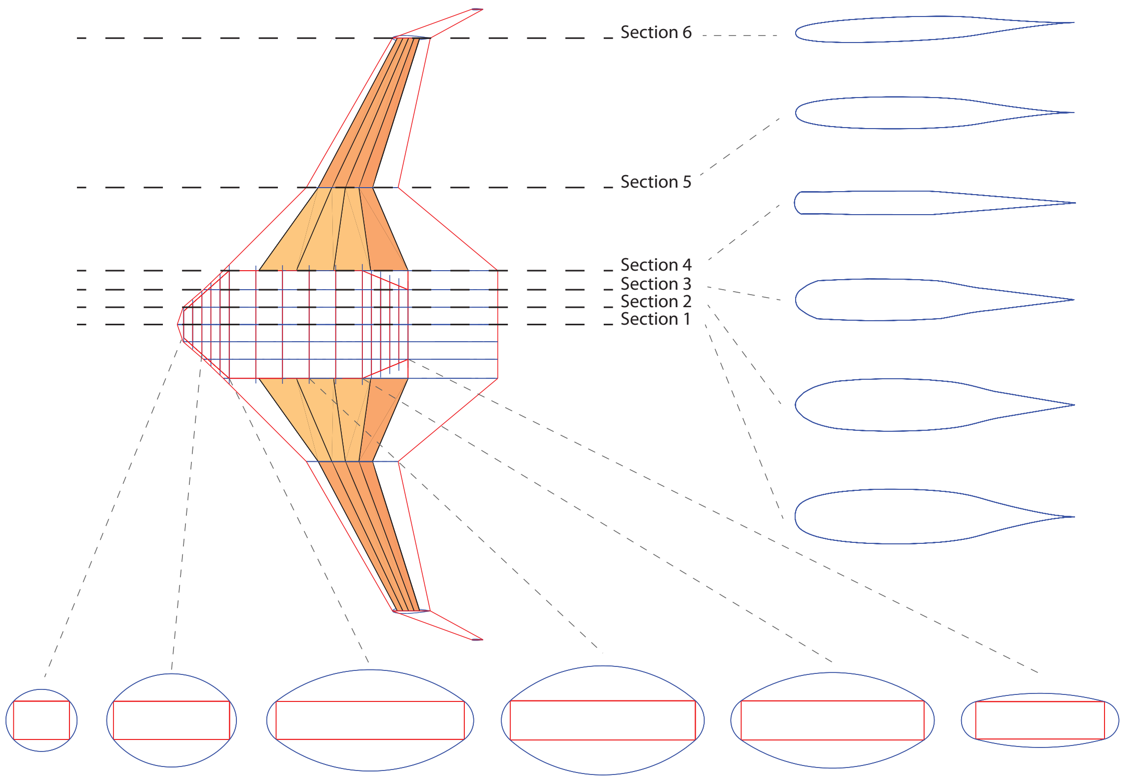

Figure 3.12: Top view of the BWB showing the definition of the airfoil sections and several cross-sections

Section 1 is located on the aircraft centre line. Section 2 is located where the width at the first fuselage station is maximum. Section 3 is positioned at the maximum width of the fuselage aft and Section 4 is positioned at the maximum width of the passenger cabin. At these four positions the airfoils are determined from the shape of the pressure shell. The trailing edges are set equal to that of Section 1, to have a straight trailing edge at the centre body (potential position of control surface). Section 5 and 6 are at the same position as for the multi-bubble BWB.

Figure 3.12 also shows the airfoils at the sections 1 through 6. Especially the airfoil at section 4 has a rather strange shape due to the fact that it is located at the edge of the cabin. Here the cabin-height determines the profile, because the outer shells intersect at this point. Therefore the airfoil has a flat profile, that may be improved by the addition of fuselage fairings, to achieve a better airfoil shape. Section 6 in this particular case shows the twist in the airfoil profile, as was found by the optimizer for this particular case.

Additionally, several fuselage cross-sections along the longitudinal axis are shown. These clearly show the effect of the the tapered cabin and the influence of the fuselage height restriction of the airfoil profile imposed on section 1. The first cross-section is almost circular, whereas the last has a large radius of curvature in the upper and lower shell, approaching the actual cabin geometry. At the stations where more fuselage height is allowed, the radius of curvature of these shells is much smaller, meaning that space for the cargohold is created.

Now that all the information is obtained, with the wingbox, outer wing, vertical tail and engines similar to the multi-bubble MMG, a 3D aircraft model can be generated. A wireframe model of an 'oval-fuselage' cabin and a 3D representation of the aircraft is shown in Figure 3.13.

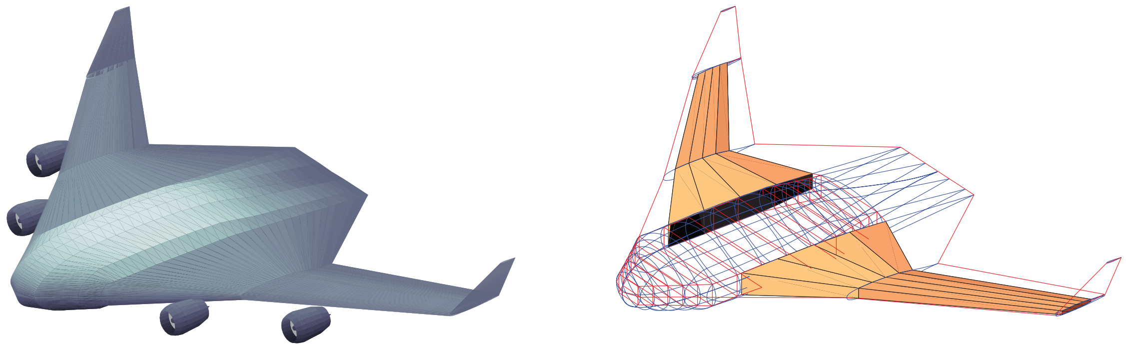

Figure 3.13: 3D model and wireframe model of an 'oval fuselage' BWB

When the geometry of the 'oval-fuselage' blended wing body has been determined, the weight and balance of the aircraft must be evaluated, before comparing its performance to the multi-bubble BWB. The weight and balance of the 'oval-fuselage' will be described in Chapter 4.

CHAPTER 4

WEIGHT AND BALANCE

This chapter presents the weight estimation of an 'oval-fuselage' BWB, which is a necessity to evaluate the aircraft's performance by means of the optimization tool presented in Chapter 3. In Section 4.1 the Class-II weight estimation method that was used to calculate all components of the OEW, except for the wing and fuselage, is introduced. Section 4.2 continues with the wing weight estimation that was used to calculate the weight of the outer sections of the BWB. The weight of the fuselage section of the BWB is determined for pressurization loads, by the method explained in Section 4.3, followed by an explanation of the checks on the longitudinal fuselage stresses in Section 4.4. The method in the latter two sections is defined per fuselage cross-section, similar to the geometry creation in the Multi-Model Generator. The chapter is concluded by Section 4.5 on the determination of the OEW centre of gravity.

4.1 Class-II Operative Empty Weight Estimation

The OEW of the blended wing body has been calculated by implementing Torenbeek's Class-II weight estimation[10]. However, for some specific estimates, more up to date, or more detailed information is used, or estimates specifically for blended wing body aircraft by Howe[4]. The complete OEW estimation is provided in Appendix A and only the additions specific to this fuselage concept are highlighted here.

APU

The installed mass of the auxiliary power unit (APU) is directly related to the dry-mass of the APU. Here a PW980 APU of the Airbus A380 is assumed, which is 10% larger than the PW901a of the Boeing 747-400[31]. The PW901a weighs in at 835 lbs according to information from Virginia Tech[32]. The installed weight can be calculated according to Equation (A.20) shown in Appendix A

Radar

The mass of the radar is estimated from that of a typical Honeywell weather radar for commercial aircraft, the Primus 880[33], at 20kg.

Paint

The weight of the paint is estimated at 0.3kg/m^2 wetted area. This based on a press release by Airbus for the A380[34].

$$W_{\text{paint}} = 0.3 \cdot S_{\text{wet}} \;\; [kg] \tag{4.1}$$

Flightdeck Furnishing

The furnishing of the flightdeck is estimated at 200kg in total, as estimated from the weight of pilot and fold-away seats in the cockpit from Torenbeek[10] and rounded upwards to account for the rest of the furnishing.

Cabin Furnishing

The cabin furnishing, including toilets and galleys and overhead luggage compartments was estimated from data for the Boeing 747. From Roskam[35] the mass of the furnishing for this aircraft was obtained and divided equally over the cabin surface to obtain a ratio of 51.5kg furnishing per squared meter of cabin area. The 747-100 was used as a reference as it is capable of transporting 400+ passengers in a 2 class configuration, and most importantly because of the availability of rare reference data on the furnishing weight from Roskam.

Crew

Flight crew and cabin crew cannot be considered equipment, however, they are indispensable for the operation of the aircraft. Because the ever changing human anthropology, the original data from 1982[10] has been adapted to better match the average human in 2012. Therefore the heavier of the two weights proposed by Torenbeek, i.e. that of the flight crew, has been considered for both the flight crew and cabin crew, including there luggage. This weight is set equal to 93kg per crew member, including luggage.

Cargo Containers

Since the lower deck cargo hold is sized for cargo containers, their weight must be considered in the operational items. The number of LD-3 containers is determined in the cargo hold analysis and multiplied with the LD-3 tare weight of 72kg each, as used by British Airways World Cargo[30].

Fuselage Trailing Edge

In Section 4.3 the weight of the fuselage section is computed, however this does not include the nose cone or the section aft of the passenger cabin. The nose cone weight can be determined by means of Equations (A.4) through (A.6), however, that of the fuselage trailing edge is not yet included. Therefore Equation (4.2) is taken from the class II.5 wing weight estimation methodology from Torenbeek[5]. This equation is used to calculate the weight of the trailing edge to complete the aerodynamic shape of the wing, based on the planform area of the trailing edge, with the wing box weight already determined. A similar methodology is adapted here, the trailing edge merely completes the aerodynamic shape of the wing. Though it must be noted that in a more detailed design, the available volume could very well be used for example for aircraft systems or fuel, implying a re-evaluation of the use of this equation. At this point it is assumed that the trailing edge section could also be used as a control surface. This is included in Equation (4.2), where Δ is normally an indication of the complexity of the flap system present on the trailing edge of a wing. It is assumed that a single slotted flap bears more resemblance to an elevator than e.g. a double slotted system. Therefore no further penalty on Δ is considered.

$$W_{\mathrm{fus_{TE}}} = S_{\mathrm{TE}} \left[60 \left(1 + 1.6 \cdot \sqrt{\frac{W_{\mathrm{TO}}}{10^6}} \right) + \Delta \right] \quad [kg] \tag{4.2}$$

For a single slotted flap[5]:

$$\Delta = 0$$

4.2 Class-II.5 Wing Weight Estimation

The weight of the outer wing, which is not yet included in the previously described airframe weight is determined by means of the Class-II.5 wing weight prediction of Torenbeek[5]. The inner wing section, or fuselage section is determined in Section 4.3.
The method for the wing weight prediction has been extensively documented by Van Dommelen[7]. Only minor corrections to the calculations in MATLAB have been made, yet the methodology has remained the same.

4.3 Fuselage Weight Estimation for Pressurization

From the geometry determined in Chapter 3, it is possible to calculate an estimate of the OEW of the BWB. For the cross-sections along the aircrafts length only the geometry is known, however, the thicknesses of the shells, walls and floor and ceiling need to be determined as well. Therefore, the internal forces must be calculated, to determine the material necessary to withstand these forces. It is assumed that the resultant force acting in one of the nodes can be decomposed in a horizontal component carried by either the floor or the ceiling, and a vertical component carried by the wall. In addition to the horizontal component of the resultant force due to pressurization, a compressive force is added because of the lateral bending moment of the wings, this is treated in Sub-section 4.3.3.
The resultant force due to pressurization is determined from the force resulting from the hoop-stress acting in each of the shells. Pressurization of a cylinder causes stresses in two directions, hoop-direction (in green) and in the longitudinal direction (in blue), as illustrated by Figure 4.1. The influence of the longitudinal stress will be covered in Section 4.4.

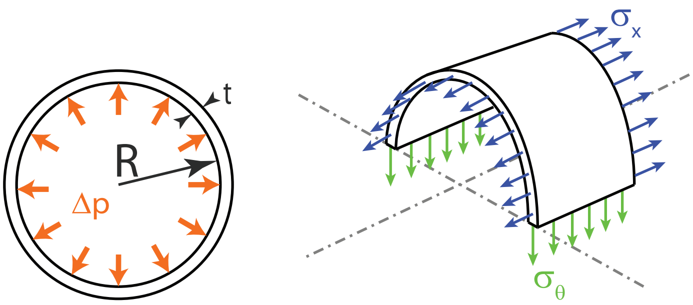

Figure 4.1: Schematic representation of stresses due to pressurization

The hoop-stress for a cylinder with radius R and thickness t may be derived as:[28]

$$\sigma_\theta = \frac{\Delta p \cdot R}{t} \tag{4.3}$$

For a section of unit length Δl, the tensile force due to pressurization may be obtained from the stress in hoop-direction as:[28]

$$F = \sigma_\theta \cdot \Delta l \cdot t = \Delta p \cdot \Delta l \cdot R \tag{4.4}$$

The tensile force can be derived for each of the shells, in each of the nodes, as illustrated by Figure 4.2. This figure schematically shows the upper node as an example with the tensile forces that originate from each of the two shells under pressurization. For this part of the analysis, the upper and lower node are treated separately in the sub-sections that follow.

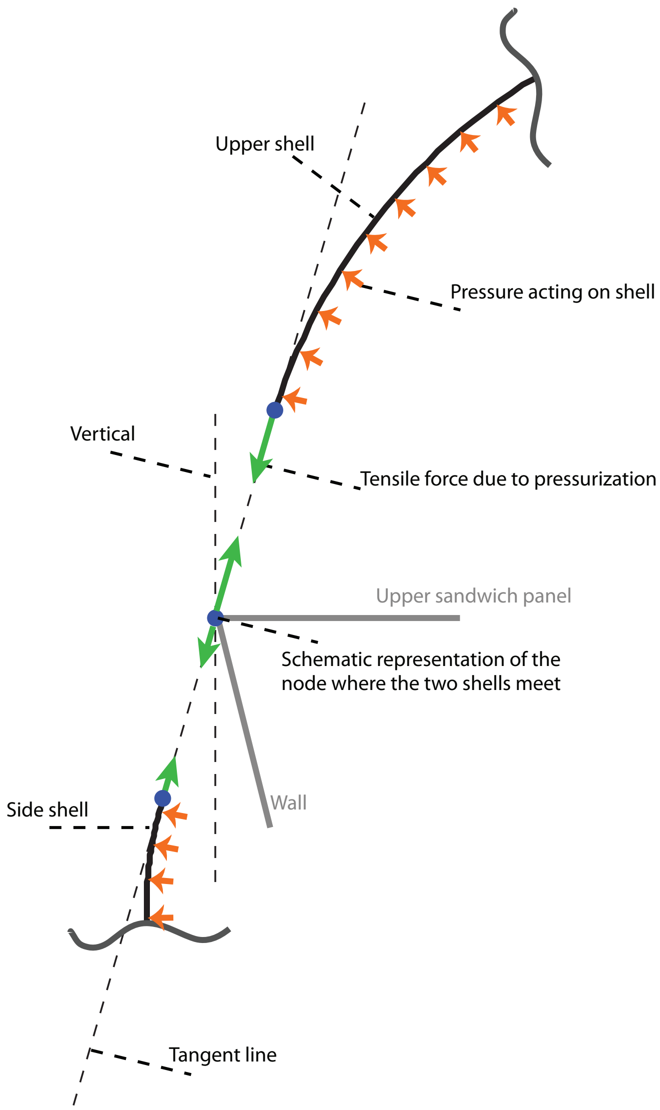

Figure 4.2: Schematic representation of the forces acting on the upper node due to pressurization

4.3.1 Resultant Forces and Decomposition of Forces

Upper node

This sub-section treats the decomposition of the resultant force due to pressurization acting in the upper node of the pressure shell. Figure 4.3 shows the Free Body Diagram (FBD) in the upper node.

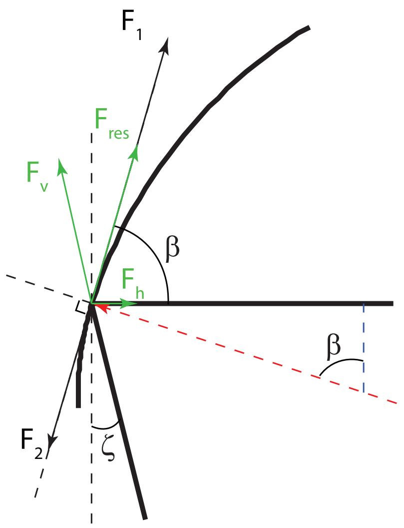

Figure 4.3: Free body diagram for pressurization in the upper node

The resultant force must be decomposed in order to determine the component in the wall and ceiling. However, as can be seen in Figure 4.4, it has to be decomposed in two non-orthogonal components because of the skewed wall. Note that the direction of the resultant force has been changed, as the figure merely serves to illustrate of the decomposition along non-orthogonal axis.

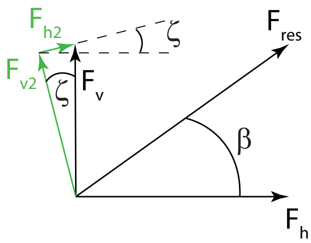

Figure 4.4: Decomposition of the resultant force in the upper node

From Figure 4.4 follow Equations (4.5) through (4.8).

$$F_{\mathrm{h}} = F_{\mathrm{res}} \cdot \cos(\beta) \tag{4.5}$$

$$F_{\mathrm{v}} = F_{\mathrm{res}} \cdot \sin(\beta) \tag{4.6}$$

$$F_{\mathrm{h2}} = F_{\mathrm{v}} \cdot \sin(\zeta) \tag{4.7}$$

$$F_{\mathrm{v2}} = F_{\mathrm{v}} \cdot \cos(\zeta) \tag{4.8}$$

However, only F_{h} and F_{v2} are in the direction desired for sizing the wall and the ceiling. Yet, F_{h2} remains. This small component can again be decomposed along the horizontal and vertical axis. And subsequently an even smaller component of this force along the axis of F_{h2} and F_{v2}. This repeating decomposition of forces is described by a sum, as shown in Equations (4.9) and (4.10).

$$F_{\mathrm{h_{bar}}} = F_{\mathrm{res}} \cdot \cos(\beta) + F_{\mathrm{res}} \cdot \sin(\beta)\cos(\zeta) \cdot \sum_{n=1}^{\infty} \sin^{2n-1}(\zeta) \tag{4.9}$$

$$F_{\mathrm{v_{bar}}} = F_{\mathrm{res}} \cdot \sin(\beta)\cos(\zeta) \cdot \sum_{n=0}^{\infty} \sin^{2n}(\zeta) \tag{4.10}$$

Lower node

A similar FBD can be made for the lower node, as illustrated by Figure 4.5.

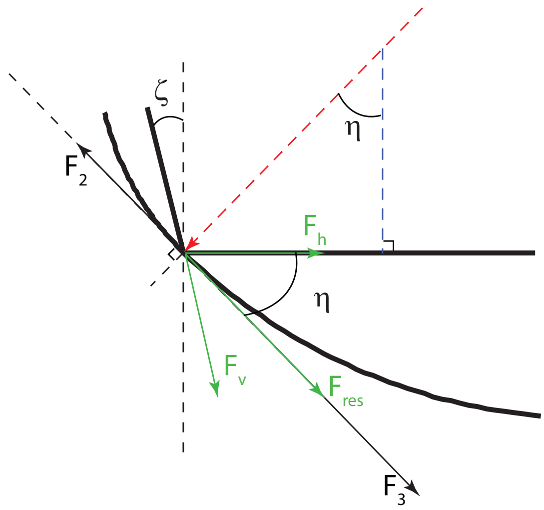

Figure 4.5: Free body diagram for pressurization in the lower node

The resultant force can again be decomposed as a sum, with the help of Figure 4.6.

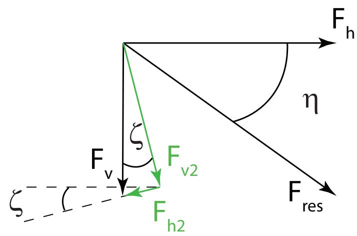

Figure 4.6: Decomposition of the resultant force in the lower node

For the lower node, Equations (4.11) through (4.14) describe the first two steps of the decomposition. Note that this time the component F_{h2} is in the direction opposite of F_{h}, resulting in a minus sign in Equation (4.15).

$$F_{\mathrm{h}} = F_{\mathrm{res}} \cdot \cos(\eta) \tag{4.11}$$

$$F_{\mathrm{v}} = F_{\mathrm{res}} \cdot \sin(\eta) \tag{4.12}$$

$$F_{\mathrm{h2}} = F_{\mathrm{v}} \cdot \sin(\zeta) \tag{4.13}$$

$$F_{\mathrm{v2}} = F_{\mathrm{v}} \cdot \cos(\zeta) \tag{4.14}$$

Rewriting the decomposition as a sum yields Equations (4.15) and (4.16) for the floor and the wall, respectively. It must be noted that two equations for the force in the "vertical" wall have been found. However, it is proven in Sub-section 4.3.2 that the normal forces resulting from Equations (4.10) and (4.16) are equal for geometries satisfying the tangency condition, maintaining static equilibrium at the nodes.

$$F_{\mathrm{h_{bar}}} = F_{\mathrm{res}} \cdot \cos(\eta) - F_{\mathrm{res}} \cdot \sin(\eta)\cos(\zeta) \cdot \sum_{n=1}^{\infty} \sin^{2n-1}(\zeta) \tag{4.15}$$

$$F_{\mathrm{v_{bar}}} = F_{\mathrm{res}} \cdot \sin(\eta)\cos(\zeta) \cdot \sum_{n=0}^{\infty} \sin^{2n}(\zeta) \tag{4.16}$$

Rewriting the equations

The sums in Equations (4.9), (4.10), (4.15) and (4.16) are not very convenient for any calculations. Therefore, the sums are rewritten as series of which the limit of $n \to \infty$ can be taken. This sub-section is used to explain the process of rewriting the equations into more convenient expressions. First, for the sum in Equations (4.9) and (4.15):

$$\sum_{n=1}^{\infty} \sin^{2n-1}(\zeta) = S_{\mathrm{n}} \tag{4.17}$$

$$S_{\mathrm{n}} = \sin(\zeta) + \sin^3(\zeta) + \sin^5(\zeta) + ... + \sin^{2n-1}(\zeta) \tag{4.18}$$

$$\sin^2(\zeta) \cdot S_{\mathrm{n}} = \sin^3(\zeta) + \sin^5(\zeta) + ... + \sin^{2n-1}(\zeta) + \sin^{2n+1}(\zeta) \tag{4.19}$$

Subtracting the previous two equations from each other yields:

$$S_{\mathrm{n}} - \sin^2(\zeta) \cdot S_{\mathrm{n}} = \sin(\zeta) - \sin^{2n+1}(\zeta) \tag{4.20}$$

$$S_{\mathrm{n}} = \frac{\sin(\zeta) - \sin^{2n+1}(\zeta)}{1 - \sin^2(\zeta)} \tag{4.21}$$

With $n \to \infty$ the limit of the series must taken, as is shown below.

$$\lim_{n\to\infty} S_{\mathrm{n}} = \lim_{n\to\infty} \frac{\sin(\zeta) - \sin^{2n+1}(\zeta)}{1 - \sin^2(\zeta)} \tag{4.22}$$

$$\lim_{n\to\infty} S_{\mathrm{n}} = \frac{\sin(\zeta)}{1 - \sin^2(\zeta)} - \lim_{n\to\infty} \frac{\sin^{2n+1}(\zeta)}{1 - \sin^2(\zeta)} \tag{4.23}$$

$$\lim_{n\to\infty} S_{\mathrm{n}} = \frac{\sin(\zeta)}{1 - \sin^2(\zeta)} - \frac{1}{1 - \sin^2(\zeta)} \lim_{n\to\infty} \sin^{2n+1}(\zeta) \tag{4.24}$$

Since the sine function is bounded by $0 < \sin(\zeta) < 1$ the following limit always goes to zero for $n \to \infty$

$$\lim_{n\to\infty} \sin^{2n+1}(\zeta) = 0 \tag{4.25}$$

The boundary case where $\sin(\zeta) = 1$, hence $\zeta = 90°$ describes the orthogonal axis for the decomposition, and is therefore not relevant here. The other boundary case where $\sin(\zeta) = 0$, hence $\zeta = 0°$ is the case where there is no vertical wall. This would result in a perfectly cylindrical fuselage where floor and ceiling would be at the same height. Hence the following equation describes the limit of the series:

$$\lim_{n\to\infty} S_\mathrm{n} = \frac{\sin(\zeta)}{1 - \sin^2(\zeta)} \tag{4.26}$$

From trigonometry:

$$\sin^2(\zeta) + \cos^2(\zeta) = 1 \tag{4.27}$$

Therefore the limit of the series, and hence the sum in Equations (4.9) and (4.15), can be written according to Equations (4.28)

$$\lim_{n\to\infty} S_\mathrm{n} = \frac{\sin(\zeta)}{\cos^2(\zeta)} \tag{4.28}$$

Similarly, for the sums in Equations (4.10) and (4.16), a series expansion can me made and the limit of the series can be evaluated.

$$\sum_{n=0}^{\infty} \sin^{2n}(\zeta) = S_\mathrm{n} \tag{4.29}$$

$$S_\mathrm{n} = 1 + \sin^2(\zeta) + \sin^4(\zeta) + ... + \sin^{2n}(\zeta) \tag{4.30}$$

$$\sin^2(\zeta) \cdot S_\mathrm{n} = \sin^2(\zeta) + \sin^4(\zeta) + ... + \sin^{2n}(\zeta) + \sin^{2n+2}(\zeta) \tag{4.31}$$

Subtracting the previous two equations from each other yields:

$$S_\mathrm{n} - \sin^2(\zeta) \cdot S_\mathrm{n} = 1 - \sin^{2n+2}(\zeta) \tag{4.32}$$

$$S_\mathrm{n} = \frac{1 - \sin^{2n+2}(\zeta)}{1 - \sin^2(\zeta)} \tag{4.33}$$

With $n \to \infty$ the limit of the series must taken, as is shown below.

$$\lim_{n\to\infty} S_{\mathrm{n}} = \lim_{n\to\infty} \frac{1-\sin^{2n+2}(\zeta)}{1-\sin^2(\zeta)} \tag{4.34}$$

$$\lim_{n\to\infty} S_{\mathrm{n}} = \frac{1}{1-\sin^2(\zeta)} - \lim_{n\to\infty} \frac{\sin^{2n+2}(\zeta)}{1-\sin^2(\zeta)} \tag{4.35}$$

$$\lim_{n\to\infty} S_{\mathrm{n}} = \frac{1}{1-\sin^2(\zeta)} - \frac{1}{1-\sin^2(\zeta)} \lim_{n\to\infty} \sin^{2n+2}(\zeta) \tag{4.36}$$

Again, the same bounds apply to the sine function in the series where $0 < \sin(\zeta) < 1$ and the cases for $\sin(\zeta) = 1$ and $\sin(\zeta) = 0$ are not relevant for this part of the analysis. Hence:

$$\lim_{n\to\infty} \sin^{2n+2}(\zeta) = 0 \tag{4.37}$$

This yields the following result for the limit:

$$\lim_{n\to\infty} S_{\mathrm{n}} = \frac{1}{1-\sin^2(\zeta)} \tag{4.38}$$

From trigonometry:

$$\sin^2(\zeta) + \cos^2(\zeta) = 1 \tag{4.27}$$

Hence the limit may be written as show in Equation (4.39), which can be substituted in the sum of Equations (4.10) and (4.16)

$$\lim_{n\to\infty} S_{\mathrm{n}} = \frac{1}{\cos^2(\zeta)} \tag{4.39}$$

Finally Equations (4.9), (4.10), (4.15) and (4.16) can be rewritten using the result from the series expansion and limit-analysis. The results are shown in Equations (4.40) through (4.43). Again noting that, in Sub-section 4.3.2, it is proven that Equations (4.41) and (4.43) are equal.

For the upper node:

$$F_{\mathrm{h_{bar}}} = F_{\mathrm{res}} \cdot \cos(\beta) + F_{\mathrm{res}} \cdot \sin(\beta) \tan(\zeta) \tag{4.40}$$

$$F_{\mathrm{v_{bar}}} = F_{\mathrm{res}} \cdot \sin(\beta) \frac{1}{\cos(\zeta)} \tag{4.41}$$

And for the lower node:

$$F_{\mathrm{h_{bar}}} = F_{\mathrm{res}} \cdot \cos(\eta) - F_{\mathrm{res}} \cdot \sin(\eta)\tan(\zeta) \tag{4.42}$$

$$F_{\mathrm{v_{bar}}} = F_{\mathrm{res}} \cdot \sin(\eta)\,\frac{1}{\cos(\zeta)} \tag{4.43}$$

Decomposed forces

Now that the resultant force has been decomposed in (non-)orthogonal components, depending on the cabin definition, the magnitude of the components may be determined. For the forces due to the hoop-stresses in each of the shells for sections of unit length Δl, it follows that:

$$F_1 = \sigma_{\theta_1} \cdot \Delta l \cdot t_1 \tag{4.44}$$

$$F_2 = \sigma_{\theta_2} \cdot \Delta l \cdot t_2 \tag{4.45}$$

$$F_3 = \sigma_{\theta_3} \cdot \Delta l \cdot t_3 \tag{4.46}$$

Where the hoop-stress, for pressure differential Δp, can be found using Equations (4.47), (4.48) and (4.49).

$$\sigma_{\theta_1} = \frac{\Delta p \cdot R_1}{t_1} \tag{4.47}$$

$$\sigma_{\theta_2} = \frac{\Delta p \cdot R_2}{t_2} \tag{4.48}$$

$$\sigma_{\theta_3} = \frac{\Delta p \cdot R_3}{t_3} \tag{4.49}$$

The resultant force in the upper node can now be rewritten according to Equation (4.50) yielding Equations (4.51) and (4.52) for the components in the horizontal and “vertical” direction.

$$F_{\mathrm{res_{top}}} = F_1 - F_2 = \Delta p \cdot \Delta l \cdot (R_1 - R_2) \tag{4.50}$$

$$F_{\mathrm{h_{bar}}} = \Delta p \cdot \Delta l \cdot (R_1 - R_2) \cdot (\cos(\beta) + \sin(\beta)\tan(\zeta)) \tag{4.51}$$

$$F_{\mathrm{v_{bar}}} = \Delta p \cdot \Delta l \cdot (R_1 - R_2) \cdot \sin(\beta)\,\frac{1}{\cos(\zeta)} \tag{4.52}$$

The same can be done for the resultant force in the lower node (4.53), yielding Equations (4.54) and (4.55).

$$F_{\mathrm{res_{bottom}}} = F_3 - F_2 = \Delta p \cdot \Delta l \cdot (R_3 - R_2) \tag{4.53}$$

$$F_{\mathrm{h_{bar}}} = \Delta p \cdot \Delta l \cdot (R_3 - R_2) \cdot (\cos(\eta) - \sin(\eta)\tan(\zeta)) \tag{4.54}$$

$$F_{\mathrm{v_{bar}}} = \Delta p \cdot \Delta l \cdot (R_3 - R_2) \cdot \sin(\eta)\,\frac{1}{\cos(\zeta)} \tag{4.55}$$

4.3.2 Normal Force in the "Vertical" Wall

It can be proven that, for all fuselage constructions, with the tangency condition in the nodes fulfilled, the "vertical" component of the resultant force in the upper node is exactly the same as the one derived for the lower node. This condition is also a requirement for static equilibrium. The proof follows below. The resultant forces in the vertical wall for the upper and lower node from Equations (4.52) and (4.55), respectively, must be equal. Hence, the following must hold:

$$(R_1 - R_2) \cdot \sin(\beta) \frac{1}{\cos(\zeta)} = (R_3 - R_2) \cdot \sin(\eta) \frac{1}{\cos(\zeta)} \tag{4.56}$$

$$(R_1 - R_2) \cdot \sin(\beta) = (R_3 - R_2) \cdot \sin(\eta) \tag{4.57}$$

$$R_1 \sin(\beta) - R_3 \sin(\eta) = R_2 (\sin(\beta) - \sin(\eta)) \tag{4.58}$$

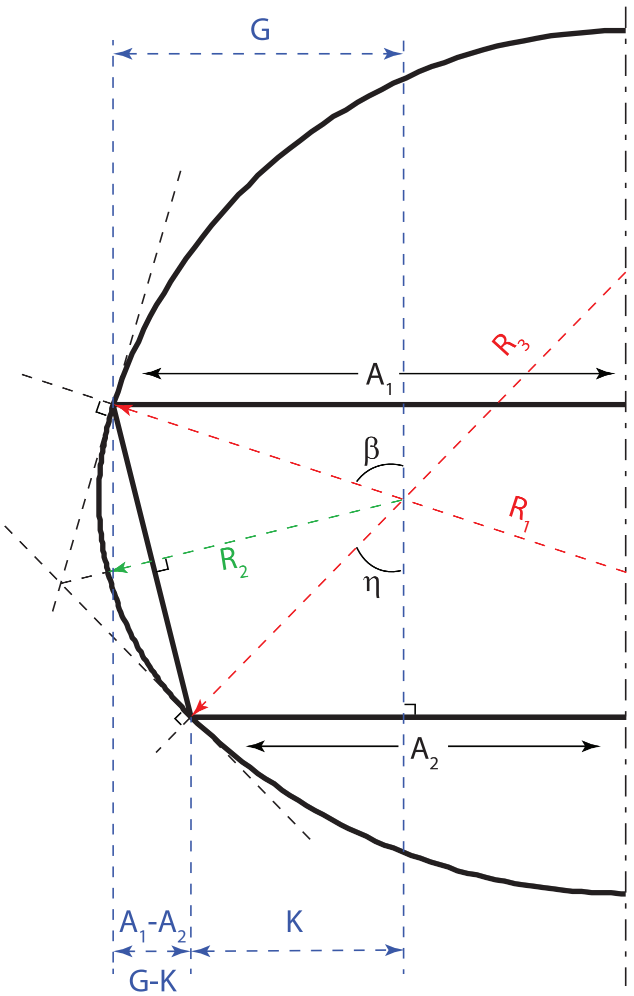

Figure 4.7: 'Oval-Fuselage' semi cross-section for geometric analysis

From Figure 4.7 the following geometric relations can be obtained:

$$\sin(\beta) = \frac{G}{R_2} = \frac{A_1}{R_1} \tag{4.59}$$

$$\sin(\eta) = \frac{K}{R_2} = \frac{A_2}{R_3} \tag{4.60}$$

Using these relations Equation (4.58) can be rewritten as:

$$A_1 - A_2 = R_2 \left(\frac{G}{R_2} - \frac{K}{R_2} \right) \tag{4.61}$$

$$A_1 - A_2 = G - K \tag{4.62}$$

Examining Figure 4.7, it can be seen that for this specific geometry this relation is always true when the tangency condition is satisfied. Hence the "vertical" components are always identical, satisfying static equilibrium.

4.3.3 Dimensions of the Fuselage Cross-Section

Now that the radii of the shells and the resultant forces are determined, the dimensions of the shells, walls and floor and ceiling can be calculated.

Shells

The thickness of the shells is determined from the hoop-stress for a certain inner radius, assuming that this stress may not exceed the fatigue stress in tension. Imposing a safety factor j yields the following relations for the thickness of the shells:

$$t_1 = \frac{j \cdot \Delta p \cdot R_1}{\sigma_{\mathrm{fatigue_t}}} \tag{4.63}$$

$$t_2 = \frac{j \cdot \Delta p \cdot R_2}{\sigma_{\mathrm{fatigue_t}}} \tag{4.64}$$

$$t_3 = \frac{j \cdot \Delta p \cdot R_3}{\sigma_{\mathrm{fatigue_t}}} \tag{4.65}$$

Walls

The walls are sized for tension, since R_2 is always smaller than R_1 and R_3, according to the magnitude of the "vertical" component of the resultant force. Hence the thickness of the wall, for a unit fuselage length Δl can be related to the fatigue stress and the normal force.

$$t_{\mathrm{wall}} = \frac{j \cdot F_{\mathrm{v_{bar}}}}{\sigma_{\mathrm{fatigue_t}} \cdot \Delta l} \tag{4.66}$$

Floor and Ceiling

The floor and ceiling are modeled as sandwich panels, where the stiffness of the core is not included in the analysis, making the analysis rather conservative. The sandwich panels are considered to be buckling critical. From literature[28], the maximum buckling force for the first buckling mode of an unsupported member of length L, is given by:

$$F_{\mathrm{crit}} = \frac{\pi^2 E_{\mathrm{f}} I_{\mathrm{f}}}{L^2} \tag{4.67}$$

The area moment of inertia of the facings in Equation (4.67) is given by:

$$I_{\mathrm{f}} = 2 \cdot \left(\frac{1}{12} \Delta l \cdot t_{\mathrm{f}}^3 + t_{\mathrm{f}} \cdot \Delta l \cdot \left(\frac{t_{\mathrm{c}}}{2} + \frac{t_{\mathrm{f}}}{2} \right)^2 \right) \tag{4.68}$$

$$I_{\mathrm{f}} = \Delta l \cdot \left[\frac{1}{6} t_{\mathrm{f}}^3 + \frac{1}{2} t_{\mathrm{f}} \left(t_{\mathrm{c}} + t_{\mathrm{f}} \right)^2 \right] \tag{4.69}$$

In addition to the horizontal forces in the floor and ceiling due to pressurization, a compressive force due to the wing bending moment is added to obtain the critical buckling force. The wing bending moment at the intersection of the wing and the fuselage is modeled as a force couple acting at the upper and lower node in horizontal direction. This is schematically illustrated in Figure 4.8, for a certain lift distribution over the wing, causing the bending moment.

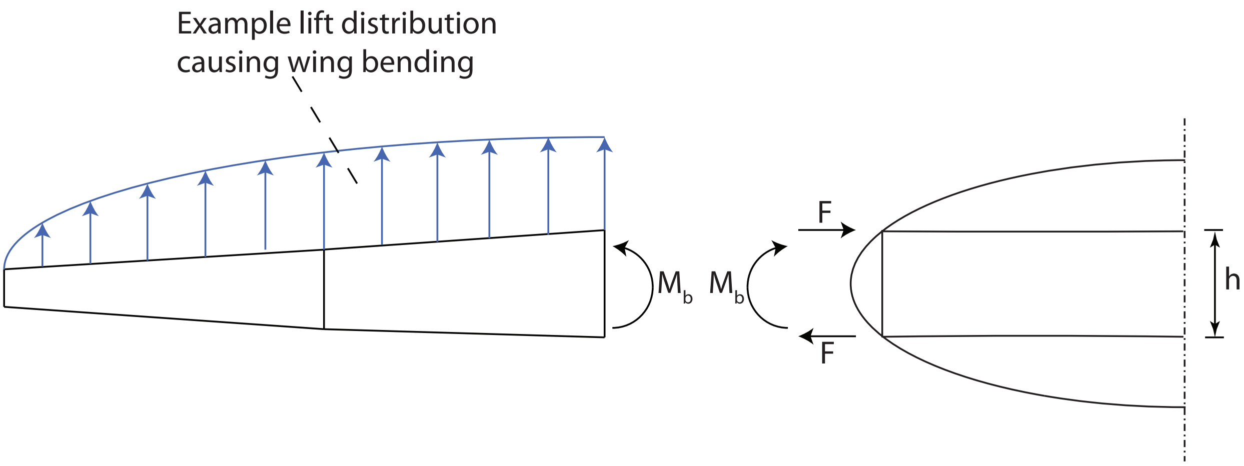

Figure 4.8: Schematic of the force couple due to wing bending at positive load factors

For positive load factors, the upper node will experience a compressive force and the lower node an additional tensile force, as shown in Figure 4.8. However, in the case of negative load factors, the opposite will occur.

The wing bending moment is determined following the application by Van Dommelen[7] of Torenbeek's method[5]. Here the bending moment in $1g$ flight at MTOW and maximum cruise angle of attack is determined from the lift distribution. This moment is multiplied by Van Dommelen with either the maneuvering load factor or the gust load factor, whichever is critical. From airworthiness regulations[9] the maximum maneuvering load factor ($n_{\mathrm{max}} = 2.5$), multiplied by a safety factor of 1.5, yields $n_{\mathrm{ult_{max}}} = 3.75$. The maximum gust load factor is determined by Van Dommelen[7], following the explanation by Torenbeek[5]. In both cases bending relief due to the engines is considered. Bending relief due to fuel is only considered when the maneuvering load is critical. The minimum maneuvering load factor according to regulations[9] is given by $n_{\mathrm{ult_{min}}} = -1$, which is also multiplied with a safety factor of 1.5 to obtain $n_{\mathrm{min}} = -1.5$, and again the minimum gust load factor is determined as explained in Torenbeek[5].
As shown in Figure 4.8, the upper member should be sized for positive load factors and the lower should be sized for negative load factors. This way the dimensions of both members are determined for the maximum force occurring. The bending moment corrected for bending relief is decomposed in a force couple, as shown in Figure 4.8 and a compressive force equal to one of the components is added to the buckling equation. The force couple is related to the bending moment from the wings, the distance between the floor and ceiling and the length of the wingbox chord at the wing fuselage intersection. The resulting compressive forces are shown in Equations (4.70) and (4.71):

$$\frac{F_{\mathrm{n_{max}}}}{\Delta l} = \frac{n_{\mathrm{ult_{max}}} \cdot (M_{\mathrm{BL}} - M_{\mathrm{Bf}} - M_{\mathrm{Beng}})}{h \cdot d} \tag{4.70}$$

$$\frac{F_{\mathrm{n_{min}}}}{\Delta l} = \frac{|n_{\mathrm{ult_{min}}}| \cdot (M_{\mathrm{BL}} + M_{\mathrm{Bf}} + M_{\mathrm{Beng}})}{h \cdot d} \tag{4.71}$$

Here, M_{Bf} and M_{Beng} are the bending moments due to fuel and engines, respectively, h is the distance between the upper and lower horizontal members and d is the distance over which the wing is connected to the centre section, the wing box chord. Note the sign-change in (4.71), as in case of negative load factors, the engine and fuel do not cause relief, as they act in the same direction as the bending moment due to lift.
Combining this information with the decomposed forces means that both the ceiling and the floor can be sized according to the following relations, respectively:

$$F_{\mathrm{n_{max}}} + j \cdot \Delta p \Delta l \left(R_1 - R_2\right)\left(\cos\left(\beta\right) + \sin\left(\beta\right)\tan\left(\zeta\right)\right) = \frac{\pi^2 E_{\mathrm{f}}}{\left(2A_1\right)^2} \cdot \Delta l \cdot \left[\frac{1}{6} t_{\mathrm{f_1}}^3 + \frac{1}{2} t_{\mathrm{f_1}} \left(t_{\mathrm{c_1}} + t_{\mathrm{f_1}}\right)^2\right] \tag{4.72}$$

$$F_{\mathrm{n_{min}}} + j \cdot \Delta p \Delta l \left(R_3 - R_2\right)\left(\cos\left(\eta\right) - \sin\left(\eta\right)\tan\left(\zeta\right)\right) = \frac{\pi^2 E_{\mathrm{f}}}{\left(2A_2\right)^2} \cdot \Delta l \cdot \left[\frac{1}{6} t_{\mathrm{f_2}}^3 + \frac{1}{2} t_{\mathrm{f_2}} \left(t_{\mathrm{c_2}} + t_{\mathrm{f_1}}\right)^2\right] \tag{4.73}$$

Here Δl drops out of the equation, still leaving two unknown thicknesses per equation. Therefore each of the equations is minimized for the mass per unit length according to the following optimization:

$$\min(J) = 2t_\mathrm{f} \cdot \rho_\mathrm{f} + t_\mathrm{c} \cdot \rho_\mathrm{c} \tag{4.74}$$

subject to:

$$F_{\mathrm{n_{ult}}} + j \cdot F_{\mathrm{h_{bar}}} - \frac{\pi^2 E_\mathrm{f}}{L^2} \cdot \Delta l \cdot \left[\frac{1}{6}t_\mathrm{f}^3 + \frac{1}{2}t_\mathrm{f}\left(t_\mathrm{c} + t_\mathrm{f}\right)^2\right] < 0 \tag{4.75}$$

$$-t_\mathrm{f} < 0 \tag{4.76}$$

$$-t_\mathrm{c} < 0 \tag{4.77}$$

In the MATLAB code, this is performed by using an input range for the facing thickness and calculating the corresponding thickness of the core that would be required according to Equations (4.72) and (4.73).

4.3.4 Mass of the Fuselage Cross-Section

When all thicknesses of the components have been found, the total mass per unit length, Δl, of a fuselage section can be calculated by multiplying the cross-sectional area of each section with its density. The following sub-sections show the equations to calculate the mass per structural component.

Mass of the "vertical" walls

The mass of the two "vertical" walls of length B is given by:

$$\frac{m_\mathrm{walls}}{\Delta l} = 2 \cdot t_\mathrm{wall} \cdot B \cdot \rho_\mathrm{wall} \tag{4.78}$$

Mass of the sandwich floor and ceiling

The mass of the sandwich panels is split in the upper and lower panel in Equations (4.79) and (4.80), respectively.

$$\frac{m_\mathrm{top}}{\Delta l} = 2A_1 \cdot 2t_{\mathrm{f}_1} \cdot \rho_\mathrm{f} + 2A_1 \cdot t_{\mathrm{c}_1} \cdot \rho_\mathrm{c} \tag{4.79}$$

$$\frac{m_\mathrm{bottom}}{\Delta l} = 2A_2 \cdot 2t_{\mathrm{f}_2} \cdot \rho_\mathrm{f} + 2A_2 \cdot t_{\mathrm{c}_2} \cdot \rho_\mathrm{c} \tag{4.80}$$

Mass of the shells

The mass of the shells is calculated per part of the total pressure shell. However, first the frames to prevent general buckling instability of the shell must be accounted for. The actual frame pitch is not calculated, however an approach for the sizing of buckling critical structures from the National Aeronautics and Space Administration (NASA) is adopted[36] to calculate the weight penalty. The methods derives that for buckling critical shells, the equivalent thicknesses of the shell and frames at a certain frame spacing to be $\frac{3}{4}\bar{t}$ and $\frac{1}{4}\bar{t}$, respectively. Where the total equivalent thickness of the structure for buckling critical structure is given by:

$$\bar{t} = \bar{t}_{\mathrm{S_B}} + \bar{t}_{\mathrm{F_B}} \tag{4.81}$$

For the oval fuselage it is assumed that the buckling critical thickness of the shell can be made equal to the previously computed thickness to cope with pressurization. This means that the equivalent thickness of the frames is $\frac{1}{3}$ of that of the shell thickness. Therefore a factor $\frac{4}{3}$ is included when computing the mass of the shells. The extra thickness is disregarded in any structural calculations, as it merely serves as a mass estimate and in its equivalent form does not yield any structural benefits. In Equations (4.82), (4.83) and (4.84), the additional factors $K_{\mathrm{lg}} = 1.12$ and $K_{\mathrm{doors}} = 1.25$, taken from Raymer[26] are added. Raymer has been used such that the same factors as for the multi-bubble design are used. Moreover, this method was the only weight estimation method found, that imposed a factor for both the landing gear and aperture cut-outs. These factors account for weight penalties imposed on the shell due to cut-outs in the shell for doors, windows and landing gear. The mass of the top shell, the mass of the sum of the two side shells and the mass of the bottom shell are given by Equations (4.82), (4.83) and (4.84), respectively.

$$\frac{m_{\mathrm{R_1}}}{\Delta l} = K_{\mathrm{lg}} \cdot K_{\mathrm{doors}} \cdot \frac{4}{3} \cdot \beta \left((R_1 + t_1)^2 - R_1^2 \right) \rho_{\mathrm{shell}} \tag{4.82}$$

$$\frac{m_{\mathrm{R_2}}}{\Delta l} = K_{\mathrm{lg}} \cdot K_{\mathrm{doors}} \cdot \frac{4}{3} \cdot 2 \cdot \theta \left((R_2 + t_2)^2 - R_2^2 \right) \rho_{\mathrm{shell}} \tag{4.83}$$

$$\frac{m_{\mathrm{R_3}}}{\Delta l} = K_{\mathrm{lg}} \cdot K_{\mathrm{doors}} \cdot \frac{4}{3} \cdot \eta \left((R_3 + t_3)^2 - R_3^2 \right) \rho_{\mathrm{shell}} \tag{4.84}$$

Total mass of the fuselage cross-section

Combining the masses of the structural components yields the total mass per unit length:

$$\frac{m}{\Delta l} = \frac{m_{\mathrm{walls}}}{\Delta l} + \frac{m_{\mathrm{top}}}{\Delta l} + \frac{m_{\mathrm{bottom}}}{\Delta l} + \frac{m_{\mathrm{R_1}}}{\Delta l} + \frac{m_{\mathrm{R_2}}}{\Delta l} + \frac{m_{\mathrm{R_3}}}{\Delta l} \tag{4.85}$$

The computed mass accounts for structural penalties due to cut-outs and also takes into account the lateral forces transfered by the wing bending moment. However, before finalizing the weight prediction of the fuselage section of the BWB, the longitudinal stresses are checked against the limiting compressive and tensile fatigue stresses. This is described in Section 4.4.

4.4 Longitudinal Fuselage Stresses

From Section 4.1, Section 4.2 and Section 4.3 an estimate of the operative empty weight of the BWB has been determined. The fuselage section has only been sized for pressurization and an extra weight penalty has been imposed for the frames preventing buckling instability, however, it must also be checked whether the structure is capable of withstanding the longitudinal stresses, caused by longitudinal bending, axial acceleration and pressurization stress in longitudinal direction.

This check is performed according to a method described by a NASA technical memorandum on fuselage and wing weight estimation of transport aircraft [36]. For the sake of completeness all three stresses will be considered in the elaboration in this section. However, in the actual sizing of the aircraft, it is assumed that the aircraft is operating in steady flight, hence without axial acceleration in flight direction. This can be assumed since the acceleration in g has a small contribution to the overall stress, as not to disrupt the comfort of the passengers. The aircraft is considered at maximum take-off weight, with maximum payload.

4.4.1 Stress Contributions

This sub-section illustrates the contributions to the longitudinal stress that are considered in the MATLAB program. The equation of the three contributions with there variables are briefly introduced.

Pressurization

Pressurization stresses in longitudinal direction is always tensile, as illustrated by Figure 4.1, and follows from the equation for hoop stress. For the three shells, the stress is dependent on the thickness of the shell and its radius in meters and the pressure differential in Pascals according to Equations (4.86), (4.87) and (4.88).

$$\sigma_{\mathrm{x_{p1}}} = \frac{\Delta p \cdot R_1}{2t_1} \tag{4.86}$$

$$\sigma_{\mathrm{x_{p2}}} = \frac{\Delta p \cdot R_2}{2t_2} \tag{4.87}$$

$$\sigma_{\mathrm{x_{p3}}} = \frac{\Delta p \cdot R_3}{2t_3} \tag{4.88}$$

Figure 4.9 illustrates the tensile stresses due to pressurization at some location in the fuselage.

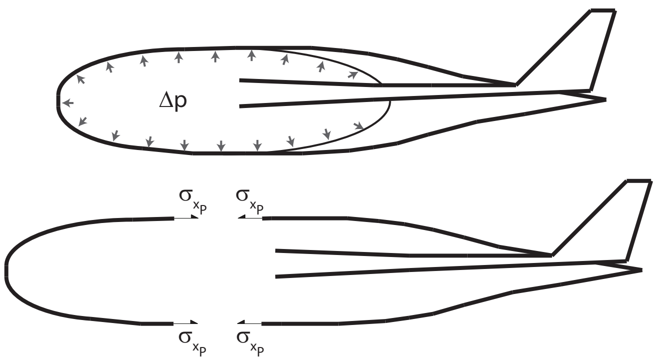

Figure 4.9: Schematic illustration of pressurization stresses in longitudinal direction

Axial Acceleration

Though the axial acceleration in flight direction, N_x, is set to zero, the equation is still modeled in MATLAB . Stress due to axial acceleration is dependent on the weight in front of the x-station when x is in front of the engine inlet and the mass aft of the station when x is aft of the engine exhaust. The area, A, is the total area of all structural material in the cross-section. Even when considering the total weight of the aircraft, of the order 10^6, an axial acceleration in the order of $10g$ would be required when the area is in the order of $1\mathrm{m}^2$ to have a significant contribution to the longitudinal stress. This would then be 10MPa with a maximum fatigue stress in the order of 130MPa to 160MPa, whereas any axial acceleration larger than $1g$ will already disrupt passenger comfort significantly.

$$\sigma_{\mathrm{x_A}} = \frac{N_\mathrm{x} \cdot W}{A} \tag{4.89}$$

Figure 4.10 illustrates stresses due to axial acceleration at two locations. In front of the engine inlet compressive stresses will occur and aft of the engine exit tensile stresses will occur.

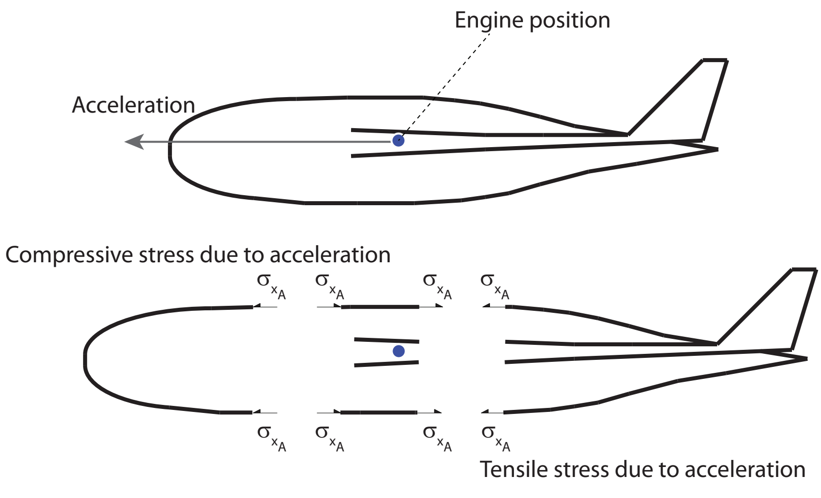

Figure 4.10: Schematic illustration of acceleration stresses in longitudinal direction

Longitudinal Bending

Longitudinal bending, due to sagging of the fuselage is modeled according to Equation (4.90), which depends on the distance z from the centroid of the section and the second moment of area about the y-axis through this centroid, I_{yy}.

$$\sigma_{\mathrm{x_B}} = \frac{M \cdot z}{I_{\mathrm{yy}}} \tag{4.90}$$

The area moment of inertia of all structural members shown in Figure 3.9 about centroid of the cross-section is determined using Steiner's theorem, or parallel axis theorem [37]. The centroid of the cross-section is determined by weighing the structural members according to their area, assuming the same material density for all aluminium members and ignoring the core of the sandwich panels. This core is also ignored in the sizing, however, not in the weight, to find a conservative estimate. The bending moment stresses in the fuselage are illustrated in Figure 4.11.

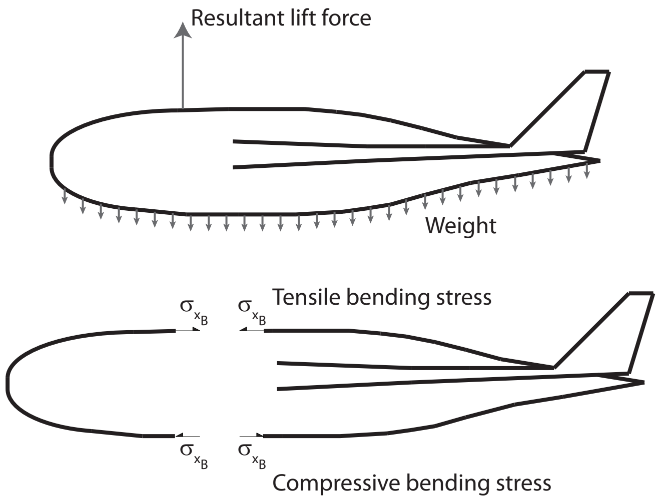

Figure 4.11: Schematic illustration of bending stresses in longitudinal direction

The front and aft of the fuselage are unsupported and the aircraft is 'suspended' from the resultant lift force, causing the fuselage to sag. This sagging introduces bending in the aircraft, tension at the top and compression at the bottom, as illustrated by Figure 4.11. In the calculation, the total mass of the fuselage is taken into account, including payload. The wings are assumed to carry themselves, including the fuel and any wing-mounted tail planes. Therefore, only the lift resultant over the fuselage sections is taken into account, as calculated by Tornado [27]. In reality the lift force would be a distributed load, however, a worst-case scenario is modeled to evaluated the stresses. In this worst-case scenario the lift resultant over the fuselage sections acts in one point, whereas the weight is distributed. The resultant lift force is modeled in the centre of pressure over all fuselage sections.

4.4.2 Longitudinal Stresses

From the different stress contributions, the compressive and tensile stresses are determined by adding the contributions as explained in Sub-section 4.4.1, depending on the position along the fuselage length that is considered. The stresses are determined at four locations per cross-section:

- Top of the fuselage cross-section in the upper shell
- Bottom of the fuselage cross-section in the lower shell
- Upper node for the side shell
- Lower node for the side shell

At these positions, the distance with respect to the centroid is maximum for each particular shell. Hence, the bending stress will be maximum. The addition of these contributions yields the total longitudinal stress, which is then compared with the maximum compressive or tensile stress, determined from fatigue loading. Should the longitudinal stresses be larger than the limiting fatigue stresses, then the shell thickness of the considered fuselage section is increased until this is no longer the case.

4.5 Balance

The centre of gravity (CG) depends on the positions of all components of the empty aircraft and that of payload and fuel. For the method to calculate the CG position, consult the thesis on the multi-bubble BWB by Van Dommelen[7]. With respect to the multi-bubble BWB only the calculation of the empty weight CG has been significantly recoded. The effect of fuel and payload determination has remained the same, for more information on this, consult the thesis work on the multi-bubble[7]. This section briefly explains the calculation of the empty weight CG and lists the CG position of the various components.

The CG position of the aircraft in OEW configuration can be calculated before payload and fuel are taken into account, by taking the moment of all OEW components about a reference point. The nose of the aircraft is used as a reference position and the sum of the moments is divided by the sum of the mass of all components to find the x-position of the centre of gravity with respect to the nose of the BWB. A similar approach is adopted for the y- and z-position of the CG, where the centre line of the aircraft and the line through $z = 0$ are used as reference points, respectively. Table 4.1 shows an overview of the different components and their centre of gravity locations.

Table 4.1: Location of weight components

Component	Centre of Gravity Location
Wingbox	Outer wing sections, per trunk. Dependent on geometry and amount of material
Wing LE's	Outer wing sections, per trunk. Halfway between LE and front spar
Wing TE's	Outer wing sections, per trunk. At a third of the distance between aft spar and TE
Cabin components	Overall CG computed via the weight of the cross-sections, includes all OEW items located in the cabin weighted for surface area per section
Flight deck	All OEW items in the nose and on flight deck, estimated at 2 meters from the nose
Vertical tail	40% of MAC of the fin[35]
Landing gear	At calculated positions, halfway between length
Engine group	Halfway between engine position
Fuel systems	At fuel tank centre of gravity, volume weighted
APU	90% chord of first wing section[7]
Trapped fuel/oil	At fuel tank's centre of gravity
Cargo handling floor	Calculated over cargo deck grid for upper and lower deck, dependent on amount of cargo per grid cell

Some of the components listed in this table actually contain multiple OEW items, as these are distributed over the component. The items are then averaged by e.g. volume or surface area of the considered section, the paint for example is split amongst wing and cabin. In Figure 4.12 an example of the overall CG position of a BWB for 400 passengers is shown. The locations of the CG positions of the different groups are also shown. The cabin group in this figure includes the flight deck, cabin, APU and cargo handling. The wing group includes the fuel systems, trapped fuel and oil and primary and secondary structure of the outer wings.

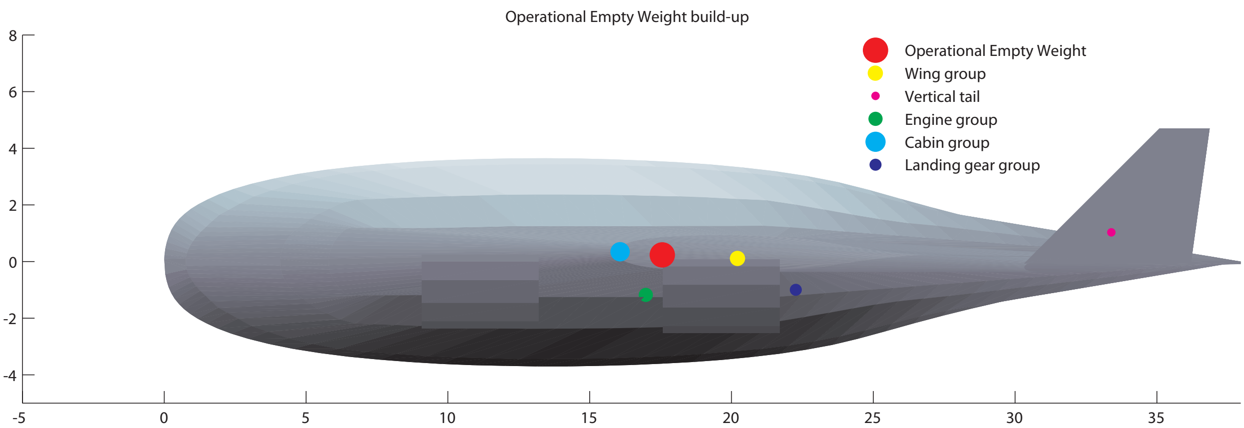

Figure 4.12: Longitudinal CG positions of the main mass groups

CHAPTER 5

CONCEPT ANALYSIS

This chapter presents the results of the performance analysis of the 'oval-fuselage' BWB. The previously discussed weight estimation methodology and geometry parameterization have been integrated in the optimization program that was presented in Chapter 3. Section 5.1 deals with the definition of the concepts and their configuration as inputs to the actual optimizer. The results are presented and analyzed in Section 5.2, with a more detailed explanation of the 400 passenger concept than for the others, to demonstrate the capabilities of the optimization tool. The 'oval-fuselage' is then compared to the multi-bubble BWB and conventional aircraft in Section 5.3, to form a critical judgment on the feasibility of the concept.

5.1 Concept Definition

As explained in Chapter 3, every optimization is run from a predefined concept. This concept is a general description of the BWB under consideration and is nothing more than a data structure containing the configuration of the BWB and an input vector for the optimization. The configuration used for all concepts examined in this chapter feature wing mounted engines, with aft-swept wings. As a vertical stabilizer, winglets are used. The aft-swept wings and wing-mounted stabilizer are commonly found in literature[2, 21, 38]. The positioning of the engines under the wings was chosen for accessibility and convenience. With body mounted engines, the aft section of the fuselage could for example not, or rather difficultly, be used as a control surface. Moreover the conventional high-bypass ratio turbo-fan engines are supplied with cleaner airflow and provide bending relief to the wings.

The components of the data structure used for the concept definition has remained unchanged with respect to the one used for the multi-bubble BWB. Their content however, has changed. The data structure used for all 'oval-fuselage' concepts is shown in Table 5.1

Table 5.1: Data structure for the 'oval-fuselage' BWB

Variable	**Data**
Vertical tail configuration	winglet
Engine vector	'wing' 'wing' 'wing' 'wing'
	'wing' 'wing' for 200 passenger concept
Airfoil vector	'customnocamber' 'customnocamber' 'customnocamber'
	'customnocamber' 'customnocamber' 'customnocamber'
Input vector	x0(1:19) see Sub-section 5.1.1

The airfoil vector is not changed with respect to the original program, however, only the fifth and sixth entry of its inputs are used. The other airfoils are derived in the multi-model generator, as explained in Section 3.2. The actual airfoil that is used for the outer wing sections is also used for the centre line of the aircraft, it is explained in more detail in Sub-section 5.1.2. Note that the engine vector for the 200 passenger concept only has two engines, instead of four, for the larger 400 and 800 passenger concepts. The input vector has also been altered, it now contains 19 variables instead of the 30 variables used in the original program. A typical input vector is explained in Sub-section 5.1.1. Sub-section 5.1.3 and Sub-section 5.1.4 deal with a general description of the optimizer outputs and the discussion of the bounds and additional constraints to the optimization.

5.1.1 Input Vector

The input vector consists of 19 variables that describe the aircrafts outer and cabin geometry. In combination with the input data in Appendix B and the other entries in the data structure in Table 5.1, the entire aircraft can be created. As explained in Chapter 3, the input vector defines the starting point of the optimization. In Table 5.2 an overview of these 19 variables is shown. Figure 5.1 shows the cabin and section definition from Chapter 3 as a reference.

Table 5.2: Overview of the input vector for the 'oval-fuselage' optimizer

Input	**Description**
x1	Maximum width of the centre body, b_2 in Figure 5.1
x2	Length of the mid section, L_2 in Figure 5.1
x3	Maximum width of aft of the cabin, b_3 in Figure 5.1
x4	Length of front section, L_1 in Figure 5.1
x5	Length of aft section, L_3 in Figure 5.1

Continued on next page...

Table 5.2 – Continued

Input	Description
x6	Chord of section 5 (outer wing), in Figure 5.1
x7	Chord of section 6 (outer wing), in Figure 5.1
x8	Span wise position of section 5
x9	Span wise position of section 6
x10	Wing twist of the trunk between section 4 and section 5
x11	Wing twist of the trunk between section 5 and section 6
x12	LE sweep of the trunk between section 4 and section 5
x13	LE sweep of the trunk between section 5 and section 6
x14	Wing dihedral of the trunk between section 4 and section 5
x15	Wing dihedral of the trunk between section 5 and section 6
x16	Maximum thickness to chord ratio of the airfoil at section 5
x17	Maximum thickness to chord ratio of the airfoil at section 6
x18	Maximum thickness to chord ratio of the centre line airfoil, section 1
x19	Height of the vertical stabilizer

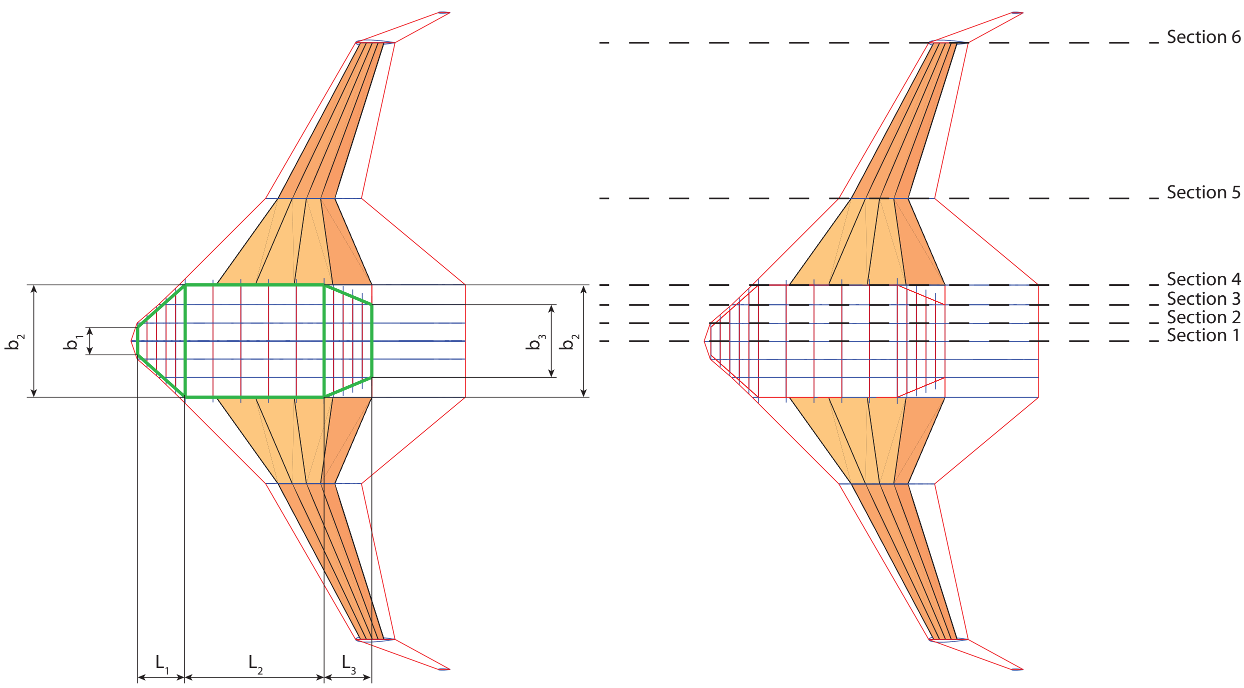

Figure 5.1: Schematic top view of an 'oval-fuselage' BWB, with wingbox, cabin and airfoil sections definition

5.1.2 Centre Line Airfoil

Input variable number 18 defines the maximum thickness to chord ratio of the centre line airfoil. This airfoil is the same type that is used for sections 5 and 6, in Figure 5.1. It is a customized version of a Whitcomb[39] supercritical airfoil. The customized airfoil, however, has no camber, making this airfoil suitable for the 'oval-fuselage', with a large, relatively thick section, that can provide the necessary clearance for the cabin section, with an upper and lower deck cargo hold. The camber has been removed, as the airfoil generated a too large pitch-down moment, too much lift and because symmetric airfoils have been assumed for the analysis, as the program cannot yet handle asymmetric airfoils (see Chapter 3). The trailing edge of the airfoil is relatively slender, such that the mass of a large trailing edge control surface is limited.

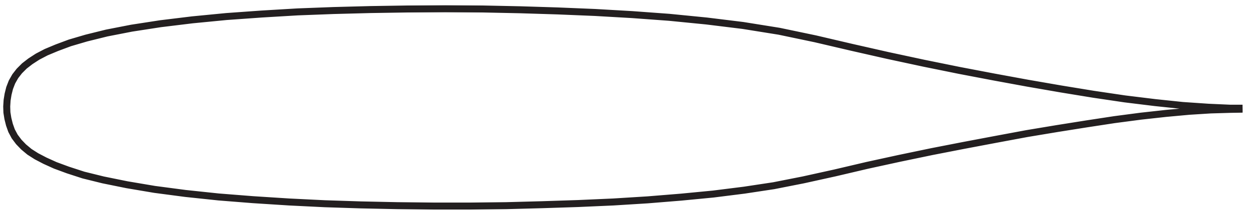

Figure 5.2: Customized supercritical airfoil profile

5.1.3 Optimizer Output

The output of the optimizer consists of a data structure containing the BWB per iteration. The data structure lists all geometric, weight, performance and stability properties of this particular aircraft. It also contains an array with the values of the non-linear constraints imposed on the aircraft. After an optimization, a post-processor can be run, that loads the data of every iteration and determines which iterates satisfy the constraints and then selects the aircraft with the best value for the objective function, i.e. the longest range with maximum payload on board. The post-processor also generates several plots. These are briefly listed here, however, for more information the thesis of Van Dommelen[7] should be consulted. The first plot shows the objective value, constraint violation and function value of all iterates up to the best performing aircraft. Another plot shows the shift in CG-position of the OEW and the planform. Furthermore a plot containing top, side and front view of the aircraft and a 3D view can be created. Also a performance summary is made, together with some output values on how the aircraft performs for the design range. New to the post-processor is the possibility to calculate the aircraft's pressurized volume and create a wireframe plot of the fuselage section and the wingbox structure. Also a print-out of the MMG input vector is shown. Examples of some plots can be found in Sub-section 5.2.1, on the analysis of the results for the 400 passenger 'oval-fuselage'.

5.1.4 Bounds and Constraints

The design space of the optimizer must constrained by means of bounds on the design values and linear and non-linear constraints on the model, otherwise the optimizer may find unrealistic solutions. The bounds are chosen such that an adequate design space is left for the optimizer to play with for aircraft of different dimensions, without the aircraft becoming too large or have unrealistic sweep angles or dihedrals etc. The thickness to chord ratio of the airfoils is also limited, for the outboard airfoil the lower bound is used to constrain the airfoil to realistic values, the upper to reduce the design space and thereby the optimization time, as higher thicknesses are not desirable for these high sweep angles and Mach numbers. The centre line airfoil is restricted by a minimum of 11%, although airfoils thinner than 15% are unlikely to be found for BWB aircraft and it has an upper limit of 20%, because too thick airfoils will dramatically decrease the aerodynamic performance. The bounds are presented in Table 5.3. The bounds for x6 upto and including x15 have been taken from the work of Van Dommelen[7]. For the 200 passenger configuration the upper bounds of x4 and x5 have been reduced to 7 meters, to avoid unfeasible solutions.

Table 5.3: Overview of the upper and lower bounds of the 'oval-fuselage' optimizer

Input	Description	Lower Bound	Upper Bound
x1	Maximum width of the centre body	7 [m]	20 [m]
x2	Length of the mid section	7 [m]	32 [m]
x3	Maximum width of aft of the cabin	6 [m]	15 [m]
x4	Length of front section	2 [m]	12 [m]
x5	Length of aft section	2 [m]	12 [m]
x6	Chord of section 5	4 [m]	20 [m]
x7	Chord of section 6	0.1 [m]	10 [m]
x8	Span of section 5	10 [m]	30 [m]
x9	Span of section 6	20 [m]	50 [m]
x10	Twist between section 4 and 5	-3°	3°
x11	Twist between section 5 and 6	-5°	5°
x12	LE sweep between section 4 and 5	10°	60°
x13	LE sweep between section 5 and 6	10°	60°
x14	Dihedral between section 4 and 5	-5°	5°
x15	Dihedral between section 5 and 6	-5°	5°
x16	Thickness to chord ratio at section 5	0.065	0.12
x17	Thickness to chord ratio at section 6	0.065	0.12
x18	Thickness to chord ratio of the centre line airfoil	0.11	0.2
x19	Height of the vertical stabilizer	2 [m]	6 [m]

Constraints

The optimization is subjected to the non-linear constraints listed in Table 5.4, for the description of these constraints, the thesis of J.L. van Dommelen[7] should be consulted.

Table 5.4: Constraints summary[7]

Parameter	Symbol	Constraints	Unit	Type
Wing span	b	< 80	m	Operational
Aircraft overall length	-	< 80	m	Operational
Cabin floor area	S_{cabin}	Cabin analysis	m^2	Payload
Cargo volume	V_{cargo}	Cabin analysis	m^2	Payload
Take-off distance	s_{TO}	Requirement	m	Top-level req
Landing distance	s_{landing}	Requirement	m	Top-level req
Stall speed TO/land	$V_{\text{stall}_{\text{TO}}}$	Requirement	m/s	Top-level req
Stall speed clean	V_{stall}	Requirement	m/s	Top-level req
Climb OEI1	γ_{OEI1}	> 0.012	-	Certification
Climb OEI2a	γ_{OEI2a}	> 0.000	-	Certification
Climb OEI2b	γ_{OEI2b}	> 0.000	-	Certification
Climb OEI2c	γ_{OEI2c}	> 0.012	-	Certification
Climb OEI3	γ_{OEI3}	> 0.032	-	Certification
Climb AOE1	γ_{AEO1}	> 0.021	-	Certification
Maximum trim deflection	-	< 12	deg	Feasibility
Minimum static margin	SM	> -10	%	Feas/Certification
Weathercock stability	C_{n_β}	> 0	-	Feas/Certification
Effective dihedral	C_{l_β}	< 0	-	Feas/Certification
Take-off rotation speed	$V_{\text{rot}_{\text{mc}}}$	$< V_{\text{stall}_{\text{TO}}}$	m/s	Feas/Certification
OEI rudder deflection	dr_{OEI}	< 25	deg	Certification
Drag div Mach outer trunk	M_{DD}	$\geq M_{\text{cr}}$	-	Feasibility
Drag div Mach outer trunk -1	M_{DD}	$\geq M_{\text{cr}}$	-	Feasibility
Minimum nose load	-	> 0.05	-	Certification
Maximum nose load	-	< 0.20	-	Certification
Nose landing gear x	x_{nlg}	$> x_{\text{nose}} + 0.5$	m	Feasibility
Main landing gear x	x_{mlg}	$> x_{\text{LE}}$	m	Feasibility
Main landing gear x	x_{mlg}	$< x_{\text{TE}}$	m	Feasibility

In addition to these constraints, several geometric constraints are active:

- Spanwise position of each section must be larger than that of the previous section
- Chord has to decrease along the span
- The thickness has to decrease along the span
- The leading edge sweep must decrease along the span

The decreasing thickness to chord ratio constraint is relaxed for the fuselage section, otherwise the creation of an oval fuselage would be very difficult, as the airfoil at section 4 may have a small thickness to chord ratio. Its absolute thickness however is larger than that of section 5. Additionally, a straight trailing edge on the fuselage section is implemented in all designs, to allow for the use of this section as a control surface.

5.2 Analysis & Results

In this section the results for the optimization of the 'oval-fuselage' BWB are presented, for a 200, 400 and 800 passenger configuration, with 10,000kg, 20,000kg and 40,000kg of additional cargo, respectively. The 400 passenger configuration is discussed in more detail, to give an overview of the attainable plots and to demonstrate the feasibility of the 'oval-fuselage' concept. A general overview of the 200 and 800 passenger concept is given, together with an alternative configuration for 400 passengers with a lower thickness to chord ratio. Several variables are summarized for later comparison to the multi-bubble BWB in Sub-section 5.3.1. The program generates a vast amount of data, of which only the most important to the concept comparison is discussed. The input variables for the optimization can be found in Appendix B.

5.2.1 400 Passenger 'Oval-Fuselage'

Figure 5.3 shows the resulting geometry of the 'oval-fuselage' BWB for 400 passengers and 20,000kg of payload. A three view drawing of the aircraft, with an additional 3D view, is shown. The aircraft looks familiar to what is commonly understood as a blended wing body. A significantly swept wing, to achieve a high enough critical Mach number on the outer sections and a large enough moment of the winglets around the centre of gravity, such that the rudder deflection in one engine inoperative conditions is within the certification limit. The fuselage section can be blended in more smoothly through the use of body-fairings, which may be applied in a more detailed design step.

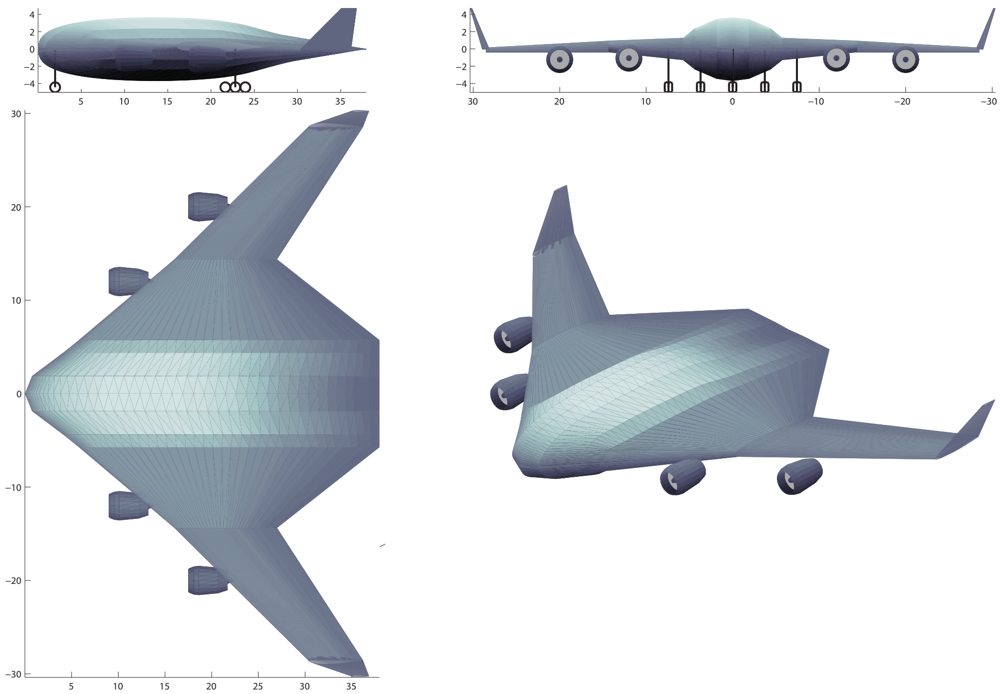

Figure 5.3: Three dimensional and 3-view drawing of the optimized 400 passenger BWB

Constraints Summary

Geometric constraints

Wing span	57 m	80 m
Aircraft length	37.9 m	80 m

Cabin constraints

Floor area	273 m^2	273 m^2
Cargo volume	283 m^3	158 m^3

Landing gear constraints

Min nose load	6.47 %	5 %
Max nose load	18.5 %	20 %
Nose gear pos	1.98 m	0.5 m
Min main gear pos	22.8 m	7.79 m
Max main gear pos	22.8 m	35.8 m

Field and climb performance

Take–off dist	2128 m	2500 m
Landing dist	2499 m	2500 m
Stall speed TO	63.3 m/s	70 m/s
Stall speed clean	69.1 m/s	80 m/s
Climb OEI1	5.38 %	1.2 %
Climb OEI2a	1.65 %	0 %
Climb OEI2b	5.38 %	0 %
Climb OEI2c	9.39 %	1.2 %
Climb OEI3	15.8 %	2.1 %
Climb AEO	14.9 %	3.2 %

Trim and stability

Max trim deflection	2.32°	12°
Min static margin	−3.01%	−10% MAC
Weathercock, Cn_β	0.0158	> 0
Eff dihedral, Cl_β	−0.0436	< 0
TO rot speed	28.9 m/s	70 m/s
OEI dr	24.7°	25°

Critical Mach number

Outer trunk	0.965	0.82
Outer trunk −1	0.821	0.82

Objective Function

Harmonic range:	15358 km	Target:	11000 km

Aircraft properties

Weights

MTOW	394.5 10^3 kg	100%
OEW	169 10^3 kg	42.8%
W_{pl}	64.4 10^3 kg	16.3%
W_f	161.1 10^3 kg	40.8%
EW	158.3 10^3 kg	40.1%

Aerodynamics

L/Dmax	25.7
Min α	1.69°
Max α	3.54°
Min δ	−0.526°
Max δ	2.32°
L/Dave	24.6
Wing area	1020 m^2
Aspect ratio	3.19

Performance

Fuel/Pax/km	0.0216
Best load case	1
Inner tanks loaded first,	
Inner tanks emptied first	
Max range BLC	20486 km
BLC CG travel	8.53 %
Clean CLmax	1.09
CLmax slats	1.3

Figure 5.4: Summary of design constraints for 400 passenger BWB

Figure 5.4 shows the summary of constraints of the optimized concept. Here, the aircraft's performance is presented. The 400 passenger concept has a harmonic range of 15358 kilometers, 4358 more than the design range of the aircraft. An OEW fraction of 42.8 percent is found, which is higher than the fraction often claimed in literature, however, it is comparable to, or even slightly lower than that of conventional airliners, to which the aircraft is compared in Sub-section 5.3.2. A maximum lift over drag ratio of 25.7 is found, with an average of 24.6 over cruise flight. Fuel consumption in cruise is low at 0.0216 kilograms per passenger kilometer. The aircraft has a maximum trim deflection of only 2.32°. Overall the results show an aircraft that is meeting the requirements and indicating the feasibility of the 'oval-fuselage' concept. One point of attention though, is the maximum angle of attack during cruise. At 3.54° it is slightly higher than the 3° stated as a maximum for passenger comfort in Liebeck[21], this angle of attack can be lowered by improving the aerodynamic performance of the aircraft, e.g. by using fairings or asymmetric airfoils. Whether or not 3.54° angle of attack, or 3° for that matter, is satisfactory for passenger comfort requires additional research. When proceeding with a more detailed design stage, it is possible to set an additional constraint on the maximum angle of attack during cruise. The 400 passenger configuration described here, has a maximum thickness to chord ratio of 19.4 % over the centre line. Since this is relatively large, a concept with a lower thickness, of 16.3% has been evaluated, as described in Sub-section 5.2.2. Also, the cabin design is close to the requirements for the optimized aircraft, though the cargo volume is oversized.

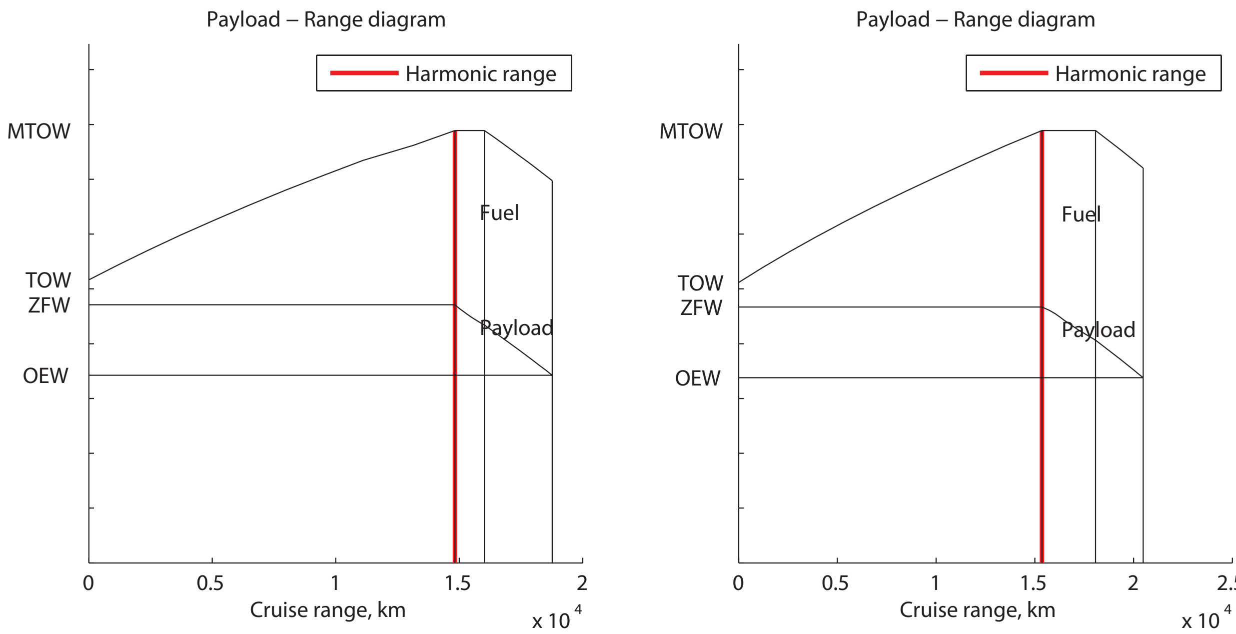

Figure 5.5: Payload-range diagram for 400 passenger BWB

In Figure 5.5, a comparison between the payload-range diagram of the input aircraft and the optimized aircraft is shown. The diagram clearly shows the improvements to the objective, namely the harmonic range of the aircraft, indicated in red. It also shows that the maximum fuel capacity is reached, after trading some payload for fuel weight. At full tank capacity, the aircraft could reach approximately 18,000km whilst still carrying more than half the maximum payload.

The CG position of the optimized aircraft at OEW and the CG travel, between 30.6% and 39.1% of the mean aerodynamic chord (MAC), are shown in Figure 5.6. The landing gear has been positioned at 49.5% MAC such that it is always aft of the CG position . The aerodynamic centre, at 36.2% MAC, can be slightly in front of the most aft CG position, requiring active stability systems.

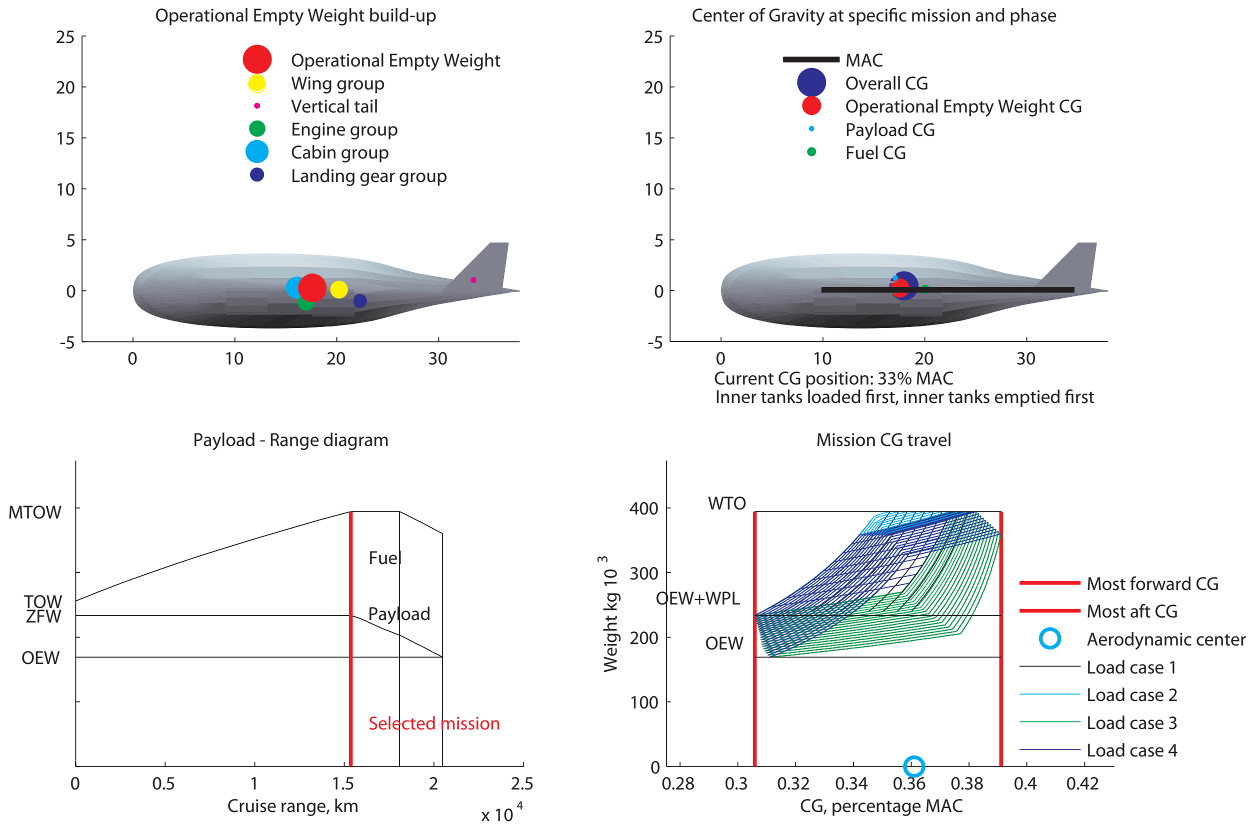

Figure 5.6: OEW centre of gravity position and loading diagram for 400 passenger BWB

The top view of the CG position in Figure 5.7 clearly shows the CG always being in front of the main landing gear. It also illustrates the changes in the planform from the initial aircraft to the optimized BWB very nicely. The increase in sweep is clearly noticeable and also a slight decrease in span.

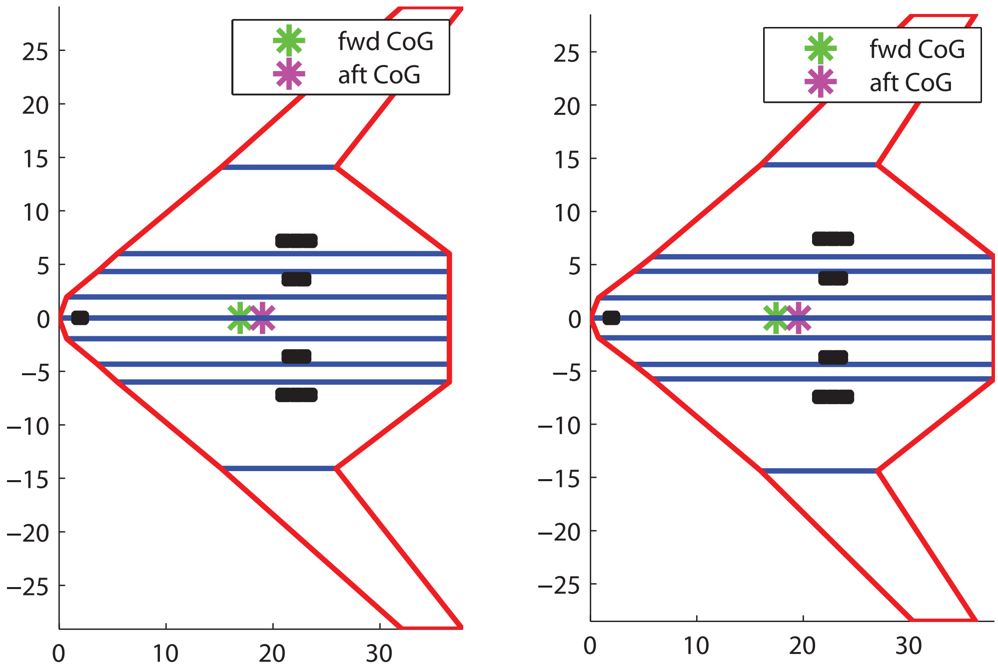

Figure 5.7: Top view of the CG positions for 400 passenger BWB, non-optimized on the left and optimized on the right

Figure 5.8 shows a schematic illustration of a cross-section of the aircraft's interior at the maximum width of the cabin. 12 meters of cabin width allow for 20 economy class seats and 4 aisles of 50 centimeters each and no more than 2 excuse-me seats to access a seat furthest from an aisle. 3 LD-3 unit load devices fit the inside of the lower cargo hold. The unused pressurized volume is indicated in light-grey, also high-lighting the bulk cargo area on the upper deck. Off-course the other pressurized area is accessible to allow the cargo to be secured.

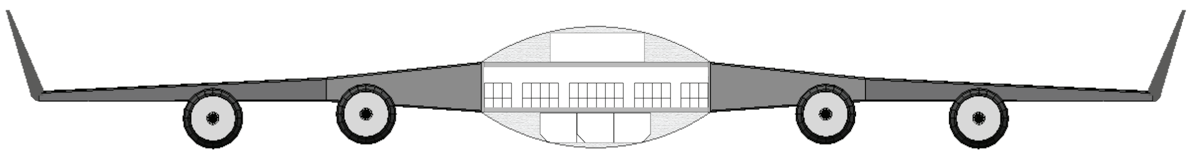

Figure 5.8: Interior schematic for 400 passenger BWB

Finally, in Figure 5.9 a 3D wireframe drawing is shown next to a 3D drawing of the surface to illustrates the aircraft's structural interior. The aft spar of the wingbox has been set to match the position of the rear pressure bulkhead of the cabin and the lateral load from the wings is applied to the sections within the wingbox chord at the intersection with the cabin. The drawing also shows that the trailing edge of the cabin section is unused and could be converted into a control surface.

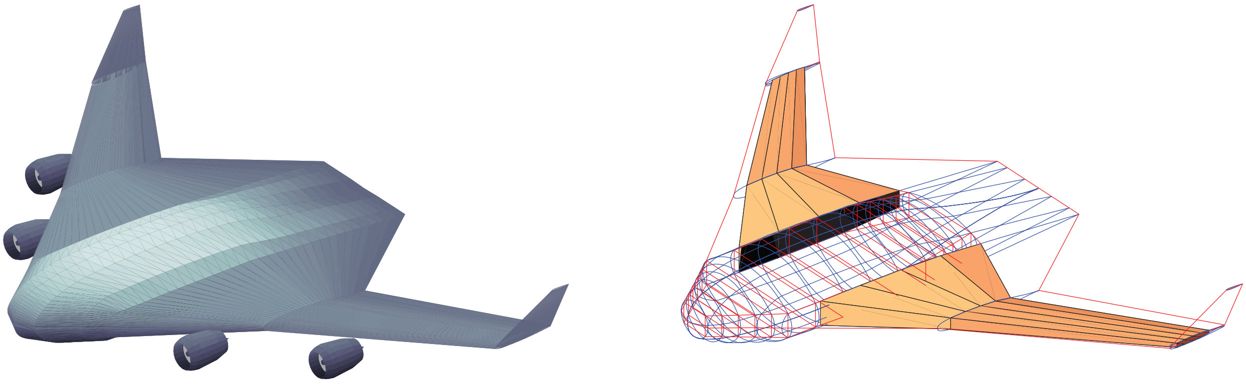

Figure 5.9: Surface and wireframe drawing, showing structural cabin of 400 passenger BWB

The aircraft's shell at the maximum cross-section has thicknesses of 7.1mm for the upper and lower arc and 1.2mm for the side arcs to withstand pressurization. The upper and lower shell are relatively thick because of the very large radius of curvature of these arcs. The OEW of the aircraft however is still at a respectable 42.8% as shown before. From data analysis it also followed that the structure is well capable of withstanding the longitudinal stresses. Shear forces and torques however have been outside of the scope and the level of complexity of this phase, therefore it is recommended for future research to determine the structure's resistance of these. The maximum thickness of the facings of the sandwich materials for the upper and lower beams have been found at 2.4mm and a core thickness of 50.4cm. These core thicknesses can be reached with foams, as used in this design, however, in reality multi-facing (multi-layer) sandwich members would be necessary to cope with wrinkling effects of sandwiches this thick, which have been disregarded at this design phase.

5.2.2 Alternative 400 Passenger 'Oval-Fuselage'

Since a relatively high thickness to chord ratio for the centre line airfoil of the 400 passenger oval fuselage BWB was found, it was decided to run a second optimization for this aircraft, starting with a different input vector (with an initial thickness to chord ratio of 16%), whilst maintaining the constraints. The result is a concept with a maximum thickness to chord ratio of 16.2%, shown in Figure 5.10. A 3-view drawing is presented in this case for comparison to the other 400 passenger concept, interestingly this aircraft features some anhedral in the outer most wing section. This also very clearly demonstrates the impact of choosing a different design vector for the optimization.

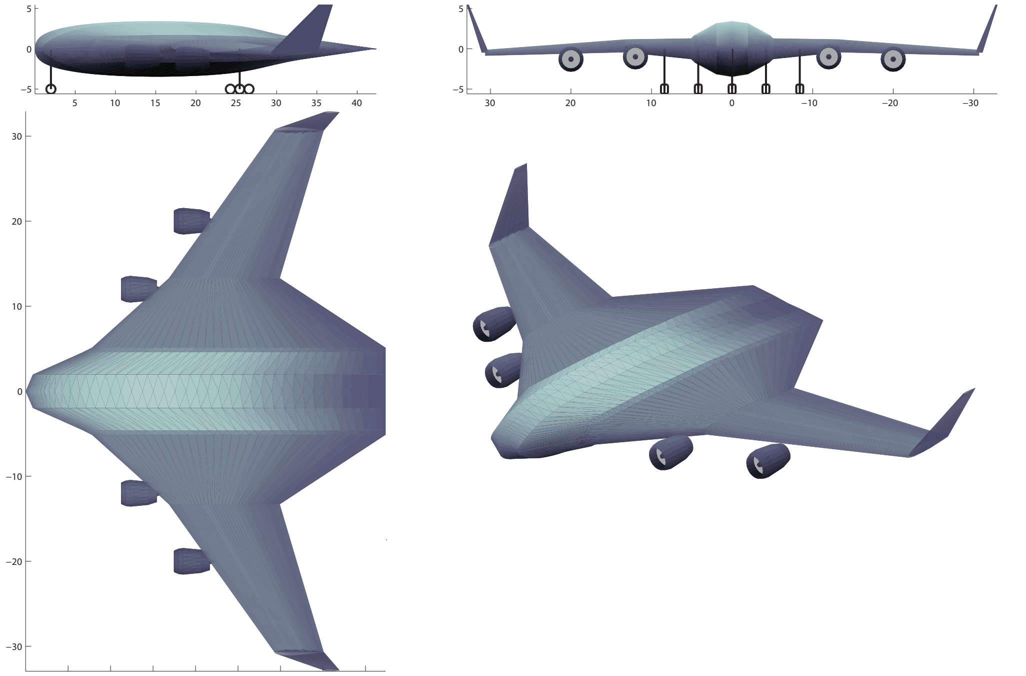

Figure 5.10: 3-view of the alternative 400 passenger oval fuselage BWB

Constraints Summary

Geometric constraints

Wing span	61.3 m	80 m
Aircraft length	42.4 m	80 m

Cabin constraints

Floor area	273 m^2	273 m^2
Cargo volume	174 m^3	158 m^3

Landing gear constraints

Min nose load	7.11 %	5 %
Max nose load	17.9 %	20 %
Nose gear pos	1.99 m	0.5 m
Min main gear pos	25.4 m	11.4 m
Max main gear pos	25.4 m	37.4 m

Field and climb performance

Take–off dist	1921 m	2500 m
Landing dist	2356 m	2500 m
Stall speed TO	59.3 m/s	70 m/s
Stall speed clean	65.1 m/s	80 m/s
Climb OEI1	5.61 %	1.2 %
Climb OEI2a	1.96 %	0 %
Climb OEI2b	5.61 %	0 %
Climb OEI2c	9.65 %	1.2 %
Climb OEI3	16.1 %	2.1 %
Climb AEO	15.2 %	3.2 %

Trim and stability

Max trim deflection	2.73°	12°
Min static margin	−4.14%	−10% MAC
Weathercock, Cn_β	0.0144	> 0
Eff dihedral, Cl_β	−0.041	< 0
TO rot speed	26.1 m/s	70 m/s
OEI dr	24.8°	25°

Critical Mach number

Outer trunk	0.866	0.82
Outer trunk −1	0.82	0.82

Objective Function

Harmonic range:	16024 km	Target:	11000 km

Aircraft properties

Weights

MTOW	394.5 10^3 kg	100%
OEW	172.3 10^3 kg	43.7%
W_{pl}	64.4 10^3 kg	16.3%
W_f	157.8 10^3 kg	40%
EW	162.4 10^3 kg	41.2%

Aerodynamics

L/Dmax	27.6
Min α	1.55°
Max α	2.99°
Min δ	−0.514°
Max δ	2.73°
L/Dave	26.5
Wing area	1121 m^2
Aspect ratio	3.35

Performance

Fuel/Pax/km	0.0201
Best load case	1
Inner tanks loaded first,	
Inner tanks emptied first	
Max range BLC	24838 km
BLC CG travel	8.77 %
Clean CLmax	1.12
CLmax slats	1.35

Figure 5.11: Constraints summary for the alternative 400 passenger BWB

From Figure 5.11 it can be concluded that this aircraft is slightly better performing than the other concept for 400 passengers, with a longer range (16,024km compared to 15,358km), higher lift over drag ratio (26.5 compared to 24.6), better fuel efficiency (0.0201kg/passenger/km compared to 0.0216kg/passenger/km), even though the OEW/MTOW fraction is higher (43.7% compared to

42.8%), and a lower maximum angle of attack during cruise (2.99°compared to 3.54°). Which is even below to the desired maximum of 3 degrees[21], only maximum trim deflection is larger for this aircraft. Figure 5.12 shows the payload range diagram of this alternative 400 passenger BWB. It

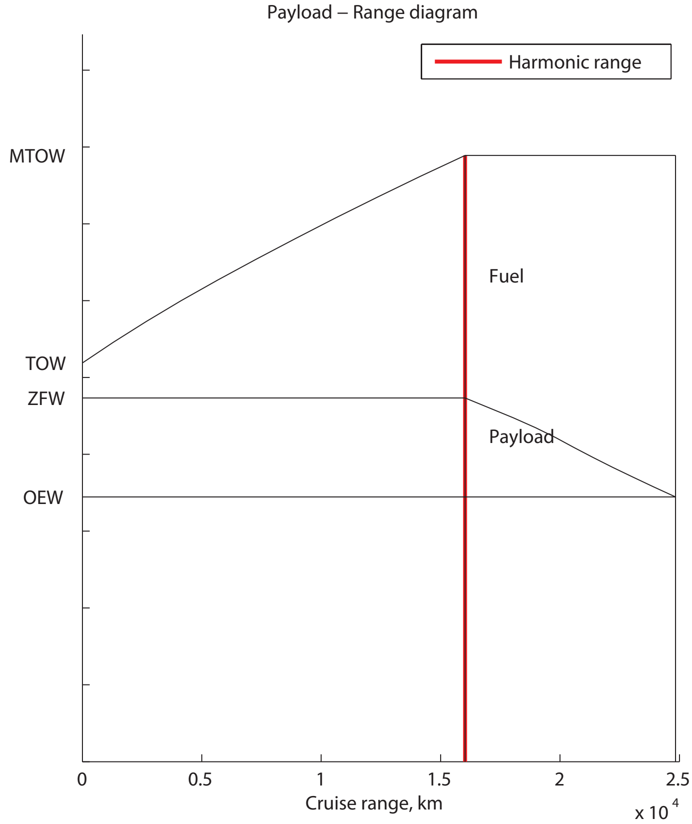

Figure 5.12: Payload-range diagram of the alternative 400 passenger BWB

can be seen that the harmonic range is larger than that of the other 400 passenger configuration, and that full tank capacity is not reached for this aircraft. This may be caused by the 3.3 metric ton higher OEW, or a larger tank capacity for this design.

5.2.3 200 Passenger 'Oval-Fuselage'

Another configuration that has been evaluated using the MATLAB program is a twin engine BWB concept with an oval fuselage for 200 passengers and 10,000kg of cargo. A three dimensional representation of the optimized aircraft is shown in Figure 5.13. This aircraft has a maximum thickness to chord ratio of 17.9%, within the range mentioned by Liebeck[21]. The aircraft looks much less like a flying wing, with a very large taper ratio on the second most outboard wing trunk and a longer centre body.

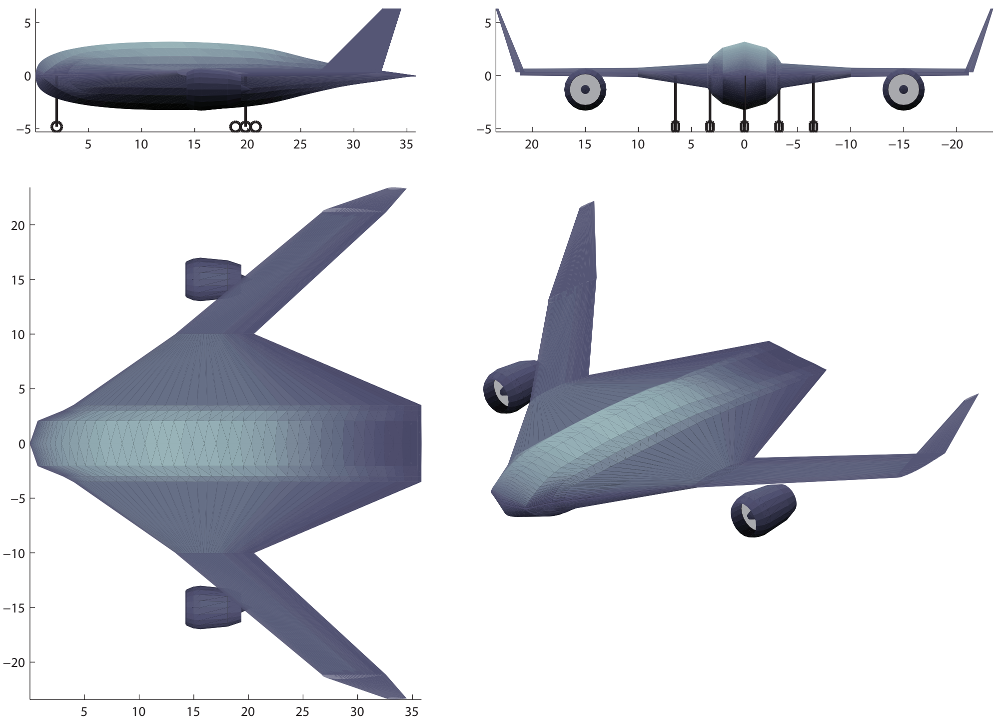

Figure 5.13: Three dimensional representation of a 200 passenger BWB

Constraints Summary

Geometric constraints

Wing span	42.3 m	80 m
Aircraft length	35.8 m	80 m

Cabin constraints

Floor area	165 m^2	143 m^2
Cargo volume	83.2 m^3	78.9 m^3

Landing gear constraints

Min nose load	9.31 %	5 %
Max nose load	15.7 %	20 %
Nose gear pos	1.99 m	0.5 m
Min main gear pos	19.8 m	8.29 m
Max main gear pos	19.8 m	28.8 m

Field and climb performance

Take−off dist	1651 m	2500 m
Landing dist	2497 m	2500 m
Stall speed TO	62.5 m/s	70 m/s
Stall speed clean	69.8 m/s	80 m/s
Climb OEI1	5.27 %	1.2 %
Climb OEI2a	1.3 %	0 %
Climb OEI2b	5.27 %	0 %
Climb OEI2c	9.73 %	1.2 %
Climb OEI3	29.7 %	2.1 %
Climb AEO	29 %	3.2 %

Trim and stability

Max trim deflection	1.52°	12°
Min static margin	−4.02%	−10% MAC
Weathercock, Cn_β	0.0597	> 0
Eff dihedral, Cl_β	−0.117	< 0
TO rot speed	24.7 m/s	70 m/s
OEI dr	24.7°	25°

Critical Mach number

Outer trunk	1.06	0.82
Outer trunk −1	0.82	0.82

Objective Function

Harmonic range:	15299 km	Target:	11000 km

Aircraft properties

Weights

MTOW	211 10^3 kg	100%
OEW	93.68 10^3 kg	44.4%
W_{pl}	32.2 10^3 kg	15.3%
W_f	85.17 10^3 kg	40.4%
EW	88.77 10^3 kg	42.1%

Aerodynamics

L/Dmax	25.6
Min α	1.4°
Max α	3.1°
Min δ	−0.263°
Max δ	1.52°
L/Dave	25
Wing area	640.7 m^2
Aspect ratio	2.79

Performance

Fuel/Pax/km	0.0228
Best load case	2
Inner tanks loaded first,	
Outer tanks emptied first	
Max range BLC	24159 km
BLC CG travel	5.3 %
Clean CLmax	0.909
CLmax slats	1.13

Figure 5.14: Constraints summary of the 200 passenger BWB

In Figure 5.14 the constraints summary of this aircraft is shown. The aircraft easily reaches the design range, with a harmonic range of 15299km. Yet, the OEW/MTOW fraction of 44.4% and a average lift over drag ratio of 25, with a maximum of 25.6 are not as good as for the 400 passenger concept. The maximum angle of attack of 3.1°is again slightly larger than suggested by Liebeck[21].

However, the maximum trim deflection is well within the bounds at 1.52°. It also has a relatively low fuel consumption in cruise of 0.0228kg/pax/km, though again worse than the 400 passenger concept. The cabin dimensions have been optimized very close to the requirements, though still some over-dimensioning exists.

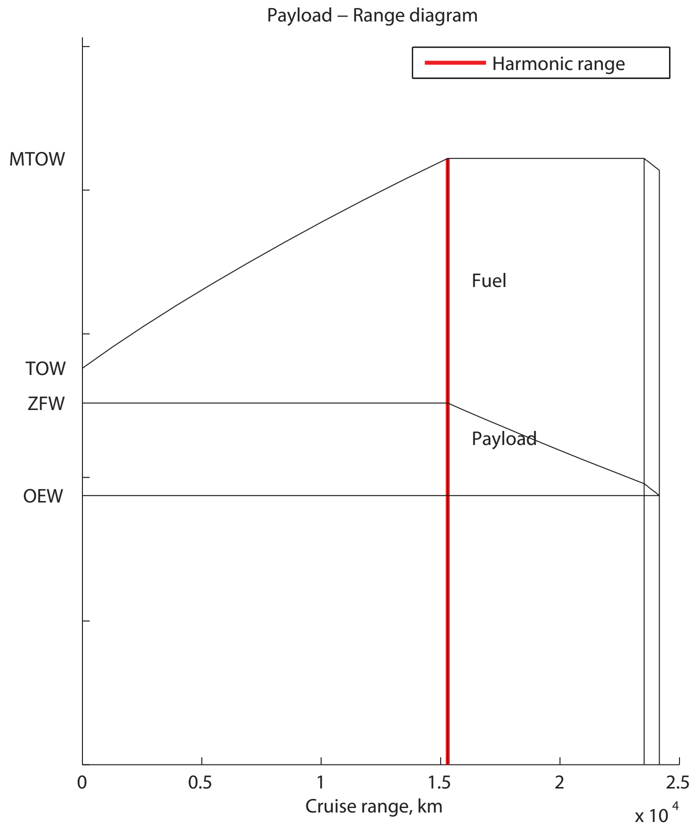

Figure 5.15: Payload-range diagram of the 200 passenger BWB

As can be seen in Figure 5.15, the aircraft has a large enough maximum payload range to fly from Amsterdam to Australia, non-stop with 200 passengers and 10,000kg cargo. If the cargo weight is reduced, the aircraft can still take 200 passengers and their luggage around the globe with just one stop for refueling.

5.2.4 800 Passenger 'Oval-Fuselage'

The third concept that was evaluated was a 800 passenger oval fuselage with an additional 40,000kg of cargo. Again, a 3D representation of this aircraft is shown in Figure 5.16. This aircraft has a maximum thickness to chord ratio of 19.9%, very close to the upper bound. The design is also approaching the limits of the 80 meter span by 80 meter length box for airports[8], as can be observed from the constraints summary in Figure 5.17.

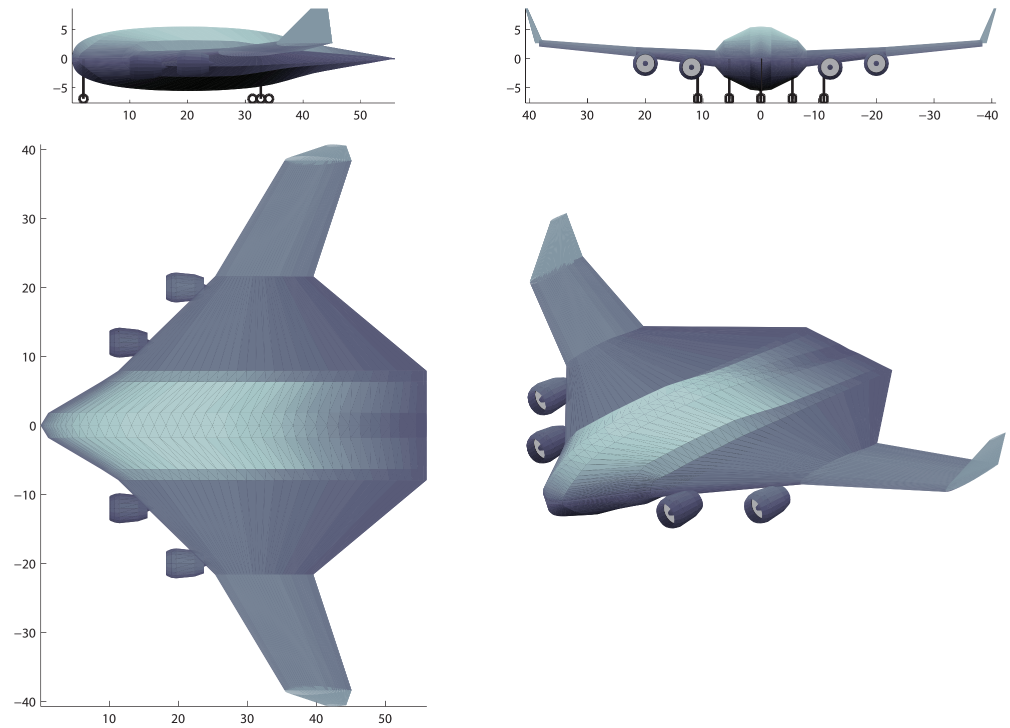

Figure 5.16: 3D representation of an 800 passenger BWB

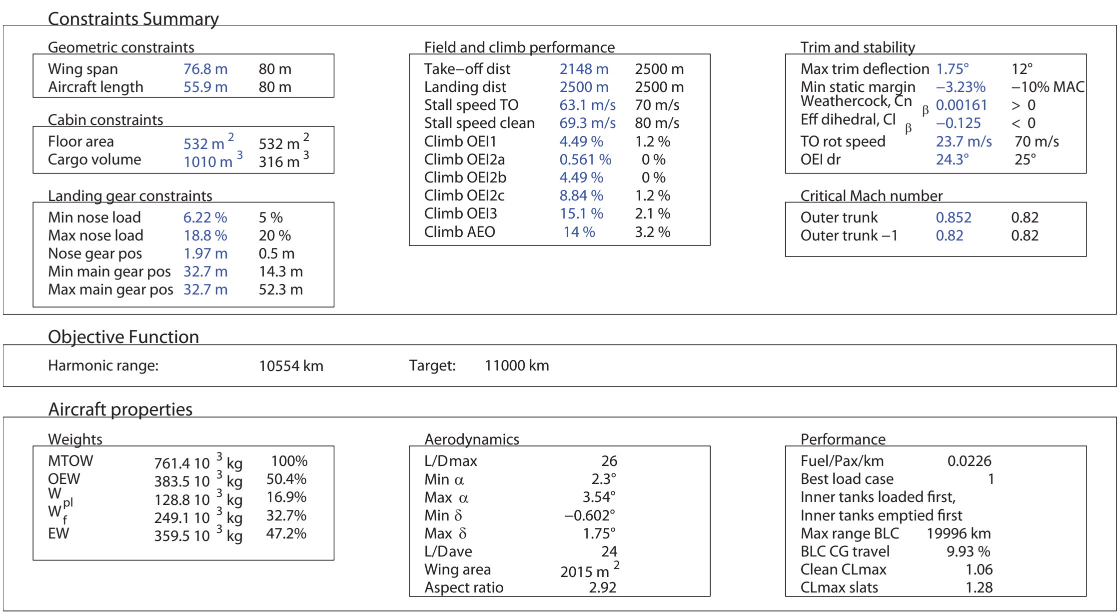

Figure 5.17: Constraint summary of the 800 passenger BWB

From the constraints summary the reason for the bulky look of the aircraft can be deduced. For an aircraft this large, there is a very large cargo volume available due to the conflicting requirements of floor area, maximum thickness, cabin width and required cargo height. Therefore simply reducing the thickness to chord ratio to lower the cargo volume may yield an aircraft that cannot fit LD-3 containers. This is a design choice that could be made, however, perhaps not without consequences in aircraft acceptance. The aircraft also has a higher OEW/MTOW fraction as the other blended wing bodies, at 50.4%. Most importantly though, the aircraft is not capable of reaching the required 11,000km range, it is about 500km short of this requirement. The maximum trim deflection of 1.75°is very low, though, and the maximum angle of attack during cruise of 3.54°is similar to the previously discussed aircraft. Lift over drag ratios are 24 on average and 26 maximum, which is still around the value to be expected for a BWB. Also the fuel consumption during cruise is not too high at 0.0226kg/pax/km. It is even better than that of the 200 passenger concept. However, considering the shear size of the aircraft and the unused cargo volume, it may be concluded that the oval-fuselage concept is less suited for passenger aircraft for this amount of payload.

From the payload-range diagram in Figure 5.18 it can also be seen that the fuel tank capacity is not yet reached when the aircraft is flying at OEW. It can also be observed that the design range of 11,000km can be reached with only a small reduction in payload.

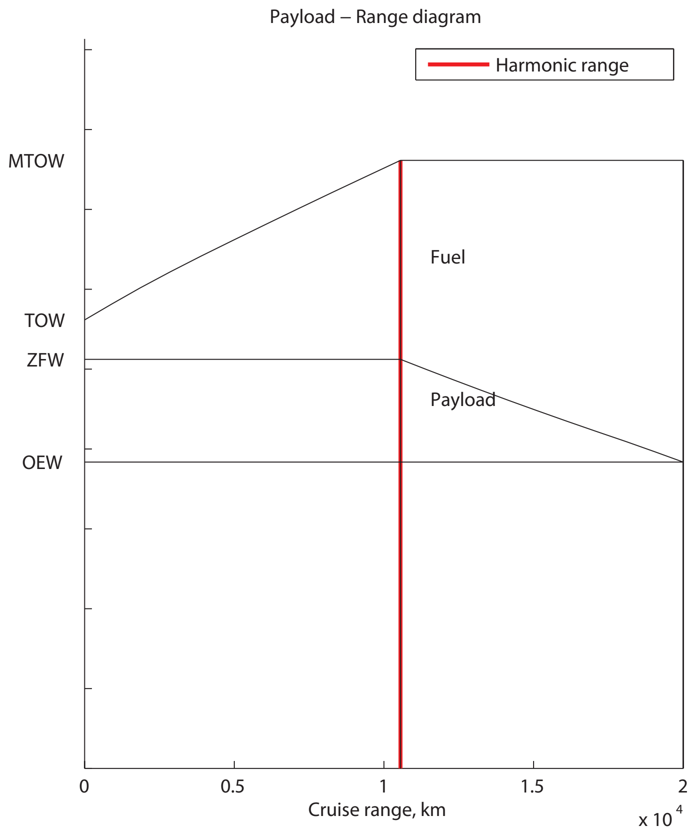

Figure 5.18: Payload-range diagram of the 800 passenger BWB

5.2.5 Summary of Results

The most important parameters of the different optimized concepts are shown in Table 5.5, since these will be used in the comparison to the multi-bubble BWB and conventional airliners in Sub-section 5.3.1 and Sub-section 5.3.2. From this table it may be concluded that the 200 and 400 passenger concepts are outperforming the 800 passenger concept in terms of OEW fraction and fuel efficiency. The 800 passenger concept is, however, not yet discarded as it is yet to be compared to the multi-bubble configuration for 800 passengers and 40,000kg cargo. Even the 200 passenger concept is outperformed by the alternative 400 passenger concept. The alternative 400 passenger concept has a better fuel consumption, a better lift over drag ratio on average and a longer range. Additionally it is also better with respect to passenger acceptance as the maximum angle of attack during cruise is slightly below to the desired 3 degrees, whilst that of the 200 passenger aircraft is a fraction too high. Indicating that the 'oval fuselage' concept may be most feasible for a long range aircraft designed for approximately 400 passengers and 20,000kg additional cargo.

Table 5.5: Summary of results for the 'oval-fuselage' concept

Variable	200 pax	400 pax I	400 pax II	800 pax
MTOW [ton]	211	395	395	761
OEW [ton]	94	169	172	384
OEW/MTOW	0.44	0.43	0.44	0.50
$(L/D)_{av}$	25	24.6	26.5	24
R [km]	15299	15358	16024	10554
δ_{max} [°]	1.52	2.32	2.73	1.75
α_{max} [°]	3.1	3.54	2.99	3.54
SFC_{cr} Harmonic Range [L/pax/100km]	2.81	2.67	2.48	2.79
SFC_{cr} Design Range [L/pax/100km]	2.72	2.56	2.37	2.79

The fuel density, as used in the MATLAB program has been used to convert the specific fuel consumption to liters. A density of 810kg/m^3 is used.

5.3 Comparison

Before drawing any more conclusions on the feasibility of the 'oval-fuselage' concept, the aircraft are compared to multi-bubble blended wing bodies that have been optimized for the same requirements in Sub-section 5.3.1, and finally to conventional aircraft to assess their feasibility with respect to the aircraft of today, in Sub-section 5.3.2.

5.3.1 Comparison to the 'Multi-Bubble' BWB

Three multi-bubble blended wing bodies have been optimized for the same requirements as the 'oval-fuselage' concept, i.e. a 200, 400 and 800 passenger aircraft. The comparisons are presented here. The optimization results of the multi-bubble concepts can be found in Appendix C.

Comparison for the 200 passenger blended wing bodies

Figure 5.19 visualizes the two different optimized blended wing body aircraft for 200 passengers and 10,000kg additional payload.

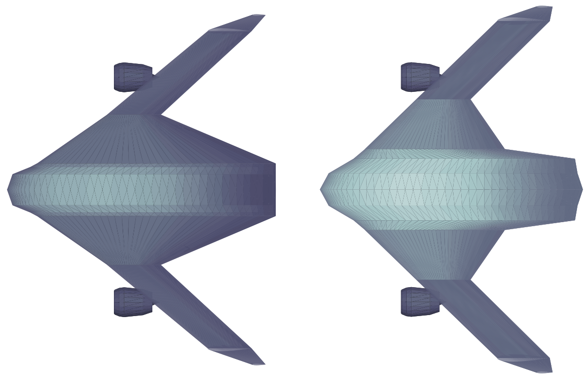

Figure 5.19: Visual comparison for the 'oval-fuselage' and multi-bubble for 200 passengers

Although the general shape of both aircraft is similar, the 'oval-fuselage' concept has a more swept wing and slightly less span. The multi-bubble has a slightly higher aspect ratio, though.

Table 5.6: Comparison for 200 passenger BWB

Variable	Oval Fuselage	Multi Bubble
MTOW [ton]	211	211
OEW [ton]	94	102
OEW/MTOW	0.44	0.48
$(L/D)_{av}$	25	24.2
R [km]	15299	12573
δ_{max} [°]	1.52	1.11
α_{max} [°]	3.1	3.72
SFC_{cr} Harmonic Range [L/pax/100km]	2.81	2.99
SFC_{cr} Design Range [L/pax/100km]	2.72	2.95

The results for the optimization of the 200 passenger multi-bubble BWB are summarized in Table 5.6, next to those of the 'oval-fuselage'. From these results it can be observed that the multi-bubble is outperformed by the new concept. The 'oval-fuselage' has a lower OEW/MTOW fraction (actually a 7.8% lower OEW), a higher average lift over drag ratio and a better fuel consumption. As a result the range is almost 3,000km (21.7%) larger for the same take-off weight. Also, with respect to passenger comfort, the 'oval-fuselage' has a lower maximum angle of attack during cruise flight. The maximum trim deflection is slightly larger thought, however, both values are well below the constraint of 12°.

Comparison for the 400 passenger blended wing bodies

In Figure 5.20, the two 'oval-fuselage' aircraft are shown next to the multi-bubble for 400 passengers and 20,000kg additional payload. The shape of the of the first 'oval-fuselage' concept is very distinctive for blended wing bodies, whereas the other two aircraft show less wing sweep. The multi-bubble also has an aspect ratio that is almost 25% larger than that of the first 'oval-fuselage'. It is also interesting to see that the best performing aircraft of the three, the 'oval-fuselage' in the middle of the illustration, seems to be a blend of the other two, when looking at the planforms.

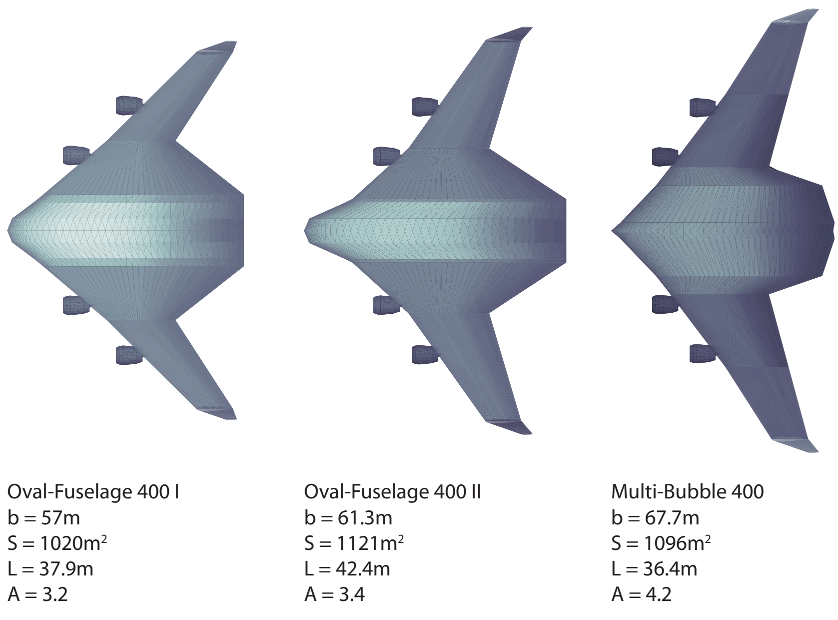

Figure 5.20: Visual comparison for the 'oval-fuselage' and multi-bubble for 400 passengers

In Table 5.7 the results are summarized, including the alternative configuration for the 'oval-fuselage'. Even though the OEW/MTOW fraction is lowest for the first 400 passenger 'oval-fuselage', it has the worst fuel consumption. The multi-bubble has a significantly higher operative empty weight fraction, yet a low fuel consumption thanks to its high average lift over drag ratio. Also in the trim angle deflection and maximum angle of attack in cruise, the multi-bubble performs

Table 5.7: Comparison for 400 passenger BWB

Variable	**Oval Fuselage I**	**Oval Fuselage II**	**Multi Bubble**
MTOW [ton]	395	395	395
OEW [ton]	169	172	198
OEW/MTOW	0.43	0.44	0.50
$(L/D)_{av}$	24.6	26.5	27.4
R [km]	15358	16024	12448
δ_{max} [°]	2.32	2.73	1.55
α_{max} [°]	3.54	2.99	2.88
SFC_{cr} Harmonic Range [L/pax/100km]	2.67	2.48	2.52
SFC_{cr} Design Range [L/pax/100km]	2.56	2.37	2.52

better than the 'oval-fuselage'. The range of the 'oval-fuselages' is 23.4% and 28.7% higher, respectively, and their OEW is 14.6% and 13.1% lower, respectively. The latter allows for more fuel to be carried with the same payload and take-off weight. The alternative 400 passenger 'oval-fuselage' is the best performing, especially in terms of fuel efficiency, which is 6% better over the design range than the multi-bubble.

Comparison for the 800 passenger blended wing bodies

The difference between the two 800 passenger aircraft with an additional 40,000kg cargo is visualized in Figure 5.21. The multi-bubble looks much more like a blended wing body. From its looks one would not immediately think that the 'oval-fuselage' is the best performing, because of its bulky shape. However, as shown in Table 5.8, its OEW is some 6% lower the multi-bubble's.

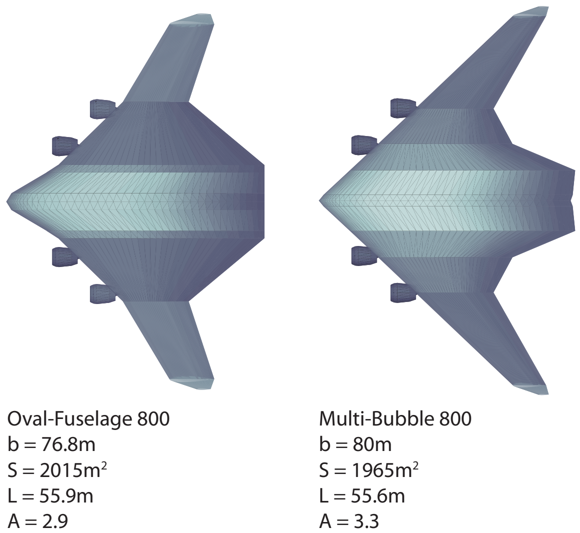

Figure 5.21: Visual comparison for the 'oval-fuselage' and multi-bubble for 800 passengers

Table 5.8: Comparison for 800 passenger BWB

Variable	Oval Fuselage	Multi Bubble
MTOW [ton]	761	761
OEW [ton]	384	408
OEW/MTOW	0.50	0.54
$(L/D)_{av}$	24	22.5
R [km]	10554	8354
δ_{max} [°]	1.75	2.33
α_{max} [°]	3.54	4.2
SFC_{cr} Harmonic Range [L/pax/100km]	2.79	3.05
SFC_{cr} Design Range [L/pax/100km]	2.79	3.09

A first observation of Table 5.8 tells that both aircraft fail to achieve the design range of 11,000km, indicating that the 800 passenger concept may be to large for a BWB aircraft. This may be caused by the restraints on the 80 meter span by 80 meter length design box for airport compatibility[8], as the optimizer would strive for a higher span to increase the aspect ratio and the gliding performance of the aircraft. The results for the 800 passenger concepts have been extrapolated, as they fail to achieve their design range. Therefore their performance is worse than before. The 'oval-fuselage' has a significantly lower OEW/MTOW fraction (thanks to a 11.5% lower OEW) and it achieves a higher average lift over drag ratio during cruise, resulting in an 8.5% lower fuel consumption and therefore a longer range. It is just under 500km short of the design range. The maximum trim deflection and angle of attack during cruise are also better for the 'oval-fuselage'.

Summary of comparison between 'oval-fuselage' and multi-bubble BWB

In comparison to the multi-bubble, the new fuselage concept shows its benefits with a lower OEW/MTOW fraction. Additionally, for all configurations a concept was found that achieves a longer range, lower fuel consumption and higher lift over drag. The alternative 400 passenger configuration shows the best results, when considering harmonic range, payload weight, fuel consumption and passenger comfort in terms of maximum angle of attack in cruise. When comparing the aircraft for their fuel efficiency over the design range of 11,000km, the 'oval-fuselage' performs better, except for the 'Oval-fuselage 400 I' concept. It is important to note though, that the difference with the multi-bubble is smaller over the design range than over the harmonic range (40 mL/passenger/km, with respect to 150mL/passenger/km). The 'oval-fuselage' thanks its larger harmonic range to the lower OEW, which is visualized in Figure 5.22, where the harmonic range of the optimized aircraft is plotted against payload. The trends of both aircraft are similar and show that the 'oval-fuselage' in all cases achieves a larger harmonic range for the same payload. In both cases the optimization objective was to maximize the harmonic range.

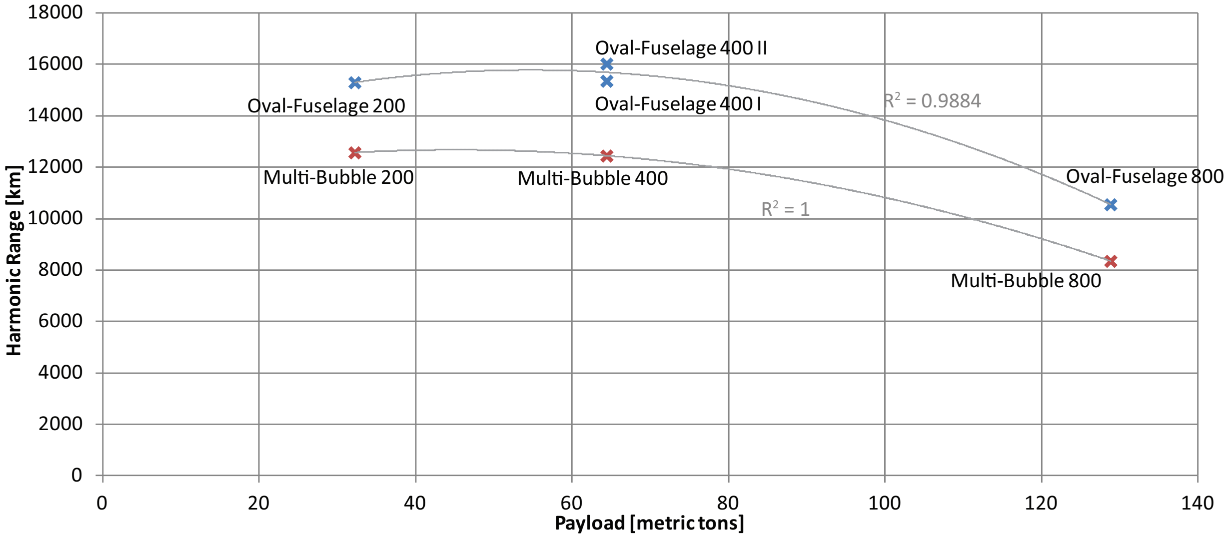

Figure 5.22: Payload vs. Harmonic Range for the optimized blended wing bodies

Part of this performance difference is also very clearly illustrated by Figure 5.23, where the OEW is plotted against the payload. Again, the trend is very clear, for all configurations over the range from 200 to 800 passengers, the 'oval-fuselage' has a lower OEW for the same payload than the multi-bubble.

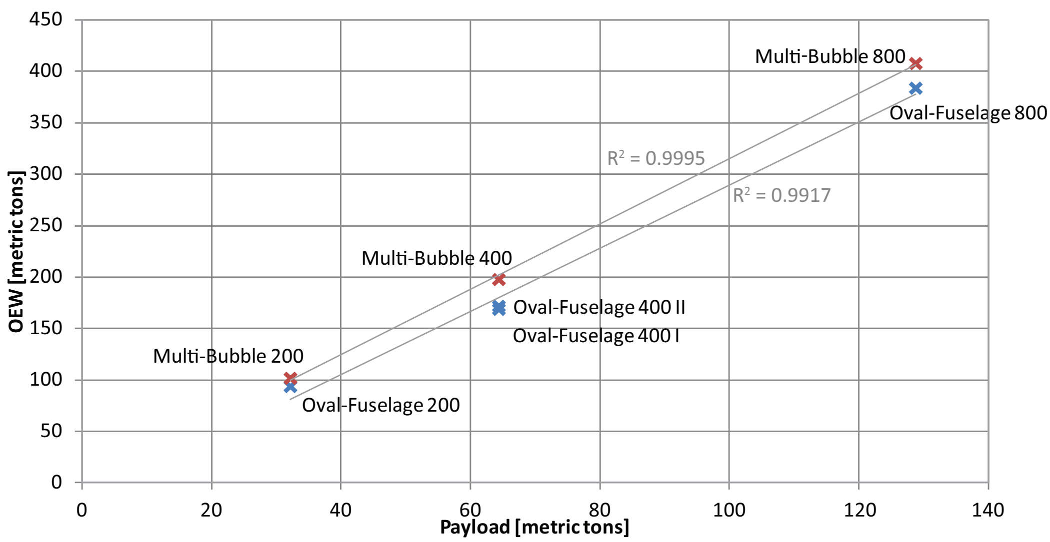

Figure 5.23: Payload vs. OEW for the optimized blended wing bodies

5.3.2 Comparison to Conventional Aircraft

In addition to the comparison with the multi-bubble BWB in Sub-section 5.3.1, the newly developed concept is compared to conventional airliners that fly around today. To properly compare the aircraft, the conventional airliners have also been assessed with the same passenger weight and payload density as the multi-bubble and 'oval-fuselage' BWB. A comparison is made on the basis of OEW/MTOW, fuel consumption and pressurized volume with respect to payload weight. The data for conventional aircraft has been obtained from the characteristics for airport planning as indicated in the tables, these are publicly available from the manufacturers websites.
Table 5.9 shows the comparison between the 'oval-fuselage' concepts and a range of different conventional airliners. The conventional airliners show a trend with lower OEW fractions for more modern aircraft. Comparing the fractions to the BWB's, it can be seen that these are on the lower end of the range for the conventional aircraft. This is also visualized in Figure 5.24.

Table 5.9: Comparison to conventional aircraft for OEW

Aircraft	MTOW [ton]	OEW [ton]	OEW/MTOW
Oval Fuselage 200	211	94	0.44
Oval Fuselage 400 I	395	169	0.43
Oval Fuselage 400 II	395	172	0.44
Oval Fuselage 800	761	384	0.50
Airbus A380-800[40]	560	271	0.48
Airbus A330-300[41]	235	125	0.53
Airbus A330-200[41]	238	121	0.51
Airbus A320[42]	78	42	0.54
Boeing 777-200LR[43]	348	145	0.42

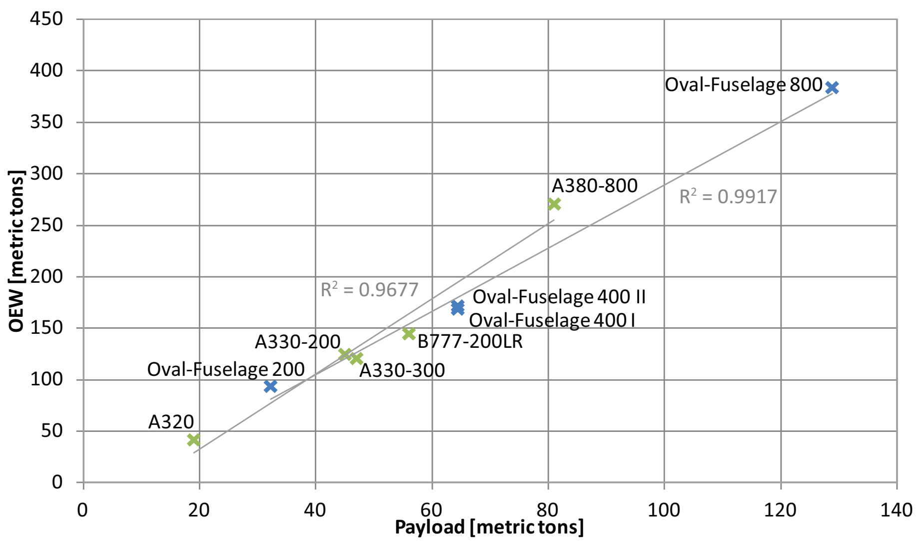

Figure 5.24: Payload vs. OEW for the 'oval-fuselage' and conventional aircraft

From this figure it can be observed that the smaller blended wing bodies have the tendency to be heavier than their conventional rivals. Whereas the 400 passenger concepts seem to perform on a similar level as the long range Boeing 777, indicating that this may be an area of application for these ‘oval-fuselage’ blended wing bodies.

When comparing for payload range, the total mission fuel consumption has been calculated for the blended wing bodies. In previous tables the listed values were cruise flight only. To make a fair comparison with the data for the conventional airliners, the values have been recalculated for the total mission for the harmonic range. Table 5.10 shows that when considering the payload the BWB’s perform better than the conventional aircraft. The fuel consumption per transported kilogram is lower for these aircraft. Although, per passenger kilometer the aircraft perform comparable to the conventional aircraft, they transport more payload kilograms per kilometer. The Oval Fuselage 400 II has a fuel consumption per transported kilogram that is approximately 10% lower than that of the best perfroming conventional aircraft.

Table 5.10: Comparison to conventional aircraft for fuel efficiency

Aircraft	**Harmonic Range [km]**	**Passengers**	**Payload [ton]**	**Fuel [m^3]**
Oval Fuselage 200	15300	200	32	105
Oval Fuselage 400 I	15300	400	64	199
Oval Fuselage 400 II	16000	400	64	195
Oval Fuselage 800	10500	800	129	308
Airbus A380-800[40]	12000	555	81	257
Airbus A330-300[41]	7000	295	45	67
Airbus A330-200[41]	8000	253	47	86
Airbus A320[42]	4500	150	19	20
Boeing 777-200LR[43]	15200	301	56	180

Aircraft	**Fuel consumption per passenger [L/pax/100km]**	**Fuel consumption per unit payload [L/kg/10,000km]**
Oval Fuselage 200	3.4	2.1
Oval Fuselage 400 I	3.3	2
Oval Fuselage 400 II	3	1.9
Oval Fuselage 800	3.7	2.3
Airbus A380-800[40]	3.9	2.6
Airbus A330-300[41]	3.2	2.1
Airbus A330-200[41]	4.2	2.3
Airbus A320[42]	3	2.3
Boeing 777-200LR[43]	3.9	2.1

In Figure 5.25 the comparison for harmonic range versus payload is visualized. For the trend line of the conventional aircraft, the Boeing 777-200LR has not been considered, as it is a specialized long range airliner. What can be observed though, is that especially the 400 passenger ‘oval-fuselage’ blended wing bodies could be competitors for this aircraft. It is also clear that the much larger 800 passenger blended wing body is approaching the limits of the design space, as an extended version of the A380 is expected to be better performing.

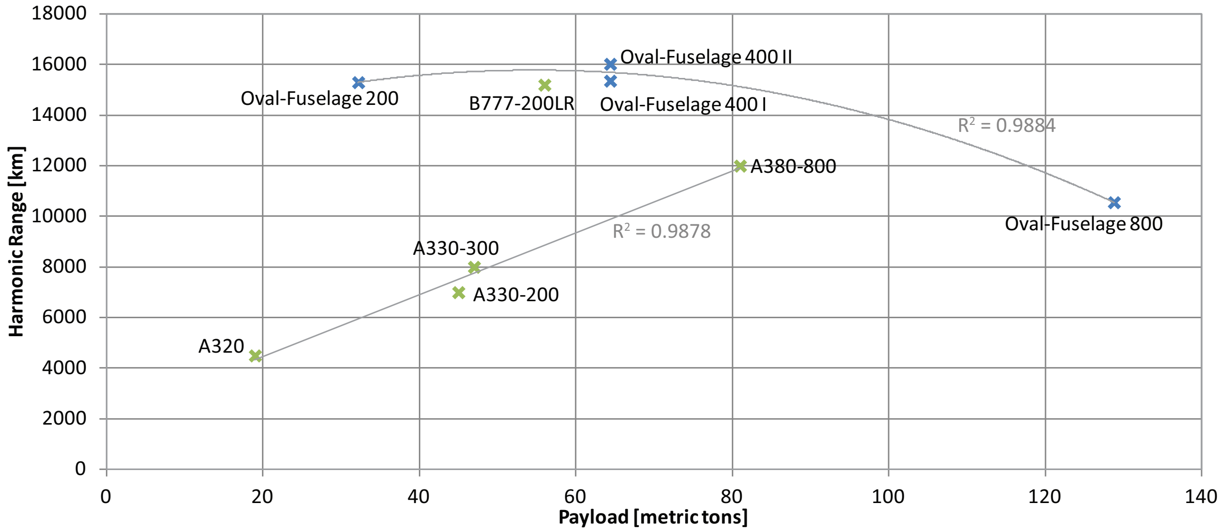

Figure 5.25: Payload vs. Harmonic Range for the ‘oval-fuselage’ and conventional aircraft

Table 5.11 shows a preliminary comparison for the pressurized volume of the ‘oval-fuselage’ concept for maximum structural payload. The values are within the range of the larger conventional aircraft, however the BWB is outperformed by a significant fraction by the A320 and A330-200. The A320 has the advantage of having specifically design unit load devices (LD3-45), which is not the case for the A330. This aircraft uses its available volume some 10 percent better than the best BWB.

Table 5.11: Comparison to conventional aircraft for pressurized volume

Aircraft	**Payload** [ton]	**Pressurized Volume** [m^3]	**Volume Usage** [m^3/ton]
Oval Fuselage 200	32	792	24.8
Oval Fuselage 400 I	64	1475	23
Oval Fuselage 400 II	64	1395	21.8
Oval Fuselage 800	129	4146	32.1
Airbus A380-800[40]	81	2100	25.9
Airbus A330-300[41]	45	1056	23.5
Airbus A330-200[41]	47	950	20.2
Airbus A320[42]	19	330	17.4
Boeing 777-200LR[43]	56	1624[44]	29

It can also be seen that what are generally considered smaller BWB’s seem to perform better for the ‘oval-fuselage’ than the very large 800 passenger concept. This suggests that the concept is perhaps better suited for smaller configurations. However, in defense of the larger A330-300 and Boeing 777-200LR, it must be noted that these aircraft are designed for long range and have substituted cargo for fuel.

Overall, the BWB can be concluded to be non-optimum in its use of volume, as a relatively large amount of the cargo area's is too low and not suitable for cargo, as was illustrated in Figure 5.8. A solution to this may be the use of asymmetric airfoils, in the larger blended wing bodies. These airfoils can reduce the volume of, for example, the upper deck, as the lower deck alone is sufficient to carry the required cargo. Additionally, the usage of custom unit load devices (wider and lower), that better fit the shape of the BWB, could result in a large improvement in the usable volume fraction. This is very clearly demonstrated by the Airbus A320, that transports customized unit load devices. The substitution of unused volume for fuel could perhaps be applied to the 'oval-fuselage' blended wing body, i.e. to lower the unused volume in the design, this volume could be fitted with additional fuel tanks.

5.4 Reflections on the Blended Wing Body

In addition to the comparison made in Section 5.3, there are several other issues that have prevented the BWB to be used as a large passenger transport aircraft, although history has shown several (unpressurized) all-lifting vehicles. The new concept has shown a solution to overcome the pressurization issue that has been troubling to blended wing body design. However, several other problems still exist. Even though the parasite drag may be reduced, as the complete aircraft contributes to the lift generation, a large profile drag is to be expected for the fuselage section, with its thick profiles and long chords. Other challenges still being researched are the longitudinal stability, with the tendency of BWB's to be statically unstable. This was also the case for the new concept with its negative static margin, as could be observed in the constraint summaries in Chapter 5. Also controllability is difficult with the comparatively small moment arms, where certification requires control of the aircraft throughout the flight envelope. Other problems are, as mentioned in Chapter 2, the passenger comfort and emergency egress. Not to mention the most likely very high development and testing cost for blended wing body aircraft. Additionally, where conventional aircraft can be easily scaled and assembled in different sections, this introduces a problem for the blended wing body, as it requires a re-design.

CHAPTER 6

CONCLUSION AND RECOMMENDATIONS

This chapter provides an overview of the conclusions drawn from the research on the feasibility of the 'oval-fuselage' BWB concept. The material provided in the previous chapters and the analysis results have provided several conclusion on this. Additionally, recommendations for future research on the presented concept and the analysis with the optimization tool are presented in this chapter.

6.1 Conclusions

The 'oval-fuselage' concept has been presented as a solution to the problematics of the pressure cabin in blended wing body design. A concept has been developed that can withstand pressurization loads by means of four tangentially connected arcs, supported by horizontal and vertical members. The research question: **"How does the performance of the 'oval-fuselage' blended wing body compare to a multi-bubble concept, for the same configuration and a given set of top-level requirements?"** was posed to investigate the feasibility of the new concept. In addition to this research question, the following sub-question was phrased: **"How can the operative empty weight of the 'oval-fuselage' concept be estimated?"**, to determine the performance of this new concept and thereby provide the means to answer the research question.

Therefore, a method to parametrize the geometry and a weight estimation methodology for the 'oval-fuselage' concept were developed. The weight estimation determines the required thicknesses of the structural members, for a certain geometry, under pressurization and wing-bending loads. In addition to this, the longitudinal stresses in the fuselage skin due to pressurization, axial acceleration and fuselage bending are required to be below the tensile and compressive fatigue limits.

To analyze the performance of the new concept, this methodology was combined with the Torenbeek Class-II[10] weight estimation method for the OEW and the Torenbeek Class-II.5[5] wing weight estimation. A MATLAB optimization tool for the blended wing body aircraft, as developed by Van Dommelen[7] was adapted to incorporate the new design.

Four 'oval-fuselage' blended wing bodies, a 200 passenger configuration, two 400 passenger configurations and one 800 passenger configuration, were optimized for symmetric airfoils over the fuselage sections. The optimized aircraft were compared to multi-bubble blended wing bodies, optimized for the same top-level requirements. The 200 passenger concept showed a lower OEW (94 metric tons compared to 102 metric tons) and a lower fuel consumption (2.81 L/pax/100km compared to 2.99 L/pax/100km), combined with a higher average lift over drag ratio (25 compared to 24.2), resulting in a range of 15,299km (compared to 12,573km). Both 400 passenger 'oval-fuselages' outperformed their multi-bubble competitor in terms of range (15,358km and 16,024km, respectively, compared to 12448) and OEW (169 and 172 metric tons, compared to 198 metric tons). This means improvements of 23.4% and 28.7% in range, respectively, and improvements of 14.6% and 13.1% in OEW, respectively. The 400 passenger 'oval-fuselage' achieving a harmonic range of 16,024km also achieved the lowest fuel consumption for the design range of 11,000km of all evaluated aircraft, with just 2.37 L/pax/100km, 6% better than its multi-bubble competitor. The 800 passenger multi-bubble failed to achieve its design range by almost 3,000km, whereas the 'oval-fuselage' carrying the same payload was just 500km short of this design range. A 24 metric tons (6%) lower operative empty weight and an 8.5% lower fuel consumption helped to achieve this. The 'oval-fuselage' was shown to outperform the multi-bubble for every assessed payload requirement in terms of performance, except for the maximum trim deflection. However, this is still easily within the imposed constraint for all 'oval-fuselage' configurations.

When comparing the 'oval-fuselage' configurations to conventional airliners, it was found that the OEW/MTOW fractions are in the lower end of the range of the conventional airliners. For the 200, the two 400 and 800 passenger concepts, fractions of 44%, 43%, 44% and 50% were found, respectively. The best conventional airliner achieved 42%, whereas the second best already showed a 48% OEW/MTOW fraction. The fuel efficiencies per passenger kilometer were found to be in the same range as the conventional aircraft. The fuel efficiency per transported kilogram, however, was in all cases better when comparing to aircraft of similar payload capacities. The best 'oval-fuselage' achieved 1.9 liters per kg per 10,000km, whereas the best peforming long range Boeing 777-200LR and Airbus A330-300 only achieved 2.1 liters per kilogram per 10,000km, some 10% worse. Only the volume usage of the 'oval-fuselage' blended wing bodies was worse than that of the conventional aircraft. To improve this, it is suggested to use asymmetric airfoils over the fuselage sections and to use custom unit load devices for blended wing bodies. From the graphical comparison between the conventional aircraft and the 'oval-fuselage' blended wing bodies for OEW versus payload, it can be concluded that the 400 passenger configurations perform on a level similar to that of the long range Boeing 777-200LR. Therefore it may be concluded that this is an area of application for the 'oval-fuselage', with a long range and low OEW for a significant amount of payload.

In comparison to the multi-bubble, it can overall be concluded that the new 'oval-fuselage' outperforms the multi-bubble in terms of fuel efficiency, harmonic range and has a lower OEW over a range of payload weights. Additionally, the 'oval-fuselage' can have a flexible cabin design with its unobstructed spacious cabin, as was determined from the literature research into cabin requirements for blended wing bodies. Therefore it may be concluded that the oval fuselage is lighter and performs better than the multi-bubble, as well as allowing for flexible cabin configurations. It brings flying a BWB aircraft one step closer to reality.

6.2 Recommendations

From the research several recommendations can be made regarding further research into the 'oval-fuselage' concept and the MATLAB optimization tool.

Regarding the 'oval-fuselage', the first point is to investigate the effect of shear and torque at the intersection between the pressurized section and the wingbox structure and make sure these loads can be handled and transmitted to the fuselage structure. As mentioned before, also the wrinkling resistance and the design of the sandwich members needs further research.

The trailing edge of the cabin can also be investigated for its use as a control surface, or the use of the volume inside for fuel. And the nosecone/cockpit section has been integrated in the airfoil shape, however, for a feasible aircraft this shape may have to change to aid pilot visibility. Research into the weight and design of body fairings between the wing and fuselage intersection is also recommended to increase the level of detail.

When considering the most likely high profile drag, it may be worthwhile to investigate the use of asymmetric airfoils over the centre body. This could also reduce the unused pressurized volume.

With respect to the program, additional improvements to the performance of the concept may be achieved through the implementation of asymmetric airfoils. Though the method derived is capable of handling these shapes, the cabin generation in MATLAB is not. The program should therefore be adapted such that a desired asymmetric airfoil is achieved whilst maintaining a level cabin floor and sufficient cargo volume and achieving a smoother trailing edge.

The program could also be improved by implementing a different aerodynamics module, as the current vortex lattice method takes up most of the optimization time. Especially considering the importance of aerodynamics to the BWB design it may be worthwhile to use a different program. Efforts in reducing the computation time of this module will drastically decrease the overall optimization time.

It is also important to mention that the current optimization tool considers a constant MTOW from a Class-I method. To improve the results this should be recalculated after the weight estimation module and be iterated before continuing with the design. In combination with this, the design range can be set as a constraint, such that the aircraft is not over-designed. For example: $10,000\text{km} < R < 11,000\text{km}$, and setting the objective to achieve the lowest fuel consumption. Additionally, imposing a constraint on the maximum angle of attack during cruise, for example to the $3°$, as suggested by Liebeck[21], should yield designs that perform better in terms of passenger well-being. Improvements to the preliminary sizing can also be achieved by building a statistical database of optimized blended wing bodies in addition to the conventional aircraft that currently dominate the preliminary sizing module. The preliminary sizing produces an estimate for the 800 passenger configuration with with a span larger than the 80 meter constraint. The 200 passenger configuration is estimated at a too low wing surface area with the current preliminary sizing.

REFERENCES

[1] Liebeck, R. H., Page, M. W., and Rawdon, B. K., "Blended-Wing-Body Subsonic Commercial Transport," *36th Aerospace Sciences Meeting & Exhibit, January 12-15, 1998 / Reno, NV*, 1998.

[2] Hileman, J. I., Spakovszky, Z. S., Drela, M., and Sargeant, M. A., "Airframe Design for Silent Aircraft," *45th AIAA Aerospace Sciences Meeting and Exhibit 8 - 11 January 2007, Reno, Nevada*, 2007.

[3] Geuskens, F. J. J. M. M., Bergsma, O. K., Koussios, S., and Beukers, A., "Analysis of Conformable Pressure Vessels: Introducing the Multibubble," *AIAA Journal*, Vol. 49, No. 8, August 2011, pp. 1683–1692.

[4] Howe, D., "Blended wing body airframe mass prediction," *Proceedings of the Institution of Mechanical Engineers, Part G: Journal of Aerospace Engineering*, Vol. 215, 2001, pp. 319–331.

[5] Torenbeek, E., "Development and Application of a Comprehensive, Design-sensitive Weight Prediction Method for Wing Structures of Transport Category Aircraft," Tech. rep., Delft University of Technology, Faculty of Aerospace Engineering, 1992, Report LR-693.

[6] Vos, R. and Geuskens, F. J. J. M. M., *Structural design of a non-circular pressurized fuselage*, Patent Pending, N2007397, 12 September 2011.

[7] van Dommelen, J. L., *Design of a Forward-Swept Blended Wing Body Aircraft A Conceptual Design Study to Alternative Blended Wing Body Configurations*, Master's thesis, Delft University of Technology, Faculty of Aerospace Engineering, 2011.

[8] Anonymous, *Aerodrome Design Manual*, International Civil Aviation Organization (ICAO), 3rd ed., July 1999, ICAO 9157.

[9] Anonymous, *Certification Specifications and Acceptable Means of Compliance for Large Aeroplanes CS-25*, European Aviation Safety Agency, 4 July 2011, Amendment 11.

[10] Torenbeek, E., *Synthesis of Subsonic Airplane Design*, Delft University Press, Kluwer Academic Publishers, 1982.

[11] Anonymous, *The history of the flying wing*, 2011, Accessed 12 December 2011, `http://www.century-of-flight.net/new%20site/frames/flying%20wing%20frame.htm`.

[12] Wood, R. M. and Bauer, S. X. S., "Flying Wings / Flying Fuselages," *39th AIAA Aerospace Sciences, Meeting & Exhibit, 8-11 January 2001 / Reno , NV*, 2001, pp. 1–25.

[13] Bullard, D., *The Development of All-Wing Aircraft by John K. Northrop at the 35th WILBUR WRIGHT MEMORIAL LECTURE*, 2003, Accessed 28 Oktober 2011, `http://www.nurflugel.com/Nurflugel/Northrop/Northrop_address/northrop_address.html`.

[14] Anonymous, *The Northrop Grumman B2-Spirit*, Northrop Grumman Corporation, 2011, Accessed 28 Oktober 2011, `http://www.as.northropgrumman.com/products/b2spirit/assets/lgm_95006809.jpg`.

[15] Anonymous, *Various United States experimental lifting bodies*, 2008, Accessed 28 Oktober 2011, `http://www.strategypage.com/gallery/images/lifting_bodies.jpg`.

[16] Kroo, I., *Blended Wing Body concept in "Reinventing the Airplane: New Concepts for Flight in the 21st Century"*, 2011, Accessed 28 Oktober 2011, `http://adg.stanford.edu/aa241/intro/futureac.html`.

[17] Galea, E. R., Filippidis, L., Wang, W., Lawrence, P. J., and Ewer, J., "Evacuation analysis of 1000+ seat Blended Wing Body aircraft configurations: Computer Simulations and Full-Scale Evacuation Experiment," *PED 2010, NIST, Maryland USA, March 8-10 2010*, 2010, pp. 1–10.

[18] Eelman, S., Schmitt, D., Becker, A., and Granzeier, W., "Future Requirements and Concepts for Cabins of Blended Wing Body Configurations - A Scenario Approach," *Journal of Air Transportation*, Vol. 9, No. 2, 2004, pp. 4–22.

[19] Wittmann, R., "Passenger Acceptance of BWB Configurations," *ICAS 2004, 24TH INTERNATIONAL CONGRESS OF THE AERONAUTICAL SCIENCES*, 2004, pp. 1–10.

[20] Hinninghofen, H. and Enk, P., "Passenger well-being in airplanes," *Autonomic Neuroscience: Basic and Clinical*, Vol. 129, 2006, pp. 80–85.

[21] Liebeck, R. H., "Design of the BlendedWing Body Subsonic Transport," *Journal of Aircraft*, Vol. 41, No. 1, January-February 2004, pp. 10–25.

[22] Mukhopadhyay, V., "Structural Concepts Study of Non-circular Fuselage Configurations," *SAE/AIAA World Aviation Congress, October 22-24, 1996, Los Angeles, California*, 1996, pp. 1–13.

[23] Vos, R., Geuskens, F. J. J. M. M., and Hoogreef, M. F. M., "A New Structural Design Concept for Blended Wing Body Cabins," *53rd AIAA/ASME/ASCE/AHS/ASC Structures, Structural Dynamics and Materials Conference, Honolulu, Hawaii*, Apr. 23-26, 2012.

[24] Geuskens, F. J. J. M. M., Bergsma, O. K., Koussios, S., and Beukers, A., "Pressure Vessels & Pressure Cabins for Blended Wing Bodies," *ICCM-17 17th International Conference on Composite Materials 27 Jul 2009 - 31 Jul 2009, Edinburgh International Convention Centre (EICC), Edinburgh, UK*, 2009, pp. 1–12.

[25] Geuskens, F. J. J. M. M., Bergsma, O. K., Koussios, S., and Beukers, A., "Non-Cylindrical pressure fuselages for future aircraft," *49th AIAA/ASME/ASCE/AHS/ASC Structures, Structural Dynamics, and Materials Conference, 7 - 10 April 2008, Schaumburg, IL*, 2008, pp. 1–11.

[26] Raymer, D. P., *Aircraft Design: A conceptual approach*, American Institute of Aeronautics and Astronautics, Inc., Washington, DC, 1992.

[27] Anonymous, *Tornado Vortex Lattice Method*, KTH Royal institute of Technology Stockholm Sweden; University of Bristol United Kingdom; University of Linkping.

[28] Ashby, M. F., *Materials Selection in Mechanical Design*, Butterworth-Heinemann, Oxford, UK, 3rd ed., 2005.

[29] Anonymous, *747-400 Airplane Characteristics for Airport Planning*, Boeing Commercial Airplanes, DecemberJanuary 2011.

[30] Anonymous, *Unit Load Devices*, British Airways World Cargo, 2012, Accessed 24 March 2012, `http://www.baworldcargo.com/configs/BAWCconfigurations.pdf`.

[31] Anonymous, *Thrust advance*, Flight International, 20-26 May 2003, A380-special pages 23-25.

[32] Anonymous, *Secondary Power Systems*, Virginia Tech, In-house, Accessed 22 May 2012, Lecture Slides `http://www.dept.aoe.vt.edu/~mason/Mason_f/SecondaryPwrSys.ppt`.

[33] Anonymous, *Honeywell Primus 880 Weather Radar*, Accessed 16 May 2012, `http://www.honeywell.com/sites/servlet/com.merx.npoint.servlets.DocumentServlet?docid=D59602700-804D-8E92-87FC-22F9AEF5819E`.

[34] Anonymous, *Airbus starts painting first A380 for Singapore Airlines*, Airbus S.A.S., 11 April 2007, Accessed 28 May 2012, Press Release `http://www.airbus.com/en/presscentre/pressreleases/pressreleases_items/07_04_11_A380_first_paint.html`.

[35] Roskam, J., *Airplane Design*, Roskam Aviation and Engineering Corporation, 1985.

[36] Ardema, M. D., Chambers, M. C., Patron, A. P., Hahn, A. S., Miura, H., and Moore, M. D., "Analytical Fuselage and Wing Weight Estimation of Transport Aircraft," Tech. Rep. TM 110392, National Aeronautics and Space Administration, May 1996.

[37] Hibbeler, R. C., *Mechanics of Materials*, Prentice Hall, 6th ed., 2005.

[38] Morris, A., Arendsen, P., Rocca, G. L., Laban, M., Voss, R., and Hnlinger, H., "MOB, A European project on multidisciplinary design optimisation," *ICAS 2004, 24TH INTERNATIONAL CONGRESS OF THE AERONAUTICAL SCIENCES*, 2004.

[39] Whitcomb, R. T., "Advance Transonic Aerodynamic Technology," Tech. rep., NASA Langley Research Center, 1976.

[40] Anonymous, *A380 Airplane Characteristics for Airport Planning*, Airbus S.A.S., November 2011.

[41] Anonymous, *A330 Airplane Characteristics for Airport Planning*, Airbus S.A.S., January 2012.

[42] Anonymous, *A320 Airplane Characteristics for Airport Planning*, Airbus S.A.S., June 2012.

[43] Anonymous, *777-200LR Airplane Characteristics for Airport Planning*, Boeing Commercial Airplanes, May 2011.

[44] Norris, G. and Wagner, M., *Boeing 777*, Motorbooks International Publishers & Wholesalers, 1996.

[45] Anonymous, *CES Edupack 2011*, Granta Design Limited.

[46] Anonymous, *Rohacell 51A Datasheet*, Rohacell, 2012, Accessed 7 May 2012, http://www.rohacell.com/product/rohacell/en/products-services/rohacell-a/pages/default.aspx.

APPENDIX A

CLASS-II OPERATIVE EMPTY WEIGHT ESTIMATION

This appendix contains an overview of the equations used to calculate an estimate of the OEW. The method used is Torenbeek's Class-II weight estimation[10]. However, for some specific estimates, more up to date, or more detailed information is used, or estimates specifically for blended wing body aircraft by Howe[4]. In case the origin of the estimates is different than Torenbeek's method, this is indicated. Since most equations have actually been obtained from Roskam's[35] description of the Torenbeek method, imperial units are used in these equations. Therefore all units of input variables and output masses are provided with the equations presented as they are listed in literature, to avoid any conflicts converting units.

Airframe Weight

The first part of the OEW to be considered is the airframe mass of the BWB, excluding the mass of the fuselage section and the outer wings. These form the majority of the weight and are treated separately in Section 4.2 and Section 4.3.

Vertical Tail

The mass of the vertical tail (in lbs) is dependent on the number of vertical tails, $N_{\text{V-tail}}$, the surface area of a single tail plane, S_{V} in ft^2, the design dive speed of the aircraft, V_{D} in knots estimated to equal $1.25 \cdot V_{\text{cruise}}$, the wetted area of the vertical tail planes, $S_{\text{W}_{\text{V-tail}}}$ in ft^2 and a factor of $K_{\text{V}} = 1$. This factor accounts for the mounting of a horizontal tail,the value of 1 is used for non-fin-mounted horizontal tails, as there is no horizontal tail.

$$W_{\text{V-tail}} = N_{\text{V-tail}} \cdot K_{\text{V}} \cdot S_{\text{V}} \cdot \left(\frac{3.81 \cdot {S_{\text{V}}}^{0.2} \cdot V_{\text{D}}}{1000 \cdot \cos^{0.5}\left(S_{\text{W}_{\text{V-tail}}}\right)} - 0.287 \right) \quad [lbs] \tag{A.1}$$

Main Gear

The main gear mass, in lbs, is related to the take-off mass, W_{TO} in lbs and the coefficients A_{mg} through D_{mg}. From Torenbeek for low wing passenger transport aircraft; $A_{\mathrm{mg}} = 40$, $B_{\mathrm{mg}} = 0.16$, $C_{\mathrm{mg}} = 0.019$ and $D_{\mathrm{mg}} = 1.5 \cdot 10^{-5}$. Here, $K_{\mathrm{mg}} = 1$.

$$W_{\mathrm{mg}} = K_{\mathrm{mg}} \cdot \left(A_{\mathrm{mg}} + B_{\mathrm{mg}} \cdot W_{\mathrm{TO}}{}^{0.75} + C_{\mathrm{mg}} \cdot W_{\mathrm{TO}} + D_{\mathrm{mg}} \cdot W_{\mathrm{TO}}{}^{1.5}\right) \quad [lbs] \tag{A.2}$$

Nose Gear

The calculation of the mass of the nose gear, in lbs, is similar to that of the main gear, except now, $A_{\mathrm{ng}} = 20$, $B_{\mathrm{ng}} = 0.1$, $C_{\mathrm{ng}} = 0$ and $D_{\mathrm{ng}} = 2 \cdot 10^{-6}$. Here, $K_{\mathrm{ng}} = 1$.

$$W_{\mathrm{ng}} = K_{\mathrm{ng}} \cdot \left(A_{\mathrm{ng}} + B_{\mathrm{ng}} \cdot W_{\mathrm{TO}}{}^{0.75} + C_{\mathrm{ng}} \cdot W_{\mathrm{TO}} + D_{\mathrm{ng}} \cdot W_{\mathrm{TO}}{}^{1.5}\right) \quad [lbs] \tag{A.3}$$

Nose Cone Shell

Because of the specific shape of the BWB, the weight of the nose cone shell, which is not included in the mass prediction of the fuselage in Section 4.3, is calculated with an equation from the BWB weight estimation method of Howe[4]. In this equation, B is the maximum with of the nose cone in meters, S_{nc} is the nose cone wetted area in m^2, where an ellipsoidal dome is assumed, the maximum pressure differential δ_{p} in bar and $\bar{f}_{\mathrm{t}}$, which is the ratio of the maximum working stress to 10^8. In this case the fatigue stress in tension at $100,000$ cycles is used for the maximum working stress.

$$W_{\mathrm{nc}} = 1.2 \frac{B \cdot S_{\mathrm{nc}} \cdot \delta_{\mathrm{p}} \cdot \rho}{\bar{f}_{\mathrm{t}}} \times 10^{-3} \quad [kg] \tag{A.4}$$

Crew Floor

With a BWB specific nose cone, also the crew floor mass equation is taken from Howe, where S_{CF} is the area of the crew floor in m^2.

$$W_{\mathrm{cf}} = (7 + 1.2B) \cdot S_{\mathrm{CF}} \quad [kg] \tag{A.5}$$

Windscreen

Also the mass of the windscreen is estimated according to the equation by Howe, where S_{WS} is the windscreen area in m^2.

$$W_{\mathrm{ws}} = 0.75 \cdot S_{\mathrm{WS}} \cdot V_{\mathrm{D}} \cdot \delta_p \quad [kg] \tag{A.6}$$

Front Pressure Bulkhead

The front pressure bulkhead is not included in the fuselage weight estimation and is also estimated according to Howe[4]. S_{fpb} is the area of the bulkhead in m^2 where a dome shape is assumed, hence $\bar{h}_{\mathrm{fpb}} = 1$ and ρ_{mat} is the material density in $\mathrm{kg/m}^3$.

$$W_{\mathrm{fpb}} = 6.5 \cdot \bar{h}_{\mathrm{fpb}} \cdot S_{\mathrm{fpb}} \cdot \delta_{\mathrm{p}} \cdot \rho_{\mathrm{mat}} \times 10^{-3} \quad [kg] \tag{A.7}$$

Rear Pressure Bulkhead

The mass of the rear pressure bulkhead is estimated similar to that of the front pressure bulkhead, where S_{rpb} is calculated as the surface within the last fuselage section in m^2. Here a flat bulkhead is assumed, hence $\bar{h}_{\mathrm{rpb}} = 1.25$.

$$W_{\mathrm{rpb}} = 6.5 \cdot \bar{h}_{\mathrm{rpb}} \cdot S_{\mathrm{rpb}} \cdot \delta_{\mathrm{p}} \cdot \rho_{\mathrm{mat}} \times 10^{-3} \;\; [kg] \tag{A.8}$$

Cargo Floor

The upper and lower horizontal sandwich members fulfill a double function as an upper cargo floor and cabin floor, however, the cargo floor for the lower deck is not computed yet. Therefore Equation (A.9) from Howe[4] is used. Here B_{frf} is the maximum width of the cargo floor in m and S_{frf} is the surface area of the cargo floor in m^2.

$$W_{\mathrm{frf}} = 2.6\,(1 + 0.6 B_{\mathrm{frf}}) \cdot S_{\mathrm{frf}} \cdot \rho_{mat} \times 10^{-3} \;\; [kg] \tag{A.9}$$

This concludes the airframe mass, except for the fuselage trailing edge, wings and fuselage as computed in Equation (A.29), Section 4.2 and Section 4.3, respectively.

Propulsion Group

Next to be discussed is the propulsion group, which is split up according to the method of Torenbeek as discussed in Roskam[35].

Engines

The mass of the engines is taken from the number of engines installed on the aircraft with the Rolls Royce Trent 900 as a reference engine. The mass is scaled with the required thrust.

Nacelles

For podded engines, the mass of the air induction system is included in the estimation of the nacelle weight. The take-off thrust in lbs is scaled with a factor $K_{\mathrm{nac}} = 0.065$ for high by-pass ratio turbofan engines.

$$W_{\mathrm{nac}} = K_{\mathrm{nac}} \cdot T_{\mathrm{to}} \;\; [lbs] \tag{A.10}$$

Fuel System

The mass of the fuel system depends on the number of installed engines and the number of fuel tanks, the fuel mass in lbs, W_{f} and a factor $K_{\mathrm{fsp}} = 6.70938$ for the fuel density per gallon. (This factor was recalculated for modern kerosine, Jet-A1).

$$W_{\mathrm{fs}} = 80\,(N_{\mathrm{eng}} + N_{\mathrm{tanks}} - 1) + 15 \cdot {N_{\mathrm{tanks}}}^{0.5} \cdot \left(\frac{W_{\mathrm{f}}}{K_{\mathrm{fsp}}}\right)^{0.333} \;\; [lbs] \tag{A.11}$$

Accessory Drives, Powerplant Controls and Starting and Ignition

The mass of the accessory drives, the engine controls and starting and ignition system is combined into one equation, that takes into account: the number of engines and the fuel flow at take-off setting in lbs/s.

$$W_{\text{apsi}} = 36 \cdot N_{\text{eng}} \cdot \left(\frac{\mathrm{d}W_{\text{f}}}{\mathrm{d}t}\right)_{\text{TO}} \ [lbs] \tag{A.12}$$

Thrust Reverser

The mass of the thurst reverser is simply a fraction of the engine mass, as given by Equation (A.13).

$$W_{\text{tr}} = 0.18 \cdot W_{\text{eng}} \ [lbs] \tag{A.13}$$

Water Injection System

In case a water injection system should be present, Equation (A.14) can be used. However, this is uncommon for modern turbofan engines because of the complexity of the system and emission regulations, therefore no water is taken aboard.

$$W_{\text{wi}} = 8.586 \frac{W_{\text{wtr}}}{8.35} \ [lbs] \tag{A.14}$$

Oil System and Oil Cooler

The mass of the oil system and oil cooler is included in the engine weight.

Fixed Airplane Services and Equipment

Next to the airframe and propulsion system, several non-optional airplane services and equipment need to be included in the weight estimation. The equations for the their mass predictions is provided in this sub-section.

Flight Control Systems

The flight control system is related to the take-off mass of the aircraft, estimated through a Class-I weight estimation method, and a factor $K_{\text{fc}} = 0.64$ for powered flight control systems.

$$W_{\text{fc}} = K_{\text{fc}} \cdot {W_{\text{TO}}}^{0.667} \ [lbs] \tag{A.15}$$

The weight of the flight control systems includes the weight of the hydraulics and hydraulic system.

Electrical System

The mass of the electrical system is related to the volume of the passenger cabin in ft^3.

$$W_{\text{els}} = 10.8 \cdot {V_{\text{pax}}}^{0.7} \cdot \left(1 - 0.018 {V_{\text{pax}}}^{0.35}\right) \ [lbs] \tag{A.16}$$

Instrumentation, Avionics and Electronics

The weight of the instrumentation, avionics and electronics on board of the aircraft is related to the empty weight, in kg, of the aircraft, estimated by the Class-I mass prediction and the range of the aircraft, in kilometers.

$$W_{\text{iae}} = 0.347 \cdot {W_{\text{E}}}^{0.556} \cdot R^{0.25} \ \ [kg] \tag{A.17}$$

Airconditioning, Pressurization and Anti- and De-icing

The mass of the airconditioning, pressurization and anti- and de-icing equipment is determined based on the length of the passenger cabin in ft.

$$W_{\text{api}} = 6.75 \cdot {l_{\text{pax}}}^{1.28} \ \ [lbs] \tag{A.18}$$

Oxygen System

For the weight of the oxygen supply system, the equation for extended overwater flights is used, where the mass is related to the number of passengers.

$$W_{\text{ox}} = 40 + 2.4 \cdot N_{\text{pax}} \ \ [lbs] \tag{A.19}$$

APU

The installed mass of the auxiliary power unit (APU) is directly related to the dry-mass of the APU. Here a PW980 APU of the Airbus A380 is assumed, which is 10% larger than the PW901a of the Boeing 747-400[31]. The PW901a weighs in at 835 lbs according to information from Virginia Tech[32].

$$W_{\text{apui}} = 2.25 \cdot W_{\text{apu}} \ \ [lbs] \tag{A.20}$$

Radar

The mass of the radar is estimated from that of a typical Honeywell weather radar for commercial aircraft, the Primus 880, at 20kg.

Paint

The weight of the paint is estimated at 0.3kg/m^2 wetted area. This based on a press release by Airbus for the A380[34].

$$W_{\text{paint}} = 0.3 \cdot S_{\text{wet}} \ \ [kg] \tag{A.21}$$

Removables

Next to all fixed gear on board of the aircraft, there are a number of items that, even though they are considered to be removable, are part of the OEW of an aircraft.

Flightdeck Furnishing

The furnishing of the flightdeck is estimated at 200kg in total, as estimated from the weight of pilot and fold-away seats in the cockpit from Torenbeek[10] and rounded upwards to account for the rest of the furnishing.

Cabin Furnishing

The cabin furnishing, including toilets and galleys and overhead luggage compartments was estimated from data for the Boeing 747. From Roskam[35] the mass of the furnishing for this aircraft was obtained and divided equally over the cabin surface to obtain a ratio of 51.5kg furnishing per squared meter of cabin area. The 747-100 was used as a reference as it is capable of transporting 400+ passengers in a 2 class configuration, and most importantly because of the availability of rare reference data on the furnishing weight from Roskam.

Cargohandling

The cargo handling equipment is split up for the upper and lower deck cargo compartment. With the upper deck suitable for bulk cargo, such as luggage and the lower deck suitable for LD-3 unit load devices. The equations for the cargo handling weight are taken from Torenbeek[10]. For the upper deck this is related to the volume of the cargo hold, for the lower deck it is related to the surface of the lower deck cargo floor.

Luggage compartment on upper deck:

$$W_{\mathrm{ch_u}} = 1.28 \cdot V_{\mathrm{u}} \;\; [kg] \tag{A.22}$$

Cargo hold suitable for containers on lower deck:

$$W_{\mathrm{ch_l}} = 13.67 \cdot S_{\mathrm{l}} \;\; [kg] \tag{A.23}$$

Fire Detection and Extinguishing

The safety equipment, such as the fire detection and extinguishing equipment, is also part of the removable gear. This is considered to be a fraction of the aircraft take-off mass, in kg, as computed in the class-I weight estimation of the preliminary sizing.

$$W_{\mathrm{fde}} = 0.0012 \cdot W_{\mathrm{TO}} \;\; [kg] \tag{A.24}$$

Evacuation Slides and Ropes

Evacuation slides and ropes are directly related to the number of passengers on board of the aircraft, as shown in Equation (A.25).

$$W_{\mathrm{evac}} = 0.453 \cdot N_{\mathrm{pax}} \;\; [kg] \tag{A.25}$$

Operational Items

Part of the OEW are also the operational items, that are perhaps not immediately necessary to transport passengers or cargo, yet are considered necessities for operating a commercial transport aircraft.

Crew

Flight crew and cabin crew cannot be considered equipment, however, they are indispensable for the operation of the aircraft. Because the ever changing human anthropology, the original data from 1982[10] has been adapted to better match the average human in 2012. Therefore the heavier of the two weights proposed by Torenbeek, i.e. that of the flight crew, has been considered for both the flight crew and cabin crew, including there luggage. This weight is set equal to 93kg per crew member, including luggage.

Trapped Fuel and Oil

The mass of the trapped fuel and oil is computed through a multiplication of the fraction computed in the Class-I weight prediction in the preliminary sizing with the take-off weight computed in the Class-I method.

Passenger Cabin Supplies

Passenger cabin supplies, such as galley equipment, meal service, consumable food, drinks, beverages, pillows, papers, magazines, entertainment etc. are considered part of the operational items. Their combined weight can be related to the number of passenger in first class and economy class according to Equation (A.26).

$$W_{\text{pax}_{\text{supp}}} = 8.62 \cdot N_{\text{pax}_{ec}} + (2.27 + 8.62) \cdot N_{\text{pax}_{\text{1st}}} \;\; [kg] \tag{A.26}$$

Drinkable Water and Toilet Chemicals

The weight of drinkable water and toilet chemicals on board of the aircraft is calculated according to Equation (A.27) from Torenbeek[10] for long range passenger aircraft.

$$W_{\text{WC}_{\text{supp}}} = 2.95 \cdot N_{\text{pax}} \;\; [kg] \tag{A.27}$$

Safety Equipment

Other safety equipment, next to fire detectors and extinguishers and evacuation slides, such as life jackets, fire axes and emergency navigational equipment must also included in the operational items. Their weight is also directly related to the number of passengers on board of the aircraft.

$$W_{\text{safety}} = 3.4 \cdot N_{\text{pax}} \;\; [kg] \tag{A.28}$$

Cargo Containers

Since the lower deck cargo hold is sized for cargo containers, their weight must be considered in the operational items. The number of LD-3 containers is determined in the cargo hold analysis and multiplied with the LD-3 tare weight of 72kg each, as used by British Airways World Cargo[30].

Fuselage Trailing Edge

In Section 4.3 the weight of the fuselage section is computed, however this does not include the nose cone or the section aft of the passenger cabin. The nose cone weight has been determined by means of Equations (A.4) through (A.6), yet that of the fuselage trailing edge is not included. Therefore Equation (A.29) is taken from the class II.5 wing weight estimation methodology from Torenbeek[5]. This equation is used to calculate the weight to complete the aerodynamic shape of the wing, with the wing box weight already determined. A similar methodology is adapted here, the trailing edge merely completes the aerodynamic shape of the wing. Though it must be noted that in a more detailed design, the available volume could very well be used for example for aircraft systems or fuel, implying a re-evaluation of the use of this equation. At this point it is assumed that the trailing edge section could also be used as a control surface. This is included in Equation (A.29), where Δ is normally an indication of the complexity of the flap system present on the trailing edge of a wing. It is assumed that a single slotted flap bears more resemblance to an elevator than e.g. a double slotted system. Therefore no further penalty on Δ is considered.

$$W_{\mathrm{fus_{TE}}} = S_{\mathrm{TE}} \left[60 \left(1 + 1.6 \cdot \sqrt{\frac{W_{\mathrm{TO}}}{10^6}} \right) + \Delta \right] \quad [kg] \tag{A.29}$$

For a single slotted flap[5]:

$$\Delta = 0$$

OEW

The actual OEW of the BWB is the sum of the component weights computed in Equations (A.1) through (A.29) and the addition of the weight of the outer wings, as explained in Section 4.2 and the weight of the fuselage cabin, as explained in Section 4.3.

APPENDIX B

INPUT VARIABLES

This appendix presents the input variables for the optimizations. All inputs have been obtained from the thesis of J.L. Van Dommelen[7], unless otherwise indicated. These inputs have been applied to both the 'oval-fuselage' and the multi-bubble for a fair comparison.

Table B.1: Collected input variables

Parameter	**Value**	**Unit**	**Type**
LD3 internal volume	4.27	m^3	Input[30]
Minimum cabin height	2	m	Requirement
Minimum cargo hold height	1.68	m	Input[29]
Cargo density	190	m^3	Input[10]
Material density (AL7075T6)	2800	kg/m^3	Input[45]
Young's modulus (AL7075T6)	72.5	GPa	Input[45]
Fatigue stress in tension (100,000 cycles)	156	MPa	Input[45]
Fatigue stress in compression (100,000 cycles)	140	MPa	Input[45]
Core material density	52	kg/m^3	Input[46]
Pressure differential	0.8	Bar	Input
Safety factor	1.5	-	Input
Area per row (4 seats+aisle), first class	3.5	m^2	Input
Area meter per row (6 seats+aisle), economy	3.15	m^2	Input
Galley volume per passenger, first class	0.2	m^3	Input
Galley volume per passenger, economy class	0.05	m^3	Input
Lavatory area	0.2	m^2	Input
Seating area per crew member	0.5	m^2	Input
Flightdeck area	6	m^2	Input
Passengers per lavatory, first class	10	-	Input
Passengers per lavatory, economy class	40	-	Input
Number of flightdeck crew	2	-	Input

Continued on next page...

Table B.1 – Continued

Parameter	**Value**	**Unit**	**Type**
Number of passengers per crew, first class	18	-	Input
Number of passengers per crew, economy class	30	-	Input
Single person weight	86	kg	Input
Baggage weight	25	kg	Input
Crew member weight incl. baggage	83	kg	Input [10]
Trent 900 reference thrust	320000	N	Input
Trent 900 reference weight	6271	kg	Input
Trent 900 reference length	4.55	m	Input
Trent 900 reference diameter	2.94	m	Input
Trent 900 reference fuel consumption	$17.1 \cdot 10^{-6}$	1/s	Input
Start up fuel fraction	0.99	-	Input
Taxi fuel fraction	0.99	-	Input
Take off fuel fraction	0.995	-	Input
Climb up fuel fraction	0.998	-	Input
Descent up fuel fraction	0.99	-	Input
Landing, taxi and shut down fuel fraction	0.995	-	Input
Trapped fuel and oil fraction of MTOW	0.002	-	Input
MLW/MTOW	0.84	-	Input
Design range	11000	km	Input
Evasion range	500	km	Input
Loiter time	45	min	Input
Cruise altitude	11	km	Input
Cruise Mach number	0.82	-	Input
Take-off runway length	2500	m	Input
Landing runway length	2500	m	Input
Twist axis location, fraction of chord	0.5	-	Input
Front spar location, fraction of chord	0.13	-	Input
Rear spar location, fraction of chord	0.72	-	Input
Front fuel tank edge, fraction of chord	0.15	-	Input
Rear fuel tank edge, fraction of chord	0.70	-	Input
Start section of fuel tank	4	-	Input
Maximum spanwise position fuel tank	0.85	-	Input
Fuel tank scaling to account for structure	0.85	-	Input
Fuel density	810	kg/m^3	Input
Nose gear length	2	m	Input
Main gear length	2	m	Input
Vertical tail taper	0.3	-	Input
Vertical tail LE sweep	45	degrees	Input
Vertical tail dihedral	20	degrees	Input
Vertical tail aspect ratio	1.9	-	Input
Vertical tail root profile	0014	NACA	Input
Vertical tail tip profile	0012	NACA	Input
Vertical tail twist	0	degrees	Input

APPENDIX C

RESULTS FOR THE OPTIMIZED MULTI-BUBBLE AIRCRAFT

.

200 passenger multi-bubble

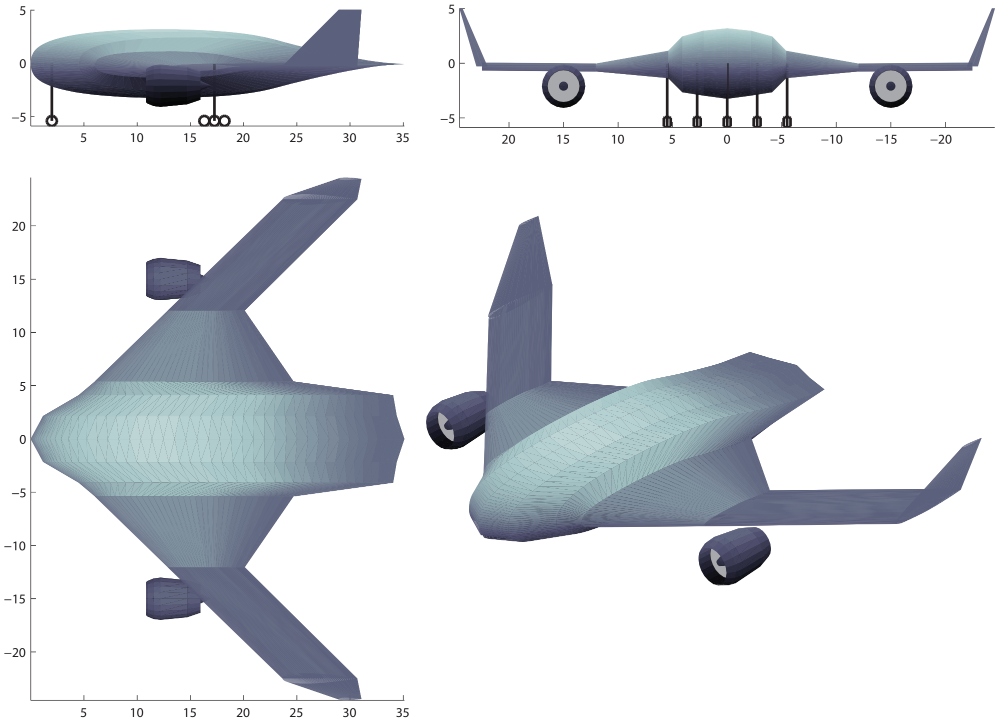

Figure C.1: 3D illustration for the 200 passenger multi-bubble BWB

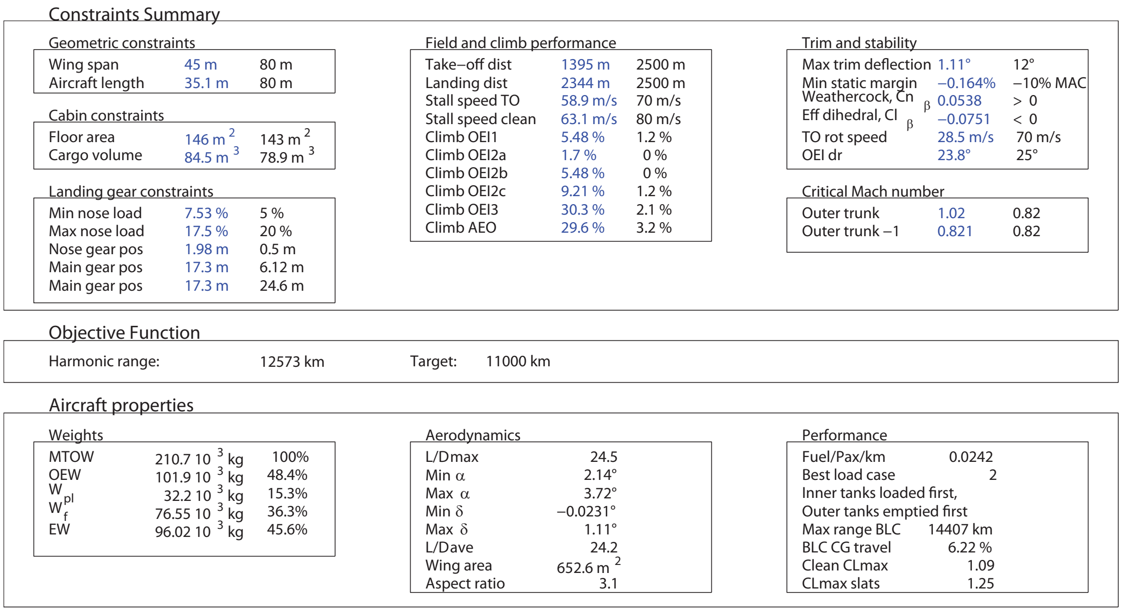

Figure C.2: Constraints summary of the 200 passenger multi-bubble BWB

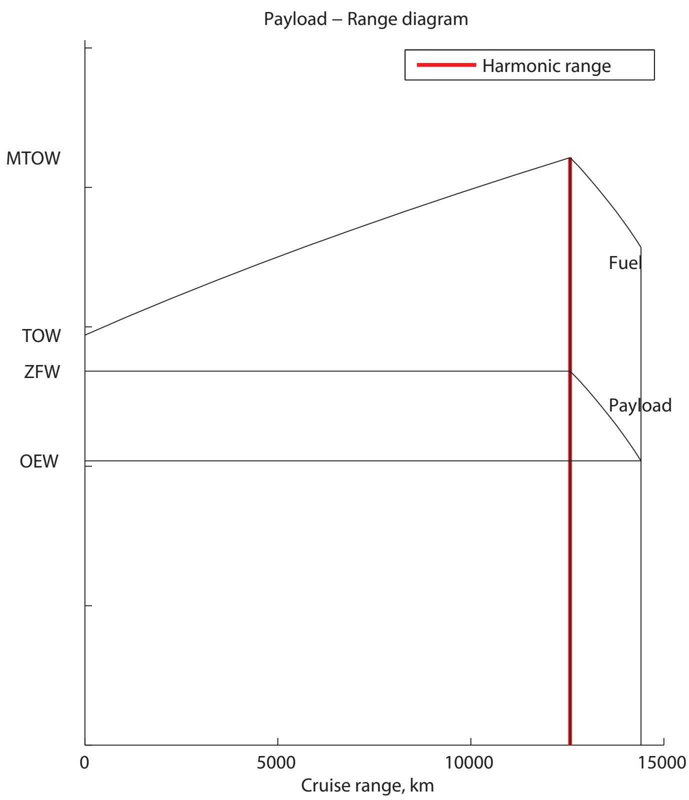

Figure C.3: Payload-range diagram of the 200 passenger multi-bubble BWB

400 passenger multi-bubble

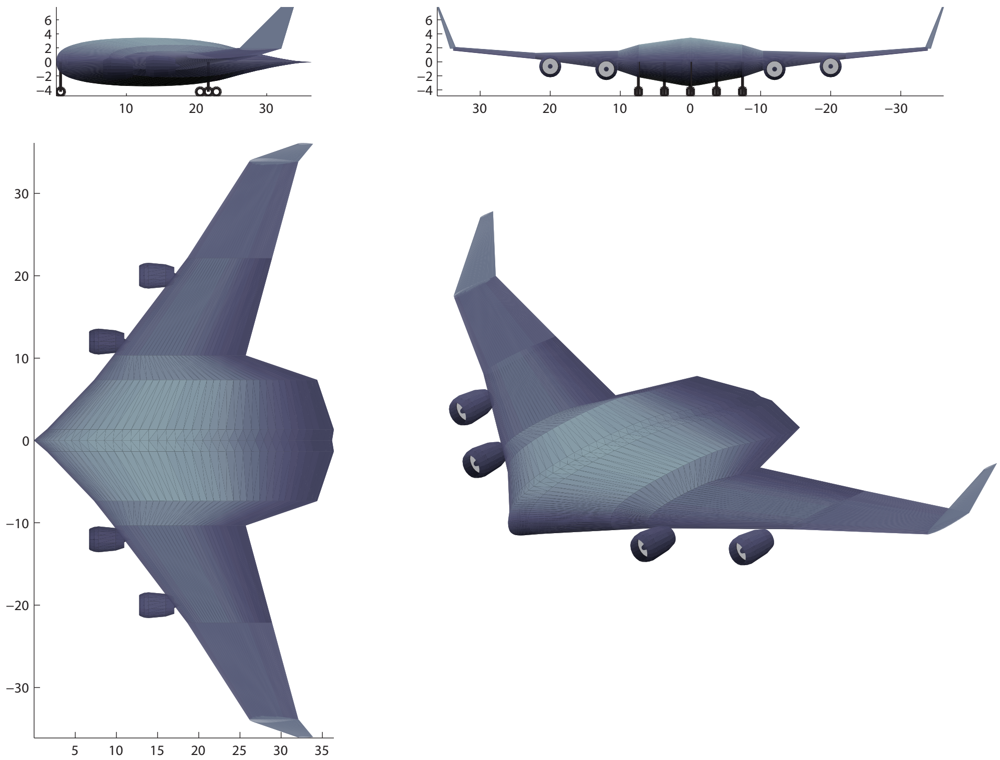

Figure C.4: 3D illustration for the 400 passenger multi-bubble

Constraints Summary

Geometric constraints

Wing span	67.7 m	80 m
Aircraft length	36.4 m	80 m

Cabin constraints

Floor area	273 m^2	273 m^2
Cargo volume	169 m^3	158 m^3

Landing gear constraints

Min nose load	5.01 %	5 %
Max nose load	20 %	20 %
Nose gear pos	0.605 m	0.5 m
Main gear pos	21.7 m	7.37 m
Main gear pos	21.7 m	34.2 m

Field and climb performance

Take−off dist	2027 m	2500 m
Landing dist	2493 m	2500 m
Stall speed TO	62.8 m/s	70 m/s
Stall speed clean	67.2 m/s	80 m/s
Climb OEI1	8.4 %	1.2 %
Climb OEI2a	5.17 %	0 %
Climb OEI2b	8.4 %	0 %
Climb OEI2c	11.4 %	1.2 %
Climb OEI3	17.4 %	2.1 %
Climb AEO	17.3 %	3.2 %

Trim and stability

Max trim deflection	1.55°	12°
Min static margin	−3.49%	−10% MAC
Weathercock, Cn_β	0.0214	> 0
Eff dihedral, Cl_β	−0.136	< 0
TO rot speed	32.7 m/s	70 m/s
OEI dr	22.1°	25°

Critical Mach number

Outer trunk	0.896	0.82
Outer trunk −1	0.82	0.82

Objective Function

Harmonic range:	12448 km	Target:	11000 km

Aircraft properties

Weights

MTOW	394.5 10^3 kg	100%
OEW	198.3 10^3 kg	50.3%
W_{pl}	64.4 10^3 kg	16.3%
W_f	131.8 10^3 kg	33.4%
EW	186.8 10^3 kg	47.3%

Aerodynamics

L/Dmax	29.5
Min α	1.87°
Max α	2.88°
Min δ	−1.06°
Max δ	1.55°
L/Dave	27.4
Wing area	1096 m^2
Aspect ratio	4.18

Performance

Fuel/Pax/km	0.0204
Best load case	1
Inner tanks loaded first,	
Inner tanks emptied first	
Max range BLC	15332 km
BLC CG travel	12.3 %
Clean CLmax	1.07
CLmax slats	1.23

Figure C.5: Constraints summary of the 400 passenger multi-bubble BWB

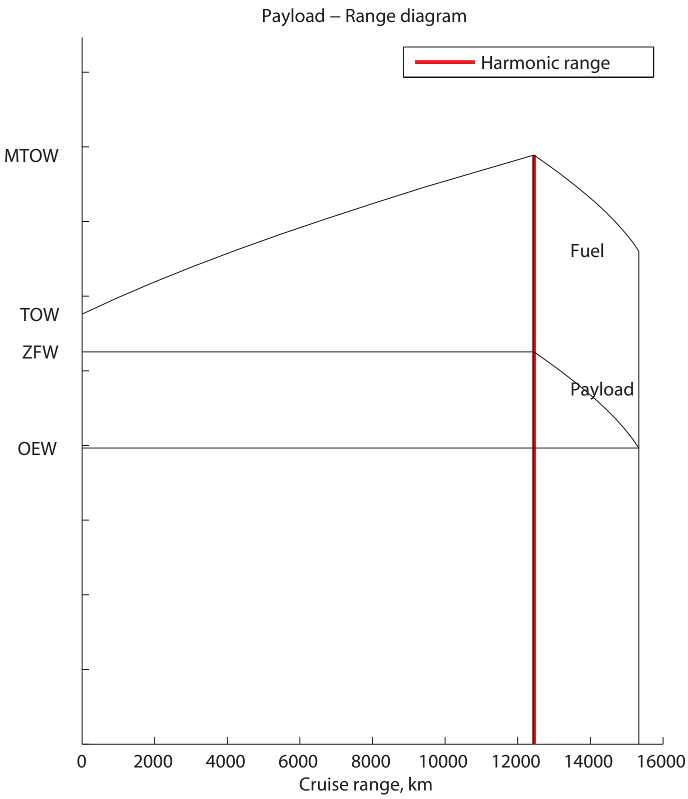

Figure C.6: Payload-range diagram of the 400 passenger multi-bubble BWB

800 passenger multi-bubble

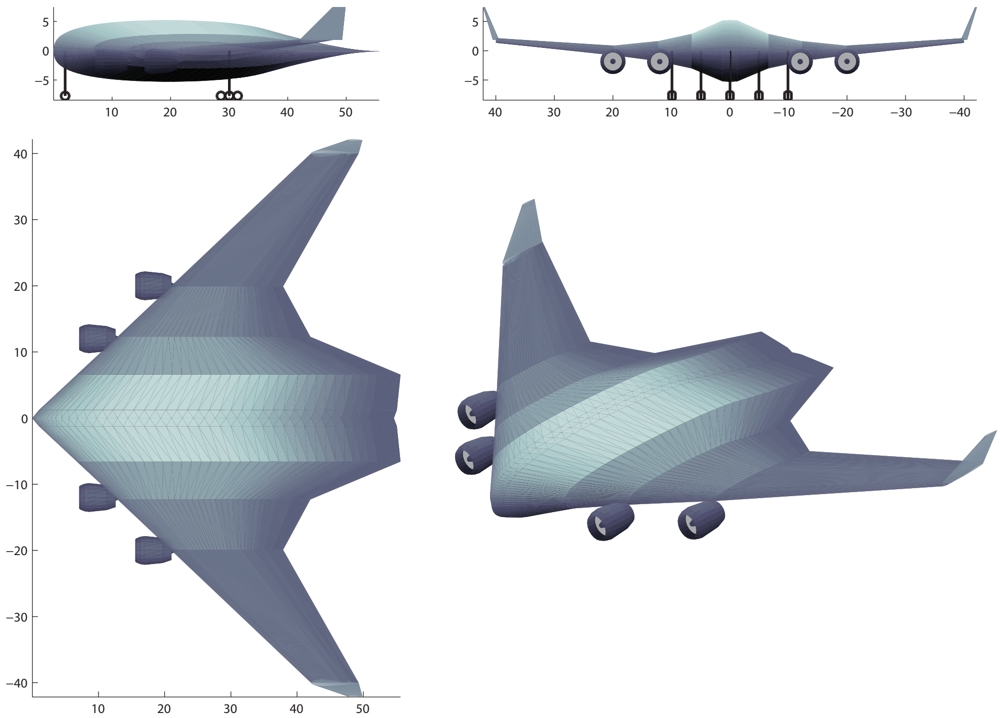

Figure C.7: 3D illustration for the 800 passenger multi-bubble

Constraints Summary

Geometric constraints

Wing span	80 m	80 m
Aircraft length	55.6 m	80 m

Cabin constraints

Floor area	566 m^2	532 m^2
Cargo volume	378 m^3	316 m^3

Landing gear constraints

Min nose load	5.35 %	5 %
Max nose load	19.7 %	20 %
Nose gear pos	1.97 m	0.5 m
Main gear pos	30 m	10.3 m
Main gear pos	30 m	47.7 m

Field and climb performance

Take–off dist	1958 m	2500 m
Landing dist	2441 m	2500 m
Stall speed TO	62 m/s	70 m/s
Stall speed clean	65.5 m/s	80 m/s
Climb OEI1	5.05 %	1.2 %
Climb OEI2a	1.33 %	0 %
Climb OEI2b	5.05 %	0 %
Climb OEI2c	8.56 %	1.2 %
Climb OEI3	15.6 %	2.1 %
Climb AEO	14.6 %	3.2 %

Trim and stability

Max trim deflection	2.33°	12°
Min static margin	−0.213%	−10% MAC
Weathercock, Cn_{β}	0.00842	> 0
Eff dihedral, Cl_{β}	−0.074	< 0
TO rot speed	26 m/s	70 m/s
OEI dr	24.3°	25°

Critical Mach number

Outer trunk	0.969	0.82
Outer trunk −1	0.83	0.82

Objective Function

Harmonic range:	8353.8 km	Target:	11000 km

Aircraft properties

Weights

MTOW	761.4 10^3 kg	100%
OEW	408.2 10^3 kg	53.6%
W_{pl}	128.8 10^3 kg	16.9%
W_f	224.4 10^3 kg	29.5%
EW	384.7 10^3 kg	50.5%

Aerodynamics

L/Dmax	23.9
Min α	2.69°
Max α	4.2°
Min δ	−1.02°
Max δ	2.33°
L/Dave	22.5
Wing area	1965 m^2
Aspect ratio	3.25

Performance

Fuel/Pax/km	0.0247
Best load case	1
Inner tanks loaded first,	
Inner tanks emptied first	
Max range BLC	11955 km
BLC CG travel	9.72 %
Clean CLmax	1.21
CLmax slats	1.35

Figure C.8: Constraints summary of the 800 passenger multi-bubble BWB

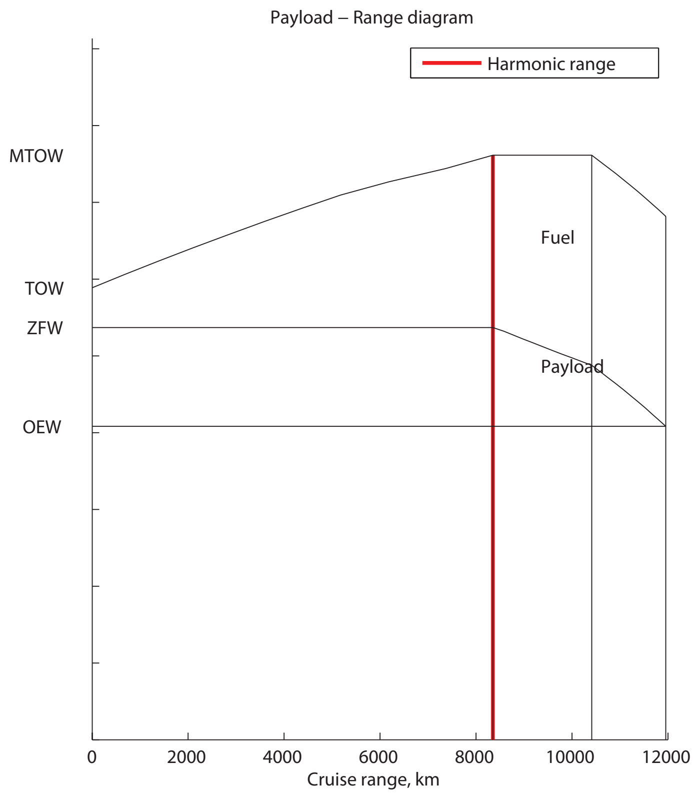

Figure C.9: Payload-range diagram of the 800 passenger multi-bubble BWB